

LAGRANGIAN ASPECTS OF  
TURBULENT TRANSPORT IN PIPE FLOW

By  
David Lee Breton

A DISSERTATION PRESENTED TO THE GRADUATE COUNCIL OF  
THE UNIVERSITY OF FLORIDA IN PARTIAL  
FULFILLMENT OF THE REQUIREMENTS FOR THE DEGREE OF  
DOCTOR OF PHILOSOPHY

UNIVERSITY OF FLORIDA  
1975

## ACKNOWLEDGMENTS

I wish to express my sincere thanks to the members of my supervisory committee: Dr. Ray W. Fahien, Chairman; Dr. Dale W. Kirmse, Co-Chairman; Dr. John G. Saw; Dr. Herbert E. Schweyer; and Dr. Mack Tyner. Special thanks are due to Dr. Fahien and Dr. Kirmse for their guidance during the course of this work.

Thanks are also due to my colleagues and friends of the Chemical Engineering department. For the assistance in the construction and the maintenance of the experimental equipment, I would like to extend my appreciation to Jack Kalway and Myron Jones.

I wish to thank my wife, Fran, for her continued support and aid in organizing and proofing. Many thanks to Mary Van Meer for the typing of the manuscript. I also wish to thank David Trissel for his computer programming assistance in data compilation.

I am very grateful to the College of Engineering for its financial aid in the form of a graduate assistantship.

## TABLE OF CONTENTS

	<u>Page</u>
ACKNOWLEDGMENTS.....	ii
LIST OF TABLES.....	v
LIST OF FIGURES.....	vi
KEY TO SYMBOLS.....	x
ABSTRACT.....	xiv
 CHAPTER	
1. INTRODUCTION.....	1
2. LITERATURE REVIEW.....	3
2.1 Dispersion of a Scalar Property in a Turbulent Flow.....	7
2.1.1 Isotropic homogeneous flow.....	8
2.1.2 Anisotropic homogeneous flow....	13
2.1.2.1 Single-particle dispersion.....	13
2.1.2.2 Two-particle dispersion.....	20
2.1.3 Shear flow.....	22
2.1.4 Interaction of molecular and turbulent dispersion.....	24
2.2 Lagrangian Characteristics of Turbulent Flow.....	26
2.2.1 Lagrangian numerical simulations.....	26
2.2.2 Lagrangian experimental studies.....	31
2.2.3 Eulerian-Lagrangian transformation.....	35
2.3 Experimental Determination of Eddy Diffusivities.....	40
2.3.1 Determination by Lagrangian analysis.....	41
2.3.2 Determination by Eulerian analysis.....	45

	<u>Page</u>
3. EXPERIMENT AND DATA ANALYSIS.....	53
3.1 Experiment.....	53
3.1.1 Flow loop.....	54
3.1.2 Lighting system.....	59
3.1.3 Camera.....	60
3.1.4 Procedure.....	65
3.1.5 Processing of photographic film.....	66
3.2 Data Analysis.....	67
3.2.1 Transformation of photographic data.....	68
3.2.2 Computation of particle velocity.....	74
3.2.3 Computation of Lagrangian correlations.....	75
4. RESULTS AND DISCUSSION.....	80
4.1 Results.....	80
4.1.1 Turbulent intensities and shear stresses.....	81
4.1.2 Lagrangian correlations.....	81
4.2 Equipment and Procedure.....	118
4.3 Data Collection and Analysis.....	121
5. SUMMARY AND CONCLUSIONS.....	150
APPENDIX	
A. DATA COLLECTION ALGORITHM.....	152
B. SOLUTION FOR COEFFICIENT TO X-Y RECORDER COORDINATE TRANSFORMATION EQUATION.....	167
C. COMPUTER PROGRAM FOR COMPUTING THE CYLINDRICAL COORDINATES OF PARTICLE PATHS.....	171
D. COMPUTER PROGRAM FOR THE COMPUTATION OF THE LAGRANGIAN TIME CORRELATIONS.....	177
BIBLIOGRAPHY.....	185
BIOGRAPHICAL SKETCH.....	199

## LIST OF TABLES

<u>Table</u>		<u>Page</u>
4.1	Relative Turbulent Intensities.....	82
4.2	Relative Turbulent Shear Stresses.....	82
4.3	Typical Particle Path Coordinates.....	125
4.4	Number of Contributions to the Correlations..	133

## LIST OF FIGURES

<u>Figure</u>	<u>Page</u>
3.1 Experiment Apparatus.....	55
3.2 Observation Enclosure and Camera Arrangement.....	58
3.3 Chopping Frequency Detection Circuit.....	61
3.4 Camera Construction.....	62
3.5 Film Mounting Arrangement.....	64
3.6 Geometry of Optics for a Typical View of the Flow Field.....	69
3.7 Arrangement of Datum Points.....	73
4.1 $\langle (r'(t))^2 \rangle / D_0^2$ Versus $t^*$ for All Radial Zones.....	91
4.2 $\langle r'(t) V_r(t) \rangle / D_0 U_{z,MAX}$ Versus $t^*$ for All Radial Zones.....	92
4.3 $\langle V_r(t_0) V_r(t) \rangle / \langle V_r^2(t_0) \rangle$ Versus $t^*$ for All Radial Zones.....	93
4.4 $\langle (z'(t))^2 \rangle / D_0^2$ Versus $t^*$ .....	94
4.5 $\langle (r'(t))^2 \rangle / D_0^2$ Versus $t^*$ .....	95
4.6 $\langle (r_0 \theta'(t))^2 \rangle / D_0^2$ Versus $t^*$ .....	96
4.7 $\langle z'(t) r'(t) \rangle / D_0^2$ Versus $t^*$ .....	97
4.8 $\langle z'(t) r_0 \theta'(t) \rangle / D_0^2$ Versus $t^*$ .....	98
4.9 $\langle r'(t) r_0 \theta'(t) \rangle / D_0^2$ Versus $t^*$ .....	99
4.10 $\langle z'(t) V_z'(t) \rangle / D_0 U_{z,MAX}$ Versus $t^*$ .....	100
4.11 $\langle z'(t) V_r(t) \rangle / D_0 U_{z,MAX}$ Versus $t^*$ .....	101
4.12 $\langle z'(t) V_\theta'(t) \rangle / D_0 U_{z,MAX}$ Versus $t^*$ .....	102

Figure		Page
4.13	$\langle r'(t)V'_z(t) \rangle / D_0 U_{z,MAX}$ Versus $t^*$ .....	103
4.14	$\langle r'(t)V_r(t) \rangle / D_0 U_{z,MAX}$ Versus $t^*$ .....	104
4.15	$\langle r'(t)V'_\theta(t) \rangle / D_0 U_{z,MAX}$ Versus $t^*$ .....	105
4.16	$\langle r_0 \theta'(t)V'_z(t) \rangle / D_0 U_{z,MAX}$ Versus $t^*$ .....	106
4.17	$\langle r_0 \theta'(t)V_r(t) \rangle / D_0 U_{z,MAX}$ Versus $t^*$ .....	107
4.18	$\langle r_0 \theta'(t)V'_\theta(t) \rangle / D_0 U_{z,MAX}$ Versus $t^*$ .....	108
4.19	$\frac{d}{dt} \langle z'(t)r'(t) \rangle / D_0 U_{z,MAX}$ Versus $t^*$ .....	109
4.20	$\frac{d}{dt} \langle z'(t)r_0 \theta'(t) \rangle / D_0 U_{z,MAX}$ Versus $t^*$ .....	110
4.21	$\frac{d}{dt} \langle r'(t)r_0 \theta'(t) \rangle / D_0 U_{z,MAX}$ Versus $t^*$ .....	111
4.22	$\langle V'_z(t_0)V'_z(t) \rangle / \langle (V'_z(t_0))^2 \rangle$ Versus $t^*$ .....	112
4.23	$\langle V_r(t_0)V_r(t) \rangle / \langle V_r^2(t_0) \rangle$ Versus $t^*$ .....	113
4.24	$\langle V'_\theta(t_0)V'_\theta(t) \rangle / \langle (V'_\theta(t_0))^2 \rangle$ Versus $t^*$ .....	114
4.25	$\frac{\langle V'_z(t_0)V_r(t) \rangle}{(\langle (V'_z(t_0))^2 \rangle \langle V_r^2(t_0) \rangle)^{1/2}}$ Versus $t^*$ .....	115
4.26	$\frac{\langle V'_z(t_0)V'_\theta(t) \rangle}{(\langle (V'_z(t_0))^2 \rangle \langle (V'_\theta(t_0))^2 \rangle)^{1/2}}$ Versus $t^*$ .....	116
4.27	$\frac{\langle V_r(t_0)V'_\theta(t) \rangle}{(\langle V_r^2(t_0) \rangle \langle (V'_\theta(t_0))^2 \rangle)^{1/2}}$ Versus $t^*$ .....	117
4.28	Projection of the Particle Paths onto the $r$ - $\theta$ Plane.....	124
4.29	Equivalent Convolution Function for the Least-Square Smoothing.....	127

<u>Figure</u>	<u>Page</u>
4.30	Energy Spectra Function for the Equivalent Convolution Function.....129
4.31	Mean Axial Velocity Profile.....131
4.32	An Estimate of the Statistical Error for $\langle (z'(t))^2 \rangle / D_0^2$ .....135
4.33	Time Symmetry in $\frac{\langle V'_z(t_0) V'_z(t) \rangle}{\langle (V'_z(t_0))^2 \rangle}$ for the Fourth Radial Zone from Center of Pipe.....136
4.34	Time Symmetry in $\frac{\langle V'_r(t_0) V'_r(t) \rangle}{\langle V'^2_r(t_0) \rangle}$ for the Fourth Radial Zone from Center of Pipe.....137
4.35	Time Symmetry in $\frac{\langle V'_\theta(t_0) V'_\theta(t) \rangle}{\langle (V'_\theta(t_0))^2 \rangle}$ for the Fourth Radial Zone from Center of Pipe.....138
4.36	Time Symmetry in $\frac{\langle V'_z(t_0) V'_r(t) \rangle}{(\langle (V'_z(t_0))^2 \rangle \langle V'^2_r(t_0) \rangle)^{1/2}}$ for the Fourth Radial Zone from Center of Pipe.....139
4.37	Axial Energy Spectra Function.....141
4.38	Radial Energy Spectra Function.....142
4.39	Tangential Energy Spectra Function.....143
4.40	Axial Autocorrelation Function Obtained from the Axial Energy Spectra Function.....145
4.41	Radial Autocorrelation Function Obtained from the Radial Energy Spectra Function.....146
4.42	Tangential Autocorrelation Function Ob- tained from the Tangential Energy Spectra Function.....147



<u>Figure</u>	<u>Page</u>
A.1 Electrical Schematic of Interface between the PDP-11 Minicomputer and the Mosely X-Y Recorder.....	154
A.2 Flow Diagram for Data Collection Algorithm.....	156

## KEY TO SYMBOLS

- a            - initial value of  $x$ ,  $L$
- $a_1$         - parameter of Equation (4.1)
- $a_2$         - parameter of Equation (4.1)
- $\underline{\underline{A}}$         - parameter tensor defined by Equations (8.14) through (8.19)
- B            - proportionality parameter for Equation (2.57)
- $\underline{c}$         - coefficient vector of Equation (3.9)
- $\underline{C}$         - height of image from photo-enlarger,  $L$
- d            - distance from object point to air-glass interface,  $L$
- $\underline{D}$         - height of object point,  $L$
- $D_0$         - diameter of pipe,  $L$
- $\underline{D}$         - relative dispersion tensor for two particles,  $L$
- $\underline{\underline{E}}$         - eddy diffusivity tensor,  $L^2/t$
- $\underline{\underline{E}}_\infty$     - asymptotic eddy diffusivity tensor,  $L^2/t$
- f            - frequency,  $1/t$
- F            - conditional p.d.f. of the separation of two particles
- $\underline{F}$         - energy spectra function vector
- $\underline{F}^{(t)}$     - turbulent flux; heat,  $M/t^3$ ; mass,  $M/L^2t$
- g            - equivalent convolution function for the least-square smoothing
- G            - Fourier transform of  $g(t)$
- $\underline{G}$         - image height on film,  $L$
- $\underline{H}$         - virtual image height at air-glass interface of observation section,  $L$

$\underline{i}_r$	- unit vector for radial direction
$\underline{i}_z$	- unit vector for axial direction
$\underline{i}_\theta$	- unit vector for tangential direction
$K_{BW}$	- proportionality parameter for Equation (2.69)
$m$	- parameter of Equation (4.1)
$\underline{m}$	- parameter vector defined by Equation (B.5)
$M$	- magnification factor for photo-enlarger
$n$	- refractive index of the glass, glycerin, and trichloroethylene
$N$	- number of contributions to a statistical sample
$P$	- probability distribution function of particle concentration with displacement and time
$Q$	- probability distribution function of particle displacement with time
$r$	- radial distance, $L$
$r_0$	- starting radial position, $L$
$\underline{R}^{(L)}$	- Lagrangian velocity correlation coefficient
$\underline{R}^{(F)}$	- autocorrelation function obtained from the energy spectra function
$\underline{\underline{S}}$	- time-stationary tensor defined by Equation (2.28), $L^2/t^2$
$t$	- time, $t$
$T$	- a specific time, $t$
$\underline{T}^{(t)}$	- Reynolds stress tensor
$\underline{u}$	- Eulerian velocity, $L/t$
$u_b$	- bulk velocity, $L/t$
$u_y$	- lateral velocity, $L/t$
$\dot{u}$	- Eulerian acceleration, $L/t^2$

$U$	- Eulerian velocity, $L/t$
$U_{z,MAX}$	- maximum mean axial velocity which occurs at the centerline of pipe, $L/t$
$U_{z,AVE}$	- average axial bulk velocity, $L/t$
$\underline{v}$	- relative velocity of two particles, $L/t$
$\dot{v}$	- Lagrangian acceleration, $L/t^2$
$\underline{V}$	- Lagrangian velocity, $L/t$
$\underline{x}$	- distance, $L$
$\underline{x'}$	- displacement from origin, $L$
$\underline{Y}$	- relative displacement of two particles, $L$
$z$	- axial distance, $L$

#### Greek Letters

$\beta$	- proportionality parameter for Equation (2.68)
$\Gamma$	- scalar property
$\zeta$	- separation distance between velocity vectors, $L$
$\theta$	- tangential angle
$\theta_i$	- incidence angle of light at air-glass interface of observation section
$\theta_r$	- refracted angle of light at air-glass interface of observation section
$\underline{\lambda}$	- parameter function defined by Equation (B.6)
$\Lambda$	- macro integral length scale, $L$
$\mu$	- distance from air-glass interface of observation section to lense, $L$
$\nu$	- distance from film to lense, $L$
$\xi$	- elapsed time, $t$
$\rho$	- density of fluid, $M/L^3$

- $\sigma$  - statistical variance
- $\tau$  - micro time scale, t
- $\omega$  - co-factor of determinant
- $\Omega$  - determinant of displacement-displacement correlation

### Subscripts

- E - Eulerian
- i - coordinate direction
- j - coordinate direction
- k - discrete time increment
- L - Lagrangian
- m - view index
- o - starting value
- y - lateral coordinate direction in 2-D
- z - longitudinal coordinate direction in 2-D

### Superscripts

- ' - fluctuation about the mean
- \*
- - time average
- < > - expected value (ensemble average)

Abstract of Dissertation Presented to the  
Graduate Council of the University of Florida  
in Partial Fulfillment of the Requirements for the  
Degree of Doctor of Philosophy

LAGRANGIAN ASPECTS OF  
TURBULENT TRANSPORT IN PIPE FLOW

By

David Lee Breton

August, 1975

Chairman: Dr. R. W. Fahien  
Co-Chairman: Dr. D. W. Kirmse  
Major Department: Chemical Engineering

A Lagrangian analysis of the turbulent dispersion process was examined by observing the motion of suspended particles in a turbulent flowing liquid. The liquid, trichloroethylene, was pressure-driven through a 0.0254 meter (1 inch) I.D. glass pipe. The average velocity was 0.969 meter/sec (3.18 feet/sec) which corresponded to a Reynolds' number of 110,000. A photographing technique was developed which enabled the photographing of particle motion over large distances. Particle positions in time were computed from the photographic images.

Lagrangian time correlations were computed from the displacement and velocity deviations obtained from the particle trajectories. The time dependence of the various correlations was obvious from an examination of the plotted results. The effect of a confining wall on the radial spread

of the particles was apparent for large times. It appeared that the assumption of a constant radial eddy diffusivity coefficient could be used as a fair approximation of the time-dependent coefficient. Within the experimental accuracy of the data, the resultant correlations agreed well with the theory and published data.

## CHAPTER 1

### INTRODUCTION

Turbulence is a common occurrence in both naturally and artificially generated flow systems. The rapid spread of smoke from chimneys and the vapor trails of high-altitude jet aircraft are examples of turbulent effects in the atmosphere. The diffusion of mass and heat in turbulent fluids in numerous chemical engineering processes is another example. Few physical phenomena have attracted more interest in the scientific and engineering fields than turbulence, which attests to its general occurrence and importance. A great deal of work has yielded only a little understanding of turbulent fluid motion, indicating its difficult and complex nature.

The Lagrangian characteristic of turbulent liquid flow is the object of study in the present work. To investigate the turbulence, paths of small particles were observed as approximations of the paths of fluid points. A distinction is made here between a "particle," a solid, rigid piece of matter immersed in the continuum, and a "fluid point," a mathematical point moving with the continuum. A fluid point is a volume of fluid so small that in the context of the continuum it may be considered as



an individual point moving along with the fluid. The system selected for study is fully developed pressure-driven flow in a pipe. Under these conditions the fluid is in shear flow, and the turbulence is nonhomogeneous and anisotropic.

## CHAPTER 2

### LITERATURE REVIEW

The concept of turbulence is widely discussed, and in a general sense, its effects and meaning are understood. Turbulence was discussed as early as the fifteenth century in the writings of Leonardo da Vinci; however, it wasn't until the nineteenth century when quantitative data were reported. The first reportings on turbulence were attempts to present the characteristics. Hagen and Poiseuille independently and qualitatively observed two modes of fluid flow in pipes, non-turbulent and turbulent (Rouse and Ince, 1963). The concept of an eddy diffusivity was introduced by Boussinesq (1877) to allow for turbulent effects analogous to Newton's law of fluid viscosity. With the aid of the Reynolds number advanced by Reynolds (1883) through an experimentally determined dimensionless ratio of fluid and system parameters, it was possible to tell when to expect turbulence in a flow system. Turbulence is said to exist in flow systems for which the Reynolds number has exceeded a critical value. Reynolds (1895) also recognized the statistical nature of turbulence. By

expressing the dynamic variables of the equation of motion as a mean value plus a deviation, and by averaging the terms formed in the equation of motion, the turbulence term

$$\tau_{ij}^{(t)} = -\rho \overline{u_i' u_j'} \quad (2.1)$$

was generated. This term can be interpreted as the turbulent stresses on an element of the fluid in addition to the stresses of pressure and viscous stress. Because Reynolds was the first to give the equation for turbulent flow, the turbulence stresses,  $\tau_{ij}^{(t)}$ , are often called Reynolds' stresses.

It was in the early twentieth century that useful and workable theories and models of turbulence appeared. It is obvious that, in the early days of turbulence investigations, when knowledge about and insight into the mechanism of turbulent fluid flow were rather poor, the turbulent processes could be studied only in a rather rough way. To describe the behavior of turbulent motion of a fluid near a wall, Prandtl (1904) proposed the boundary layer theory. The flow far from the wall is assumed uniform. Also among the theories arising from the early studies of turbulent flow are those based upon the concept of a "mixing length." These theories have

been the most fruitful, not so much because they describe the mechanism correctly, but because they have resulted in useful and practical semiempirical relationships. Taylor (1915), Schmidt (1917), Prandtl (1925), and Von Karman (1934) proposed mixing length theories for turbulence. The diffusive action of turbulence is considered to result in an eddy viscosity or eddy heat conductivity from which the distribution of mean values can be calculated, just as, in the kinetic theory of gases, molecular-transport processes result in a viscosity and heat conductivity. Basically, it is assumed in the mixing length theories, that each lump of fluid that is subjected to the turbulent motion may be considered as an individual entity. The properties of the lump are conserved during a certain time, i.e. over a certain distance. At the end of this time, the lump is assumed to mix with the surrounding fluid. These theories are purely phenomenological. Later studies have shown that the physical picture based upon the concept of a mixing length cannot be correct in all details. The mixing length theories still prove to be very useful to engineers.

The statistical theory of turbulence also began its existence in the early twentieth century. The concepts of the correlation coefficient, spectrum function, and local similarity which have proved so helpful in revealing the structure of turbulence are all a part of this theory.

Taylor (1921) advanced the concept of the Lagrangian correlation coefficient which provided a theoretical basis for turbulent diffusion. Richardson (1920, 1926) postulated the turbulence consists of a hierarchy of eddies. The energy is cascaded from the largest eddies to smaller and smaller eddies until the molecular level is reached at which point the energy is dissipated by viscous effects. Taylor (1935a,b,c,d) again considered the statistical nature of turbulence in a revised form and defined many of the properties of isotropic turbulence. This was followed by the Von Karman and Howarth (1938) demonstration of the tensor properties of the Eulerian correlation coefficient and their formulation of the relationship between the double and triple coefficients through the Navier-Stokes equations. At about the same time, Taylor (1938) showed the transform relationship between the correlation coefficient and the energy spectrum function. The Taylor concept of the energy spectrum has dominated turbulence research to the present. The first theory for the small scale structure of turbulence, presented by Kolmogorov (1941) and Obukhov (1941), served as the starting point of many investigations and led to general theories of spectral similarity such as those by Von Karman and Lin (1949) and Lin (1948). This theory predicts for any highly turbulent motion, the small scale

structure is isotropic which was empirically shown earlier by Richardson (1926).

The following publications, among others, present turbulence in general or some of its particular aspects: Prandtl and Tietjens (1934a,b), Goldstein (1938), Agostini and Bass (1950), Hopf (1952, 1957), Batchelor (1953), Frenkiel (1953), Sutton (1953), Batchelor and Townsend (1956), Corcoran et al. (1956), Opfell and Sage (1956), Townsend (1956), Hinze (1959), Lin (1959), Priestly (1959), Schlichting (1960), Lin (1961), Schubauer and Tchen (1961), Tatarski (1961), Favre (1962), Pasquill (1962), Lumley and Panofski (1964), Brodkey (1967), and Monin and Yaglom (1971). Papers considered classics on turbulence are collected by Goering (1958) and Friedlander and Topper (1961). The textbooks by Bird et al. (1960) and Brodkey (1967) also present sections on turbulence.

## 2.1 Dispersion of a Scalar Property in Turbulent Flow

Since turbulent fluid motion has an intrinsic random fluid motion, an inherent characteristic of turbulent flow is its dispersive action; accordingly, the dispersion process is more active in turbulent than in nonturbulent flow. It is not unusual then that most of the work on turbulence centers around its transport or dispersive characteristic. One of the most important analytical

inroads into the problems of turbulent dispersion was made by Taylor (1921). Taylor's work not only laid the groundwork for the Lagrangian study of turbulent dispersion but it also represented an initial step in the ideas essential to the development of a general statistical theory of turbulence. From this base, Richardson (1926), Kampé de Fériet (1939), Batchelor (1949, 1952, 1957), Taylor (1954), and Monin and Yaglom (1971) have successively expanded and deepened the theoretical foundation for understanding the statistical nature of turbulence as well as its transport processes.

### 2.1.1 Isotropic homogeneous flow

Consider a condition in which the turbulence in a fluid with no mean flow is uniformly distributed so that the average conditions of every point in the fluid are the same. The above fluid flow condition is that investigated by Taylor (1921). Within this flow field, Taylor analyzed the dispersion of a scalar property which may be associated with all or a fraction of the fluid particles. Because of the isotropy of the problem, only one direction of dispersion need be considered, say the  $x$  direction. By definition, the velocity of a fluid particle at time  $t$ ,  $V(t)$ , is

$$V(t) = \frac{d}{dt}x(t) \quad (2.2)$$

and its position at time  $t$ ,  $x(t)$ ,

$$x(t) = a + \int_0^t V(t_1) dt_1 \quad (2.3)$$

where  $a$  = position of dispersing particle at  $t = 0$ .

Let  $X'(t)$  be the displacement of the particle from  $a$ , then

$$X'(t) = x(t) - a. \quad (2.4)$$

Taylor further supposes that the statistical properties of  $V(t)$  are known, in particular the standard deviation of  $V(t)$ ,  $\langle V^2 \rangle$ ,<sup>1</sup> and the Lagrangian correlation coefficient,  $R^{(L)}(t)$ .  $R^{(L)}(t_1)$  is the correlation coefficient between the value of  $V$  for a particle at any instant, and the value of  $V$  for the same particle after an interval of time  $t_1$ , i.e.

$$R^{(L)}(t_1) = \frac{\langle V(t)V(t + t_1) \rangle}{\langle V^2(t) \rangle^{1/2} \langle V^2(t + t_1) \rangle^{1/2}} \quad (2.5)$$

It is also assumed the standard deviation is constant with time, so that

$$\langle V^2(t) \rangle = \langle V^2(t + t_1) \rangle = \langle V^2 \rangle \quad (2.6)$$

---

<sup>1</sup>The  $\langle \cdot \rangle$  indicates a statistical ensemble average.



then

$$R^{(L)}(t_1) = \frac{\langle V(t)V(t+t_1) \rangle}{\langle V^2 \rangle} . \quad (2.7)$$

One measure of the degree of dispersion is given by the variance of the displacement,  $\langle X'^2(t) \rangle$ . The rate of change in the variance can be expressed in terms of  $\langle V^2 \rangle$  and  $R^{(L)}(t_1)$  as follows:

$$\text{First } \frac{d}{dt} \langle X'^2(t) \rangle = 2 \langle X'(t) \frac{d}{dt} X'(t) \rangle = 2 \langle X'(t) V(t) \rangle \quad (2.8)$$

$$\text{and since } X'(t) = \int_{-t}^0 V(t+t_1) dt_1 \quad (2.9)$$

$$\text{then } \frac{d}{dt} \langle X'^2(t) \rangle = 2 \langle \int_{-t}^0 V(t+t_1) V(t) dt_1 \rangle \quad (2.10)$$

$$= 2 \int_{-t}^0 \langle V(t+t_1) V(t) \rangle dt_1 \quad (2.11)$$

$$= 2 \langle V^2 \rangle \int_{-t}^0 R^{(L)}(t_1) dt_1 . \quad (2.12)$$

For constant  $\langle V^2 \rangle$ ,  $R^{(L)}(t_1)$  is symmetric about zero, and therefore

$$\frac{d}{dt} \langle X'^2(t) \rangle = 2 \langle V^2 \rangle \int_0^t R^{(L)}(t_1) dt_1 . \quad (2.13)$$

Integrating Equation (2.13) yields

$$\langle X'^2(t) \rangle = 2\langle V^2 \rangle \int_0^t \int_0^{t_2} R^{(L)}(t_1) dt_1 dt_2. \quad (2.14)$$

Equation (2.14) reduces the problem of dispersion, in a simplified type of turbulent motion, to the consideration of a single quantity, the Lagrangian correlation coefficient,  $R^{(L)}(t)$ .

As mentioned above, an indication of the rate of dispersion is the rate of change in the variance. Taylor (1935a) explicitly recognized  $\langle V(t)X'(t) \rangle$  as the eddy diffusivity,  $E(t)$ , a turbulent transport property similar to the molecular diffusivity. The eddy diffusivity is also related to the Lagrangian correlation coefficient. From Equations (2.8) and (2.13)

$$E(t) = 2\langle V^2 \rangle \int_0^t R^{(L)}(t_1) dt_1. \quad (2.15)$$

Now consider the physical implications of (2.14) and (2.15). When  $t$  is so small that  $R^{(L)}(t)$  does not differ appreciably from 1, then

$$\langle X'^2(t) \rangle = \langle V^2 \rangle t^2 \quad (2.16)$$

and

$$E(t) = 2\langle V^2 \rangle t. \quad (2.17)$$

Looking further, as  $t$  becomes large

$$R^{(L)}(t) \rightarrow 0, \quad (2.18)$$

$$\langle X'^2(t) \rangle \propto t \quad (2.19)$$

and

$$E(t) \rightarrow \text{constant}. \quad (2.20)$$

Defining a Lagrangian integral time scale as

$$T_L = \int_0^{T_1} R^{(L)}(t_1) dt_1 \quad (2.21)$$

where  $R^{(L)}(t) = 0$  for  $t > T_1$ , the eddy diffusivity for large time can be expressed as

$$E_\infty = \langle V^2 \rangle T_L. \quad (2.22)$$

$T_L$  is considered a measure of the average longest time during which a particle persists in a motion in a given direction. Also a Lagrangian integral length scale may be defined as

$$\Lambda_L = \langle V^2 \rangle^{1/2} T_L \quad (2.23)$$

which leads to

$$E_\infty = \langle V^2 \rangle^{1/2} \Lambda_L. \quad (2.24)$$

This result is analogous to that obtained from the kinetic theory of gases for the molecular diffusivity. It is also consistent with Prandtl's mixing-length theory (Prandtl, 1925); however, it is obtained without having to depend on the idea of mixture by subdivision and ultimate molecular diffusion.

A Lagrangian micro time scale may also be defined (Taylor, 1935a) as

$$\frac{1}{\tau_L^2} = -\frac{1}{2} \frac{d^2}{dt^2} R^{(L)}(t) \Big|_{t=0} . \quad (2.25)$$

Physically, this time scale is taken as a measure of the time duration of the smallest eddies which are responsible for energy dissipation.

### 2.1.2 Anisotropic homogeneous flow

#### 2.1.2.1 Single-particle dispersion

Batchelor (1949) investigated the three-dimensional homogeneous turbulent flow field. Even though Batchelor started with a generalization of Taylor's (1921) single-particle dispersion which was a Lagrangian analysis, Batchelor's final results were Eulerian. The Lagrangian to Eulerian transformation was through probability arguments and some simplifying assumptions about the statistical nature of homogeneous turbulence.

To generalize Taylor's analysis to three dimensions, let  $X_i'(t)$  be the  $i$ -th component of the vector displacement of a fluid particle. The time rate of change of the covariance of two displacement components  $X_i'(t)$  and  $X_j'(t)$  is written as

$$\frac{d}{dt} \langle X_i'(t) X_j'(t) \rangle = \langle X_i'(t) V_j'(t) \rangle + \langle V_i'(t) X_j'(t) \rangle \quad (2.26)$$

or

$$\frac{d}{dt} \langle X_i'(t) X_j'(t) \rangle = \int_0^t \langle V_i'(t_1) V_j'(t) \rangle dt_1 + \int_0^t \langle V_i'(t) V_j'(t_1) \rangle dt_1 \quad (2.27)$$

Using tensor notation, define the second order tensor  $\underline{S}$  as follows:

$$S_{ij}(t-t_1) = \langle V_i'(t_1) V_j'(t) \rangle \quad (2.28)$$

If the process is assumed to be a time-stationary process, then the elements of  $\underline{S}$  depend only on the elapsed time  $\xi = (t - t_1)$ . Now Equation (2.27) can be written

$$\frac{d}{dt} \langle X_i'(t) X_j'(t) \rangle = \int_0^t (S_{ij}(\xi) + S_{ji}(\xi)) d\xi \quad (2.29)$$

and when integrated yields

$$\langle X_i'(t) X_j'(t) \rangle = \int_0^t \int_0^{t_1} (S_{ij}(\xi) + S_{ji}(\xi)) d\xi dt_1 \quad (2.30)$$

As shown by Kampé de Fériet (1939) in a study of stationary random functions, a change of variable in Equation (2.30) and a partial integration can be made to give

$$\langle X_i'(t) X_j'(t) \rangle = \int_0^t (t - \xi) (S_{ij}(\xi) + S_{ji}(\xi)) d\xi. \quad (2.31)$$

The above results can be expressed in terms of Lagrangian velocity correlation coefficients. Defining a generalized coefficient as

$$R_{ij}^{(L)}(t - t_1) = \frac{\langle V_i'(t_1) V_j'(t) \rangle}{\langle V_i'^2(t_1) \rangle^{1/2} \langle V_j'^2(t) \rangle^{1/2}} \quad (2.32)$$

$$= \frac{S_{ij}(t - t_1)}{\langle V_i'^2(t_1) \rangle^{1/2} \langle V_j'^2(t) \rangle^{1/2}} \quad (2.33)$$

and since the turbulence is homogeneous and stationary

$$\langle V_i'^2(t) \rangle = \langle V_i'^2(t_1) \rangle = \langle V_i'^2 \rangle \quad (2.34)$$

then Equations (2.29) and (2.31) become

$$\frac{d}{dt} \langle X_i'(t) X_j'(t) \rangle = \langle V_i'^2 \rangle^{1/2} \langle V_j'^2 \rangle^{1/2} \int_0^t (R_{ij}^{(L)}(\xi) + R_{ji}^{(L)}(\xi)) d\xi \quad (2.35)$$

and

$$\langle X_i'(t) X_j'(t) \rangle = \langle V_i'^2 \rangle^{1/2} \langle V_j'^2 \rangle^{1/2} \int_0^t (t - \xi) (R_{ij}^{(L)}(\xi) + R_{ji}^{(L)}(\xi)) d\xi. \quad (2.36)$$

The probability distribution of  $X_i(t)$  is intimately connected with the spatial distribution of the mean concentration of the property transported by the fluid particle. From this viewpoint Batchelor considers a volume of marked fluid particles with a probability that a fluid point defined by the position vector  $\underline{X}$  lies within the marked fluid at time  $t$ . Note that  $P(\underline{X}, 0)$  is unity or zero depending on whether the point  $\underline{X}$  lies within or outside the initial volume of marked fluid.

Now by using the probability associated with the dispersion of a fluid particle, the probability density function,  $P(\underline{X}, t)$ , can be related to its initial p.d.f.,  $P(\underline{X}, 0)$ . Each particle diffuses independently of its neighbors. Representing by  $Q(\underline{X}, t)$  the p.d.f. of the vector displacement  $\underline{X}$  of any fluid particle during a time  $t$ , then  $Q(\underline{X}, t)dv(\underline{X})$  is the probability that a fluid particle lies within a volume element  $dv(\underline{X})$  at time  $t$ . Furthermore, the p.d.f.,  $P(\underline{X}, t)$ , for a finite volume of marked fluid is

$$P(\underline{X}, t) = \int P(\underline{X}', 0) Q(\underline{X} - \underline{X}', t) dv(\underline{X}'). \quad (2.37)$$

If the form of  $Q(\underline{X}, t)$  is known, the solution for  $P(\underline{X}, t)$  can be obtained from (2.37). The experimental results of Schubauer (1935), Collis (1948), and Kalinske and Pien (1944) indicate that the separate p.d.f.'s of the

$X_i$ 's are normal for all values of  $t$ . The above data are not sufficient to define the p.d.f.  $Q(\underline{X}, t)$  in all its generality. However, in order to make the analysis as general as possible, Batchelor assumed the p.d.f.'s of the  $X_i$ 's to be jointly as well as separately normal. In this case it is known that the appropriate form of  $Q(\underline{X}, t)$  is

$$Q(\underline{X}, t) = \frac{1/3}{(8\pi^3\Omega)^{1/2}} \exp\left(-\frac{\omega_{rs} X_r X_s}{2\Omega}\right) \quad (2.38)$$

where

$$\Omega = \begin{vmatrix} \langle X_1^2 \rangle & \langle X_1 X_2 \rangle & \langle X_1 X_3 \rangle \\ \langle X_2 X_1 \rangle & \langle X_2^2 \rangle & \langle X_2 X_3 \rangle \\ \langle X_3 X_1 \rangle & \langle X_3 X_2 \rangle & \langle X_3^2 \rangle \end{vmatrix} \quad (2.39)$$

$\omega_{rs}$  is the co-factor of the typical element  $\Omega_{rs}$  of the determinant  $\Omega$ , and repeated suffixes implies summation over values 1, 2, and 3. Thus Equation (2.37) becomes

$$P(\underline{X}, t) = \frac{P(\underline{X}^0, 0)}{(8\pi^3\Omega)^{1/2}} \int \exp\left(-\frac{1}{2} \omega_{rr} (X_r X_r'') (X_s - X_s'')\right) dv(\underline{X}''). \quad (2.40)$$

Furthermore, Equation (2.40) is a solution to the diffusion equation,

$$\frac{\partial P(\underline{X}, t)}{\partial t} = E_{ij} \frac{\partial^2 P(\underline{X}, t)}{\partial X_i \partial X_j}, \quad (2.41)$$



provided the diffusion coefficient tensor  $\underline{E}$  is such as to satisfy the equations

$$E_{ij} \omega_{ij} = \frac{1}{2} \frac{d\Omega}{dt} \quad (2.42)$$

$$E_{ij} \omega_{ir} \omega_{js} = -\frac{1}{2} \Omega^2 \frac{d(\omega_{rs}/\Omega)}{dt} . \quad (2.43)$$

Remembering that by definition

$$\Omega_{ir} \omega_{jr} = \Omega \delta_{ij}$$

where  $\delta_{ij}$  is the delta function, then Equation (2.43) can be reduced to

$$E_{ij} = \frac{1}{2} \frac{d\Omega_{ij}}{dt} = \frac{1}{2} \frac{d}{dt} \langle x_i(t) x_j(t) \rangle \quad (2.44)$$

which is also consistent with (2.42).

Thus the diffusion Equation (2.41) provides a description of the turbulent dispersion process when Eulerian analysis is used, provided the p.d.f.'s of  $X_1$ ,  $X_2$ , and  $X_3$  are jointly as well as separately normal. At present, sufficient information is not available to support the above normality hypothesis rigorously; however, it is a fortunate discovery that a single differential equation describes the homogeneous turbulent dispersion

process with high accuracy. Even though this hypothesis is presently (Monin and Yaglom, 1971) thought to be exact or nearly exact, Equation (2.44) should be treated as a phenomenological and not a fundamental law of turbulent dispersion.

It is important to notice that the tensor coefficient  $E_{ij}$  is a function of time, which is in contrast to the molecular diffusion coefficient, and that Equation (2.44) is valid at all times. The tensor  $\underline{E}$  is a generalization of the eddy diffusivity coefficient. From Equations (2.29) and (2.35) the generalized eddy diffusivity coefficient can be expressed as

$$E_{ij}(t) = \frac{1}{2} \int_0^t (S_{ij}(\xi) + S_{ji}(\xi)) d\xi \quad (2.45)$$

or in terms of the Lagrangian velocity correlation coefficient

$$E_{ij}(t) = \frac{1}{2} \langle V_i^2 \rangle^{1/2} \langle V_j^2 \rangle^{1/2} \quad (2.46)$$

$$\int_0^t (R_{ij}^{(L)}(\xi) + R_{ji}^{(L)}(\xi)) d\xi.$$

In addition, a generalized Lagrangian integral time scale may be defined as

$$T_{ij} = \int_0^\infty (R_{ij}^{(L)}(\xi) + R_{ji}^{(L)}(\xi)) d\xi. \quad (2.47)$$

In view of (2.46), for large times the generalized eddy diffusivity coefficient can be expressed

$$(E_{\infty})_{ij} = \frac{1}{2} \langle v_i'^2 \rangle^{1/2} \langle v_j'^2 \rangle^{1/2} T_{ij} \quad (2.48)$$

and one may easily generalize Boussinesq's phenomenological hypothesis as

$$\underline{F}(t) = -\underline{E}_{\infty} \cdot \nabla \Gamma \quad (2.49)$$

where  $\Gamma$  is any scalar and  $\underline{F}(t)$  is the turbulent flux.

The limiting cases for the fluid element displacement covariance and eddy diffusivity are given below. For small  $t$

$$\langle x_i'(t) x_j'(t) \rangle \approx \langle v_i'^2 \rangle^{1/2} \langle v_j'^2 \rangle^{1/2} t^2 \quad (2.50)$$

and  $E_{ij}(t)$  is proportional to  $t$ . For large  $t$

$$\langle x_i'(t) x_j'(t) \rangle = \langle v_i'^2 \rangle^{1/2} \langle v_j'^2 \rangle^{1/2} T_{ij} t + \text{constant} \quad (2.51)$$

and  $E_{ij}(t)$  is constant.

### 2.1.2.2 Two-particle dispersion

To thoroughly describe turbulent dispersion in a homogeneous flow field, all  $n$ -particle interactions should

be included in the statistical analysis. The single-particle dispersion problem has been discussed in the previous section, and the two-particle dispersion is discussed in this section. Due to increasing mathematical difficulties, the analysis of the other  $n$ -particle interactions have not been made. Even though a complete statistical determination of turbulent dispersion is desirable, significant and workable models based on the presently available works have been obtained.

As in the single-particle studies, the two-particle analysis was first made for one-dimensional isotropic case. This work was done by Richardson (1926). Batchelor (1952) extended the two-particle analysis to the general homogeneous situation by investigating the relative displacement and relative velocity of two fluid particles. Batchelor shows that even though the flow field may be assumed stationary, the relative velocity covariance,  $\langle v_i(t)v_j(t) \rangle$ , is not stationary; it depends on the actual elapsed time  $t-t_0$ . The asymptotic form of the covariance is related to Eulerian correlations as follows

$$\langle v_i(t)v_j(t) \rangle \rightarrow 2\langle u'_i(t)u'_j(t) \rangle, \quad (2.52)$$

and the relative displacement asymptotic form is related to the single-particle displacement as

$$\langle Y_i(t)Y_j(t) \rangle \rightarrow 2\langle X_i(t)X_j(t) \rangle. \quad (2.53)$$

Furthermore, under the normality assumption for the joint probability distribution of the components of  $\underline{Y}(t)$ , the conditional p.d.f. of the separation of two fluid particles satisfies the diffusion equation,

$$\frac{\partial}{\partial t} F(\underline{Y}, t | \underline{Y}_0, t_0) = \mathcal{D}_{ij}(t) \frac{\partial^2}{\partial Y_i \partial Y_j} F(\underline{Y}, t | \underline{Y}_0, t_0) \quad (2.54)$$

where the relative dispersion tensor is determined by

$$\mathcal{D}_{ij}(t) = \frac{1}{2} \frac{\partial}{\partial t} (\langle Y_i(t) Y_j(t) \rangle - \langle Y_i(t_0) \rangle \langle Y_j(t_0) \rangle) \quad (2.55)$$

or

$$\mathcal{D}_{ij}(t) = \frac{1}{2} \int_{t_0}^t (\langle v_i(t) v_j(t_1) \rangle + \langle v_i(t_1) v_j(t) \rangle) dt_1 \quad (2.56)$$

Unfortunately, the diffusion equation does not apply to the p.d.f. of the relative concentration.

### 2.1.3 Shear flow

The number of contributions in which there is a theory developed on shear turbulence is very small when compared to those contributions to isotropic turbulence. Obviously this is because of the extreme complexity of the problems encountered. Though the results are still very meager, a few features of actual shear flow have been studied and give some understanding of the nature of this type turbulence.

Batchelor (1957) did some work in the area to free turbulent shear flows. He extended the single-particle analysis to the dispersion of a scalar in nonhomogeneous, self-preserving turbulent flows such as exist in steady turbulent jets, wakes, and mixing layers. Flow fields, which are self-preserving, retain their structure with elapsed time since only changes in the length, time, and velocity scales occur. Using this property of the flow field, Batchelor transformed this nonstationary dispersion problem into a stationary one by an appropriate transformation of the Lagrangian velocity of the fluid particle. An important result is that the lateral and longitudinal dispersions, as functions of time, are proportional to the average width of the shear layers at identical times. Also, the time rate of change of the dispersion becomes constant for large times. No convenient diffusion type equation was found applicable as for the homogeneous turbulence case.

The study of turbulent shear flow has been mainly directed at correlations between velocities and their derivatives. One of the most reported or discussed studies of this type is that of Laufer (1954). Laufer studied the fully developed turbulent shear flow in a large pipe. He not only investigated the second and third order correlations but some fourth order correlations as well. The importance of a detailed knowledge of flow conditions near

the wall is clearly suggested. The various turbulent energy rates, such as production, diffusion, and dissipation, were shown to reach a maximum at the edge of the viscous sublayer. It was also found that kinetic energy is transferred away from the edge of the viscous sublayer while an equally strong movement of pressure energy is transferred toward the sublayer.

#### 2.1.4 Interaction of molecular and turbulent dispersion

The effects of turbulent dispersion and molecular diffusion are not easily separated. Taylor (1935) suggested that the two are statistically independent, so that the variances due to these two effects are additive. Townsend (1954) and Batchelor and Townsend (1956) showed that the two effects are synergistic in a homogeneous turbulent field. They concluded that for short times, the dispersion of a scalar is accelerated since the stretching and rotational effects of the turbulence would enhance the molecular diffusion. It was decided that the total transport of a scalar depends on the interaction of the two modes of transport in a dependent fashion. Townsend confirmed his predictions experimentally. He studied the heat transport behind a source in homogeneous turbulence, and in addition, indicated adjustments were needed on Uberoi and Corrsin's (1953) studies of a similar transport problem. The adjustments had no

noticeable effect on the asymptotic eddy diffusivity obtained by Uberoi and Corrsin. Mickelsen (1960) also found the accelerated molecular diffusion is negligible for large times in his experimental measurements of mass transport in the flow field.

Later, Saffman (1960, 1962) added to the analysis of Townsend and Batchelor. He pointed out that the molecular diffusion reduced the turbulent dispersion since the scalar within the original fluid particle is diluted by the molecular diffusion. However the two effects, when not negligibly small, tend to balance themselves. Saffman (1960) and Okubo (1967) have shown that the interaction reduces the dispersion relative to the origin from the value it would have had if the two processes had been independent and additive. Saffman claimed that his predictions were in qualitative agreement with the measurements of Mickelsen (1960). Both Saffman and Mickelsen suggested that further experimentation was needed to resolve this problem for large times. In general the small absolute value of the molecular diffusion relative to the turbulent dispersion allows one to neglect the purely molecular diffusion. Monin and Yaglom (1971) present an excellent survey plus supplementary results covering this area of study.



## 2.2 Lagrangian Characteristics of Turbulent Flow

The fundamental analytical approaches of Taylor (1921) and Batchelor (1949) are basically derived from the Lagrangian statistics of a turbulent homogeneous flow field. Both experimental and numerical efforts have been made to obtain the Lagrangian characteristics pertinent to these studies. Ideally, the statistics should be generated from numerous individual fluid point paths. Numerically, the generation of fluid point paths is straightforward once the statistical parameters and model have been decided upon. However, to experimentally track or follow fluid particles would be a very difficult if not impossible task. Approximate Lagrangian statistics have been obtained from experiments which make possible the visualization of the paths of small particles suspended in a turbulent flow field. These small particles consist of a separate phase and retain their identity, and their paths are thought to closely approximate the paths of fluid points. In addition, attempts have been made to extract Lagrangian statistics from the concentration and temperature profiles generated by the turbulent dispersion of mass and heat, respectively.

### 2.2.1 Lagrangian numerical simulations

Several different stochastic models of turbulent dispersion have been used to obtain the different Lagrangian

statistics which are of interest. Because of the mathematical difficulties and the number of repetitive calculations involved in a numerical simulation, the digital computer is required to expedite the solution. The capacity and speed of the computer used often limits the complexity and size of the simulation to be made.

Using a Monte Carlo procedure, Kirmse (1964) simulated turbulent dispersion in pressure-driven nonhomogeneous pipe flow. A proportionality parameter was used to relate the variance of the Lagrangian acceleration,  $\sigma_{\dot{v}}$ , to measurable Eulerian variances in the expression

$$\sigma_{\dot{v}} = B\sigma_u\sigma_{\dot{u}} \quad (2.57)$$

where  $\sigma_u$  = variance of Eulerian velocity

$\sigma_{\dot{u}}$  = variance of Eulerian acceleration.

The parameter "B" is similar to Mickelsen's (1955) Eulerian to Lagrangian transformation parameter. By trial and error the parameter "B" was adjusted until concentration profiles obtained in the simulation coincided with available experimental data. From a simple random walk model, Patterson and Corrsin (1966) simulated a one-dimensional dispersion process. A homogeneous velocity field was assumed and both Lagrangian and Eulerian temporal velocity correlations were

obtained. The model generated results which appear to represent the expected turbulent behavior.

Single-particle paths and their Lagrangian statistics were simulated by Kraichnan (1970) using a normal multivariate velocity distribution. An incompressible, stationary, isotropic flow field was assumed. The velocity field was generated from a set of Fourier components obtained from Eulerian correlations and spectra. Dispersions, velocity correlations, and eddy diffusivities were computed using the simulation. The results were consistent with Taylor's earlier work.

Deardorff and Peskin (1970) generated single- and double-particle trajectories using a three-dimensional numerical model of shear flow within a channel. The study was limited to regions outside of the viscous sublayer for a large Reynolds' number. The model used was developed by Deardorff (1970) and was based on averaging the Navier-Stokes equations over grid volumes by the method of Reynolds (Reynolds, 1895; Lamb, 1932). After generating a fully developed velocity field, forty-eight fluid particles at different initial points within the turbulent core were selected and followed for two hundred time steps. A new set of fluid particles was then selected with the same initial starting points and the procedure repeated. An ensemble of ten such sets of forty-eight particles was used to compute the

Lagrangian temporal mean square displacements and velocity autocorrelation coefficients for single-particle tracks. The decay of the two-particle velocity correlation coefficients toward zero was very slow; and consequently, the two-particle mean square separation did not reach the asymptotic value of twice the single-particle mean square displacement predicted by Batchelor (1952). The Lagrangian time macroscales of the two-particle correlation were five to twenty-five times greater than the corresponding single-particle macroscales.

A numerical stochastic model depending on only three parameters was proposed by Sullivan (1971) for fully developed turbulent flow in an open channel. The two-dimensional model uses only the bulk velocity,  $u_b$ , the local Eulerian space macroscale,  $\Lambda_E$ , and the standard deviation of the local lateral velocity fluctuations,  $\sigma_{u_y}$ . With an initial lateral velocity equal to the local standard deviation, a fluid particle is allowed to retain its velocity for a time period of

$$\tau = \frac{\Lambda_E(y_0)}{\sigma_{u_y}(y_0)} \quad . \quad (2.58)$$

The longitudinal and lateral displacements at the end of the time period  $\tau$  are

$$\Delta x = \frac{\Lambda_E}{\sigma_{v_y}} \int_{y(t_k)}^{y(t_k)+t} u_b dy \quad (2.59)$$

and

$$\Delta y = \pm \frac{\Lambda_E \sigma_{u_y}}{\sigma_{u_y}} = \pm \Lambda_E \quad (2.60)$$

respectively, where

$$t_k = (k - 1)\tau. \quad (2.61)$$

From the new position, the values of  $u_b$ ,  $\Lambda_E$ , and  $\sigma_{u_y}$  are corrected, and the sign of the next lateral displacement is randomly assigned. By repeating this procedure, particle trajectories of any time length could be generated. Sullivan generated one thousand particle tracks for ten initial lateral points distributed evenly on the height of the channel. Ensemble averages of the longitudinal concentration profiles for given elapsed times and the temporal Lagrangian velocity autocorrelation coefficients were obtained. In view of the simplicity of the simulation, the agreement with experimental data is surprisingly good.

Gielow (1972) numerically studied shear flow between parallel plates using a stochastic model based on Kimse's (1964) model. Also by using the mean Lagrangian acceleration obtained from the Reynolds' stresses, deterministic velocity and position loci were found. By imposing the

condition that these deterministic loci are closed curves in a coordinate system connected by the local mean velocity, relationships were obtained to supplement and to check the consistency of available experimental data used in the stochastic model. In the model, the time derivative of the velocity signal was chosen from a probability distribution and integrated to give the velocity. Statistical and spectral analyses of the simulated velocity records were made to show the suitability of the model. Lagrangian time correlations of the nonhomogeneous pressure-drive flow were computed and compared to the same correlations for homogeneous flow computed from the stochastic model. Because of the confining walls the eddy diffusivity obtained from the Lagrangian correlations was clearly time-dependent. The model was also used to simulate the turbulent transport of a scalar such as heat or mass. The results for the steady state simulations were consistent with available experimental data.

#### 2.2.2 Lagrangian experimental studies

The Lagrangian characteristics of fluid flow have been investigated experimentally by many researchers. The experiments performed in this area used "tagged" fluid particles to observe both microscopic and macroscopic turbulent activity. "Tagging" is accomplished by the release of a visible foreign material into the flowing fluid. The bulk of the experimental investigations have

been macroscopic in nature, i.e. due to the type experiment or objectives, the attention was focused on the overall effect of the large scale nature of the turbulent activity. The microscopic type of experiments deal mainly with the individual fluid particles and their paths through the flow field.

Hagen, in 1854, appears to be the first to report the use of this "tagging" technique to study fluid particle motion (Rouse and Ince, 1963). By observing the behavior of suspended particles, Hagen discovered the existence of two different modes of flow. Reynolds (1883) also, in his well-known experiments using dye injection, demonstrated vividly the gross Lagrangian characteristic of a flowing fluid. Prandtl and Tietjens (1934b) discussed and presented results of their investigations using visual techniques for liquid and gas flows.

In confined flows, the turbulent activity has been visually observed in all regions of the flow field, the core region as well as the wall region. Turbulence has even been observed inside the viscous sublayer using the particle "tagging" technique. Fage and Townend (1932) and Fage (1936), using a microscope to view suspended particles in a confined turbulent fluid, observed significant turbulence in the viscous sublayer. In addition to observing the qualitative nature of the turbulence, Fage

and Townend made quantitative computations of local turbulent intensities. More recently, Corino and Brodkey (1969) visually observed the turbulent fluid motions very near a pipe wall, including the viscous sublayer, using a high-speed movie camera moving with the flow. This study was made in an effort to establish a physical picture which related the turbulent activities near the wall to the generation of turbulence and the turbulent transport processes. With an apparent consistent average period, fluid elements were observed to be ejected outward into the turbulent core from a thin region adjacent to the viscous sublayer. These ejections and resulting fluctuations were the most important feature of the wall region and were believed to be a factor in the generation and maintenance of turbulence. Other studies of this type have been done by Kline and Runstadler (1959), Nedderman (1961), Kim et al. (1971), and Grass (1971).

Very few Lagrangian experiments of the microscopic nature have been performed. The reason for the lack of experimental work in this area is most likely because of the laborious and tedious chore of following the particles. Even of the experiments done, the main interest was in the Lagrangian correlation of the velocity of a solid particle. The limiting case of the particle velocity correlation is the Lagrangian correlation function discussed by Taylor



(1921). Studies of the movements of neutrally buoyant particles were made by Vanoni and Brooks (1955) and later extended and improved by Frenzen (1963). Droplets of nitrobenzene and olive oil were injected into the grid-generated turbulence of a water tunnel. They made measurements of successive displacements of the particles and adjusted the velocity data to account for decay of the turbulent intensity. The Lagrangian velocity autocorrelation function was computed from the corrected data. Kennedy (1965) measured the dispersion of 1250-micron soap bubbles and 700-micron and 900-micron polystyrene beads in the grid-generated turbulence of a vertical wind tunnel. Kennedy did not measure particle velocities directly, but inferred them from the initial slope of the dispersion curve. Snyder and Lumley (1971) made some experimental measurements of the particle velocity autocorrelation function. Several types of particles were used in dispersion experiments within a wind tunnel designed after Kennedy's. Within the experimental error, the particle velocity correlations coincided with the Eulerian spatial correlations, when the separation was made dimensionless by dividing by the integral scales. Data generated using hollow glass beads, were thought to be a good estimate of the Lagrangian fluid properties. The Lagrangian time integral scale was found to be approximated by  $\Lambda_E/u'$ , where

$\Lambda_E$  is the Eulerian integral scale and  $u'$  is the turbulent intensity.

### 2.2.3 Eulerian-Lagrangian transformation

A fundamentally correct theory of turbulent dispersion of fluid points is that of Taylor (1921). The major reason this theory has not been put to common use is that it is formulated in Lagrangian terms rather than the much more easily measured Eulerian variables. As was indicated in the previous section, quantitative measurements of the Lagrangian characteristics are laborious and tedious, particularly since reliable ensemble averages required that numerous individual particle paths be investigated. Under these circumstances it is advantageous to develop a theoretical, or empirical if need be, relationship between the Lagrangian variables and the more easily measured Eulerian variables. As a start in this direction, Taylor (1938) proposed that the changes at a fixed Eulerian point are simply due to the passage of an unchanging pattern of turbulent motion through that point. This concept has been designated as frozen turbulence or Taylor's hypothesis. An immediate result of this hypothesis is that time is given by the displacement divided by the mean velocity,  $-x/U$ , and in derivative form

$$\frac{\partial}{\partial x} = - \frac{1}{\langle U \rangle} \frac{\partial}{\partial t} . \quad (2.62)$$

Taylor considered the hypothesis applicable only to uniform low intensity turbulence. Lin (1953) and Uberoi and Corrsin (1953) tested more fully the conditions under which Taylor's hypothesis is useful. For isotropic turbulence and large Reynolds' numbers, Lin found the accuracy of Taylor's hypothesis can be estimated by

$$\frac{\langle (\frac{dU}{dt})^2 \rangle}{\langle U \rangle^2 \langle (\frac{\partial U}{\partial x})^2 \rangle} \approx 5 \frac{\langle u'^2 \rangle}{\langle U \rangle^2} \quad . \quad (2.63)$$

For shear flow, the validity of the concept is less clear. Laufer (1954) and others indicated experimentally the hypothesis can be extended to fully developed shear flow outside the viscous sublayer. An important application of Taylor's hypothesis permits the analysis of Eulerian data obtained from a truly Lagrangian type dispersion experiment. Numerous Lagrangian studies have been made of turbulent dispersion from continuous sources in uniform turbulence. By applying Taylor's hypothesis to the above type experiments in which Eulerian measurements are obtained at fixed points downstream of the source, temporal mean functions can be approximated. Each fixed position is assumed to correspond to a certain elapsed time of a fluid particle flight from the originating source.

Taylor's (1921) theory reduces the dispersion problem to that of determining the Lagrangian autocorrelation

function. The Lagrangian velocity correlation may be extracted from the mean square displacement function by a double differentiation as suggested by Equation (2.14). In experiments in which the fluid particles were not followed individually, the autocorrelation function, if obtained, was found through the questionable step of doubly differentiating the second moment of the distribution of particles. Graphical differentiation is always difficult, but the double-differentiation of an empirical curve, even one in which the scatter of the data is seemingly small, can give results which vary widely from one analyst to another. Burgers (1951) proposed that the Lagrangian velocity correlation may be approximated from an easily measured Eulerian correlation as follows

$$\langle \left( \frac{\partial V}{\partial t} \right)^2 \rangle = \langle U \rangle^2 \langle \left( \frac{\partial u}{\partial x} \right)^2 \rangle . \quad (2.64)$$

It has been suggested by several authors (Mickelson, 1955; Baldwin and Walsh, 1961; Hay and Pasquill, 1959; Kirmse, 1964) that Lagrangian and Eulerian velocity correlations are similar in shape and one can be used to generate the other by scaling their arguments. For homogeneous turbulence, Mickelsen (1955) investigated the similarity between the Lagrangian velocity autocorrelation function and the Eulerian longitudinal velocity correlation. Assuming a proportionality between the Lagrangian and the Eulerian integral length scales; i.e.

$$\Lambda_E = B\Lambda_L \quad (2.65)$$

and through the definitions of the two length scales, it was derived that

$$\zeta = B\langle u^2 \rangle^{1/2} \tau \quad (2.66)$$

where

$\zeta$  is the separation distance between velocity vectors in the Eulerian correlation, and

$\tau$  is the elapsed time for the Lagrangian correlation.

Kirmse (1964) further deduced that the above implies

$$\sigma_v = B\sigma_u \sigma_u \quad (2.67)$$

The value of "B" was determined by Mickelsen to be approximately 0.6 for relative turbulent intensities of about 0.03. This value of "B" was determined by comparing the doubly integrated Eulerian longitudinal correlation evaluated from hot-wire anemometry data with the corresponding value of the Lagrangian turbulent spreading coefficient evaluated from data collected on the dispersion of helium into air. Baldwin and Mickelsen (1963) used the same value of "B" to fit heat dispersion data. Hay and Pasquill (1959) related the Lagrangian velocity correlation to the Eulerian time correlation by assuming a proportionality of the time arguments, i.e.

$$\tau = \beta t \quad (2.68)$$

where  $\tau$  is the Lagrangian time and

$t$  is the Eulerian time.

The constant  $\beta$  was evaluated from experimental data of the integral of the Eulerian time correlation and the Lagrangian dispersion in medium scale atmospheric turbulence. At a relative turbulent intensity of about 0.14,  $\beta$  varied from 1.1 to 8.5 in an uncorrelated fashion. Baldwin and Walsh (1961) also investigated the similarity in the Eulerian and Lagrangian correlation coefficients. They assumed the relationship

$$\zeta = \frac{\langle u'^2 \rangle^{1/2} \tau}{K_{BW}} . \quad (2.69)$$

By an incremental integration technique applied to both heat and mass dispersion data, a twofold variation of the empirical factor  $K_{BW}$  with  $\tau$  and turbulent intensity was observed. Applying Taylor's hypothesis,  $\beta$  can be related to  $K_{BW}$  as follows

$$\beta = \frac{\langle U \rangle}{\langle u'^2 \rangle^{1/2}} K_{BW} . \quad (2.70)$$

Philip (1967) theoretically developed a relationship for the ratio of the Eulerian and Lagrangian integral time scales for homogeneous, isotropic, stationary turbulence. The experimental results already mentioned as well as that of Angell (1964a, b) agree with Philip's results.

A general treatment and review of the theoretical considerations of the relationship between the Eulerian

and the Lagrangian velocity correlation functions can be found in Hinze (1959), Brodkey (1967), and Monin and Yaglom (1971).

### 2.3 Experimental Determination of Eddy Diffusivities

From the work of Taylor (1921) and Batchelor (1949), it was shown that turbulent dispersion has its grass roots implanted in the Lagrangian aspects of the flow field. Unfortunately, direct measurement of the physically appealing Lagrangian characteristics is a laborious and awkward task. The overwhelming majority of the experimental data available on turbulent dispersion is of the more easily measured Eulerian type. As was seen in the previous section there is no completely satisfactory Eulerian to Lagrangian transformation scheme. At this juncture there are two principal methods that may be used to analyze the Eulerian measurements of turbulent dispersion. One method is to assume the frozen turbulence hypothesis and use Taylor's analysis. The second method is to retain the Eulerian description of the phenomenon with the aid of Boussinesq's hypothesis. In either case the eddy diffusivity seems to be the common denominator of the two approaches. The concept of the eddy diffusivity is a natural extension of the more fundamental concept of the molecular diffusivity and was introduced as a consequence of the phenomenological approach to the dispersion

of a scalar in turbulent fluids. Boussinesq (1877) presented an essay on the theory of flowing water, followed by a book (Boussinesq, 1897), in which he discusses the flux of momentum in open channels. Generalizing Newton's law of viscosity, he developed the concept of an effective momentum diffusivity, later to be referred to as the eddy diffusivity. Numerous measurements of the eddy diffusivity for heat and mass transfer have been made for systems having various geometries and a wide range of Reynolds numbers. Subbotin et al. (1966) correlated numerous data on the radial component of the thermal eddy diffusivity and found an empirical relationship that fits very well the data for Prandtl numbers from zero to 10, and for Reynolds numbers ranging from 10,000 to 500,000. The relationship depends only on the Reynolds number and the dimensionless radial position. Simplifications can be imposed for the core region of the flow. General discussions of the eddy diffusivity can be found in Hinze (1959), Brodkey (1967), and Monin and Yaglom (1971).

### 2.3.1 Determination by Lagrangian analysis

Many Lagrangian type experiments have been performed in which only Eulerian type measurements have been made. In these experiments heat or mass was dispersed from different source configurations by the turbulent fluid action.



Subsequent temperature and concentration profiles, respectively, were measured at several stations located downstream from the source. Then by assuming the frozen turbulence hypothesis and applying Taylor's (1921) Lagrangian analysis to the mean square displacements obtained from the profiles, certain Lagrangian statistics were computed.

The simplest source configuration is of course the point source. This configuration is most adaptable to mass transfer experiments. Towle and Sherwood (1939) studied the turbulent dispersion of carbon dioxide and hydrogen from an injection point within the turbulent core of pipe flow using air as the carrier gas. By measuring concentrations at several points downstream from the injection point, the eddy diffusivities were computed for a Reynolds' number range from 12,000 to 180,000. The eddy diffusivity was found to increase with Reynolds' number and to asymptotically approach a constant value. Kalinske and Pien (1944) obtained eddy diffusivities using Taylor's analysis. They investigated the dispersion of liquids within water flowing in an open channel. It was revealed in this study that the scale of the turbulence enters directly into the eddy diffusion relationship and it must be measured or estimated if dispersion in turbulent fluids is to be predicted accurately. The dispersion from a point

source within packed and fluidized beds has been investigated by Hanratty et al. (1956). These experimenters injected dye into particle beds having various bulk densities ranging from the pack bed through the fluidized bed condition to the case where no particles were present. Eddy diffusivities were computed as functions of elapsed time using Taylor's analysis. A nonlinear variation of the eddy diffusivity with particle Reynolds number was observed. With a constant Reynolds number, the eddy diffusivity was found to vary also with the particle size. Finally, for a certain particle size and a constant Reynolds number, the eddy diffusivity increased with particle density to a maximum at a 0.35 solid fraction then decreased with particle density until a fixed bed condition was reached.

Some heat transfer experiments were made using a line source generated by stretching a wire across the flow field and heating it by an electrical current. Schubauer (1935) appears to be first in the use of this technique. He measured the lateral spread of heat from a line source in small scale isotropic air flow. Thermal eddy diffusivities were computed from measured temperature profiles. A thorough investigation of the dispersion of heat from a line source was made by Uberoi and Corrsin (1953) using grid-produced isotropic turbulence within a wind tunnel. The mean temperature distributions were measured for systematic

variations in wind speed, size of turbulence-producing grid, and downstream location from heat source. Temperatures and velocity fluctuations were also measured. A comparison of Lagrangian and Eulerian analysis for dispersion in the non-decaying turbulence was performed. The ratio of Eulerian to Lagrangian microscales was determined theoretically and was shown to roughly agree with the experimental results. Townsend (1954) carried out a similar experimental study. Experimental work by Brodkey (1967) supports the Eulerian-Lagrangian relationships developed by Uberoi and Corrsin. Crum and Hanratty (1965) measured mean temperature profiles, temperature fluctuations, and spatial correlations of the temperature fluctuations in the wake of a heated wire. The flow system was fully-developed turbulence inside of a pipe. Traverses of the pipe were made at fixed stations downstream from the source to obtain the measurements. The mean square of the temperature fluctuations was found to have a relative minimum at the centerline and to have a maximum at about two thirds' the radius. As the wall is approached, the mean square fluctuation tends to zero. For increasing distances downstream of the source, the maximum of the mean square temperature fluctuation increased to an apparent asymptotic value at large distances.

Other source configurations have been studied using Lagrangian analysis. Taylor (1954) investigated the dispersion

of a "plug" of foreign material instantaneously inserted into a fluid flowing in a pipe. The dispersion of the "plug" for long elapsed times was the principal point of interest in his study. Taylor adapted his one-dimensional single-particle analysis to pipe flow. In spite of the simplicity of the resulting model, the predictions for long elapsed times of the longitudinal concentrations were in excellent agreement with experimental results (Taylor, 1954; Batchelor et al. 1955). Hanratty (1956) theoretically studied the transfer of heat in isotropic turbulent flow between a line source-sink pair by superpositioning of solutions for point source-sink pairs. Using Taylor's exponential form of the Lagrangian velocity autocorrelation function and an experimental thermal eddy diffusivity, Hanratty calculated temperature profiles between the source and sink. The results agree well with experimental data for heat transfer between parallel plates.

### 2.3.2 Determination by Eulerian analysis

The transformation of Eulerian data to Lagrangian data is not necessary if a complete Eulerian analysis is used. In the Eulerian approach it is assumed that the mean-values of velocity, temperature, and concentration can be calculated with the aid of a suitably chosen eddy diffusion coefficient using Boussineq's hypothesis or the

mixing-length theories. In these theories the rate of transfer of a property is taken to be proportional to the spatial rate of change of the mean value of the property. By application of the mass, energy, or Navier-Stokes equations to experimental data, the eddy diffusivity parameter can be evaluated and used in numerical solutions to these equations.

As in Lagrangian studies, the point source has also been used in Eulerian analysis of turbulent dispersion. Various atmospheric scales of turbulence have been measured and analyzed using one-dimensional Fickian type models (Akerblom, 1908; Taylor, 1915; Schmidt, 1917; and Defant, 1921). Richardson (1926) summarized the results of these and additional workers. Roberts (1923) broadened the analysis to multidimensional problems by using a constant value of the mass diffusivity for each principal direction. Then Sutton (1932) allowed for the components to be positionally dependent as well. This model incorporated the experimental facts then known. Sutton also proposed functional forms of the Lagrangian velocity correlation and obtained diffusivities for a nonhomogenous atmosphere which depended only on the dispersion time. Sutton's model despite its limited accuracy, is still one of the few theoretical analyses that accounts for many atmospheric observations (Monin and Yaglom, 1971). Recently, measurements of medium

and large scale atmospheric turbulence have been made by Hay and Pasquill (1957, 1959), Smith (1961), and Angell (1964a,b). Pasquill (1962) discusses the experimental results up to 1962.

Based on experimental data, Pasquill (1961) and Gifford (1961) presented semi-empirical nomograms which could be used to predict scalar dispersion in the atmosphere. Meteorological services have made extensive practical use of the Pasquill-Gifford nomograms (Pasquill, 1971).

Further atmospheric studies in the early fifties by Lettau (1951) and Davies (1954) have measured the complete eddy diffusivity tensor including the off-diagonal components of the tensor.

Experiments using point sources have also been performed to investigate turbulent dispersion in nonhomogeneous confined flows. These studies have been carried out in pipe flow as well as in packed bed flow. Bernard and Wilhelm (1950) studied the dispersion of a tracer injected in a gas flowing through a cylindrical packed bed. Eddy diffusivities were found by fitting the experimental data to analytical solutions of the mass equation. The analytical solution was obtained by assuming the average axial and radial diffusivity coefficients to be equal and then solving the system of equations by separation of

variables. The diffusivities were found to increase with Reynolds' number for the particle Reynolds' number of 5 to 2,400 studied. Considerable work has been done in this area by Fahien and co-workers using a procedure developed by Fahien (1954) for a point source. The axial component of the eddy diffusivity tensor was neglected on grounds of small gradients in that direction. This assumption enabled an analytical solution of the mass equation for the axial direction to be obtained using the separation of variables technique. The radial component of the eddy diffusivity tensor is allowed to vary, and the mass equation for the radial direction is solved numerically.

This solution technique has been applied to both fully-developed pipe flow and packed bed flow. Fahien and Smith (1955) studied dispersion in a packed bed for gas flows by injecting a tracer. The radial dependence of the radial component of the eddy diffusivity tensor;  $E_{rr}$ , was determined for flow conditions having a particle Reynolds' number ranging from 12 to 15,000. This component was found to have a relative minimum at the centerline, a maximum near the wall, and tended toward zero at the wall. The value of  $E_{rr}$  observed at the centerline was in good agreement with the asymptotic values obtained by Hanratty et al. (1956) for packed beds. Dorweiler and Fahien (1959) confirmed these results and extended the interpretation of

the data. Using a modification of Fahien's procedure, Seagrave and Fahien (1961) investigated dye injection into water flowing in a pipe. They found that the turbulent eddy diffusivity was greater than the molecular diffusivity by a factor of  $10^5$  for Reynolds' numbers of about 7,500. For the lower Reynolds' numbers, axial dispersion appears to increase in its importance. Similar behavior was reported by Roley and Fahien (1960) for gaseous flows. Additional data and eddy diffusivity analysis have been obtained by Frandolig and Fahien (1964) and Konopik and Fahien (1964).

Eulerian studies of heat transfer between parallel plates have been conducted by a group of workers between the years 1947 and 1970 under the leadership of Sage and Corcoran (Corcoran, 1948; Corcoran et al., 1947, 1952, 1956; Cavers et al., 1953; Schlinger et al., 1953a,b; Schlinger and Sage, 1953, Hsu et al., 1956; Sage, 1959; Venezian and Sage, 1961; Chia and Sage, 1970). For Reynolds' numbers ranging from 8,900 to 100,000, the mean temperature profile of air was measured between a heated source wall and the parallel sink wall. Only the lateral heat flux was considered, thereby allowing only the lateral component of the thermal eddy diffusivity tensor to be calculated. The dependence of this component on lateral position was found to be similar to dependence



found for  $E_{rr}$  in pipe flow by Fahien and co-workers. The value of the thermal eddy diffusivity increases with increasing Reynolds number for a given lateral position. It was generally greater than the eddy viscosity. It was found in the latter phase of the work that the lateral heat transfer was influenced significantly by changes in viscous dissipation. Since the work of Venezian and Sage (1961), the eddy diffusivity results have been corrected. The viscous dissipation effect (Chia and Sage, 1970) manifests itself as a sigmoid increase of the lateral heat flux away from the source wall and maximizes at the sink wall. The correction required increases with Reynolds number, being about four per cent at a Reynolds number of 40,000 and thirteen per cent at a Reynolds number of 100,000. When the viscous dissipation effect is accounted for, the thermal eddy diffusivity is found to be symmetric about the centerline. Chia and Sage (1970) summarize the results of this excellent series of works.

Heat transfer within a uniformly heated pipe has been studied in the fully developed flow of air and water. The principal investigations of air flow systems were done by Deissler and Eian (1952), Nunner (1956), Schleicher (1958), Abbrecht and Churchill (1960), Tanimoto and Hanratty (1963), Ibragimov et al. (1969, 1971), and Bourke and Pulling (1970). Both the thermal entrance region and the

isothermal region have been investigated. Mean temperature profiles, mean square temperature fluctuations, and the radial thermal eddy diffusivity have been measured. Axial heat transfer was neglected, an assumption acceptable for a Peclet number greater than 100 (Schneider, 1957). The behavior of the eddy diffusivity profile for the axial and radial direction was similar to that observed in above mentioned studies of the diffusivity. In these studies Reynolds numbers ranged from 7,000 to 71,000, except for the work of Ibragimov et al.; a Reynolds number of 32,500 and 260,000 was used. The correlation between velocity and temperature fluctuations was measured by Ibragimov et al., and they also determined the axial heat flux. The ratio between the local radial and axial turbulent flux components is always smaller than one, with a maximum of about 0.70 midway between the centerline and the wall. Beckwith and Fahien (1963), Truchasson (1964), Rust and Sesonske (1966), and Smith et al. (1966) have investigated liquid flow systems. Reynolds numbers varied from 5,000 to 243,000. All used water as the liquid except Rust and Sesonske; they used mercury and ethylene glycol. The corresponding Prandtl numbers are 0.0018, 10, and 44 for mercury, water, and ethylene glycol, respectively.

Analytical and seminumerical Eulerian investigations of the mass and energy equations have been made for fully

developed turbulent flow within a pipe and between parallel plates. Beckers (1956), Schleicher and Tribus (1957), Sparrow et al. (1957) studied heat transfer for pipe flow using empirical correlations for the thermal eddy diffusivity and considered only the radial dependence. Gielow (1965) considered fully developed flow in a pipe having a constant temperature at the wall. He performed a numerical analysis of the energy equation to obtain local mean temperature profiles. Kakac and Paykoc (1968) did a similar study for flow between parallel plates with constant heat flux and constant temperature at the walls. Again, since experimental data are available for only the radial direction, only the radial dependence was considered. Seminumerical investigations of mass transfer was made by Russo (1965). Using experimentally available data for various components of the eddy diffusivity tensor, Russo obtained solutions to the mass equation.

## CHAPTER 3

### EXPERIMENT AND DATA ANALYSIS

#### 3.1 Experiment

The experiment's objective required the generation of fully developed turbulent flow with subsequent observation of individual fluid point paths. To accomplish this objective, liquid flowing in a glass pipe was chosen as the flow system. Small, spherical particles were suspended in the liquid and illuminated so their paths were made visible. Ideally, the particles should be small in size and of the same density as the fluid. However, the requirement of visibility and availability necessitated a compromise. The particles selected were hollow glass micro spheres with diameters in the range of 10 to 100 microns. Particle density was about 0.34 grams per cubic centimeter. These solid particles were assumed to approximate fluid points.

The apparatus used to photograph the particle motion consisted of three basic systems; (1) the flow loop in which the turbulent motion to be observed was generated, (2) a lighting system for illuminating small suspended particles depicting the fluid motion, and (3) a unique camera for photographing the particle motions over extended distances.

Figure 3.1 shows the integrated arrangement of these three systems.

### 3.1.1 Flow loop

To insure fully developed turbulent flow, several precautions were taken in the design of the flow loop. These included (1) a constant head fluid source, (2) a baffled entrance section to reduce disturbances caused by piping, and (3) a sufficiently long entrance region to the test section to allow the flow to develop fully.

A constant head source was necessary to eliminate the pressure fluctuations created by the pump. Process fluid, trichloroethylene (TCE), was pumped from a receiving and storage drum, through a filter, and to an elevated drum for a constant head supply of fluid. The pump was a centrifugal type equipped with a mechanical seal which provided an excellent seal for the TCE and reduced the potential of contaminating the process fluid with foreign oils and greases present in other types of sealing arrangements. A pot type filter assembly was used to remove solids and contained five 0.304 meter (1 foot) long Fram Corporation, CF10EIH filter elements.<sup>1</sup> These filter elements removed all particles above 5 microns in diameter. Both the receiving and elevated drums were constructed

---

<sup>1</sup>See Fram Corporation Bulletin No. 171.5.

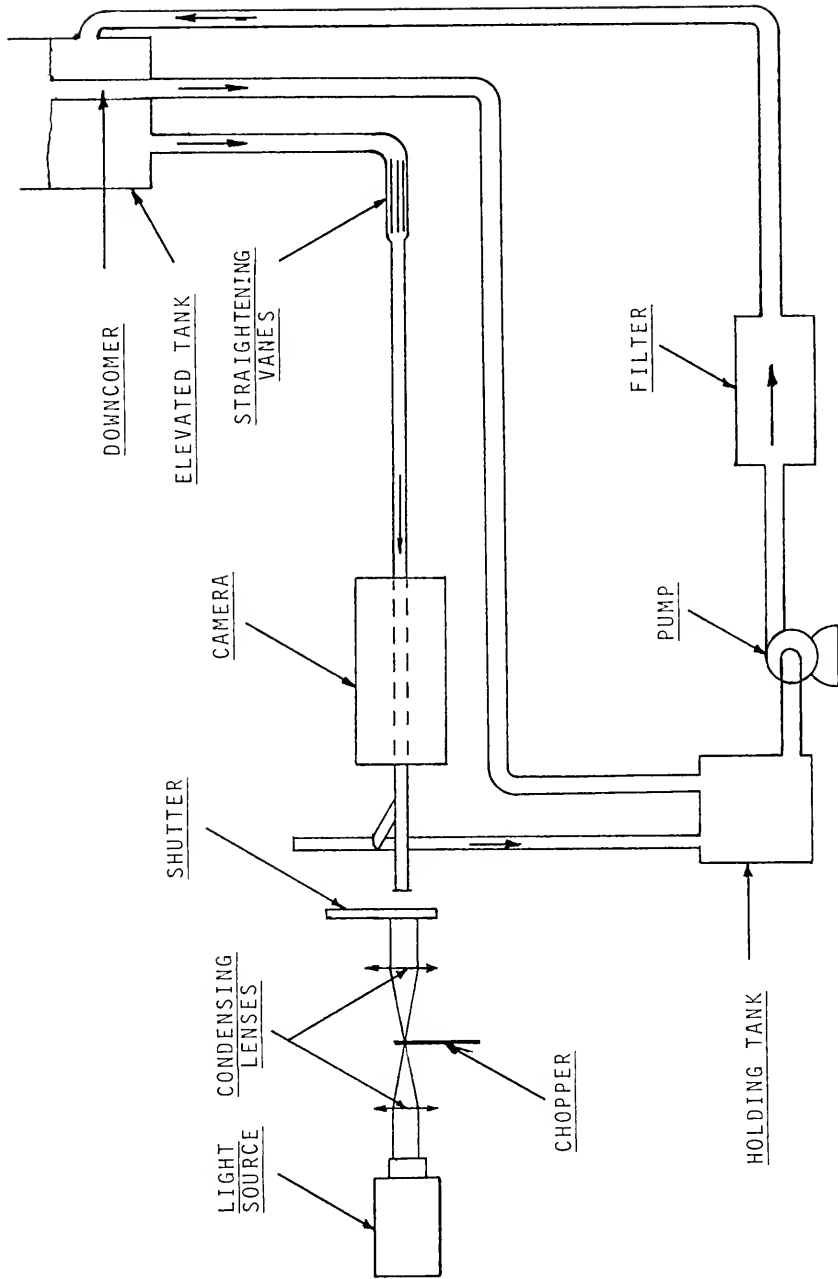


Figure 3.1 Experiment Apparatus

from standard 55-gallon drums with appropriate pipe couplings welded into their walls to accommodate piping. An internal standpipe was installed inside the elevated drum. By pumping the TCE to this drum at a faster rate than was required for the test section, the excess fluid flowed down the standpipe maintaining a constant level in the drum. The receiving drum was vented to the elevated drum so that vapors entrained in the downcoming fluid would seek their level in the upper drum without hindering liquid flow down the standpipe. Sight glasses in both drums provided a convenient method for examining the quantity of fluid in each drum.

From the bottom of the elevated drum, the TCE flowed down a 0.0508 meter (2 inch) diameter aluminum pipe to a reducing section before flowing into the horizontal test section, a glass pipe 4.56 meters (15 feet) long with an inside diameter of 0.0254 meter (1 inch). The reducing section provided a reduction of pipe size as well as damping of abnormal fluid motion created by the piping configuration. Internal straightening vanes were installed just before the reducer. The flow cross section was divided into axial quadrants by the vanes. This was thought adequate to dissipate any large scale disturbances generated by the piping configuration. Two fused glass joints were present in the test section, one at the 0.304 meter (1 foot) position

and the other at the 1.52 meter (5 foot) position. Observations were made over 1.52 meters of pipe starting 1.22 meters (4 feet) from the last fused glass joint. This arrangement provided 48 diameters of straight unobstructed pipe for flow development. The first 1.52 meters of pipe also provided a flow developing region even though two fused glass joints were present. Following the observation section, the remaining length of pipe reduced the influence of the exit region. The full length of the glass pipe was supported at several points to facilitate leveling and eliminate sagging of the pipe.

To minimize distortion of the particle visualization, an observation section was constructed so that the effects of the pipe's curvature were eliminated. Approximately 1.83 meters (6 feet) of the glass pipe were enclosed within two glass plates and a supporting frame. Care was taken in the construction of the enclosure to make sure the angle between the glass plates was 90 degrees. The space within the enclosure surrounding the flow tube was filled with glycerin to yield two undistorted perpendicular views. Glycerin has approximately the same refractive index as glass and TCE, and thereby circumvents the distortion which is present when viewing a bare circular glass pipe. It is through the two perpendicular glass plates that the particles are photographed. See Figure 3.2.



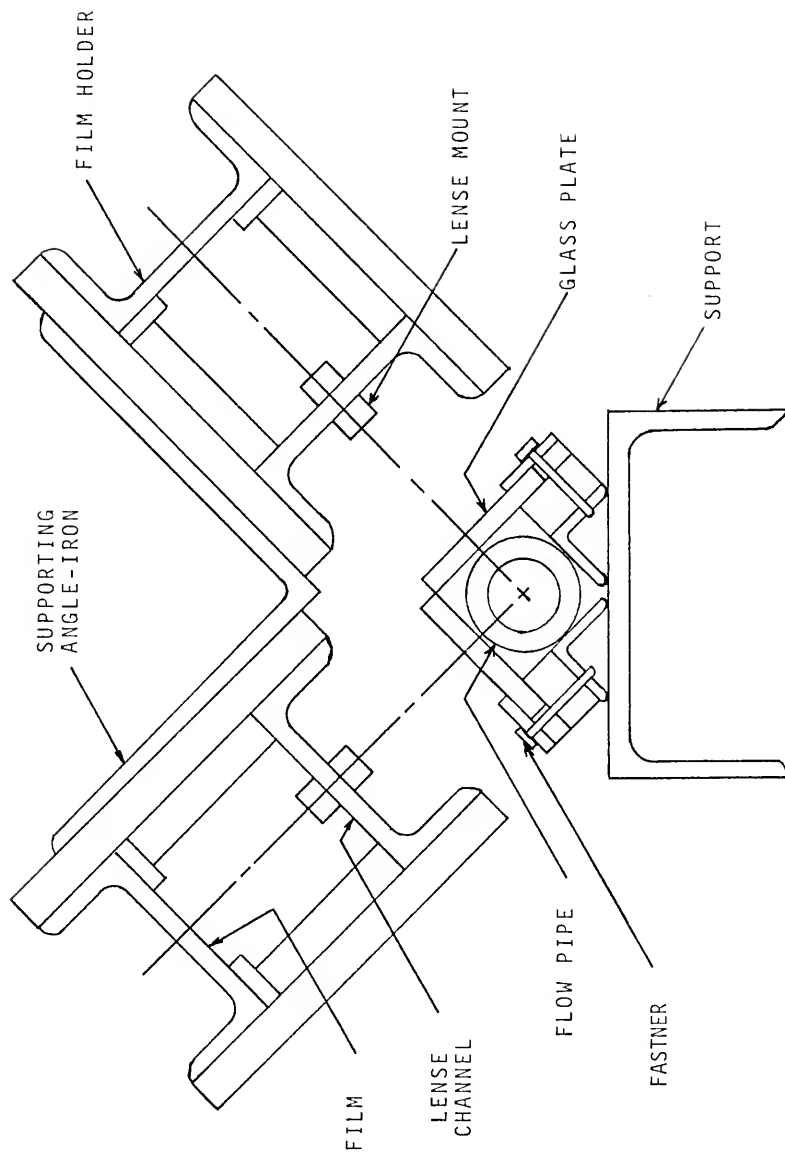


Figure 3.2 Observation Enclosure and Camera Arrangement

The process fluid was recycled to minimize the amount of TCE needed for proper circulation in the loop. The TCE exits the glass section through the side arm of a tee into an expansion section. The tee allows passage of fluid through the flow loop while enabling the flow tube to be illuminated axially through a glass port mounted to a second arm of the tee. A 0.0508-meter (2-inch) aluminum pipe was used to return the TCE through a rotameter to the receiving and storage drum. The rotameter was calibrated with TCE and had a capacity of 1.26 liters/sec (20 G.p.m.), yielding a maximum Reynolds number for the glass pipe of 200,000. The temperature of the process fluid was measured just before returning the fluid to the receiving drum.

A small stream of the process fluid was passed through a silica gel trap to remove water from the TCE. This minimized corrosion of iron materials used in the construction of the flow loop.

### 3.1.2. Lighting system

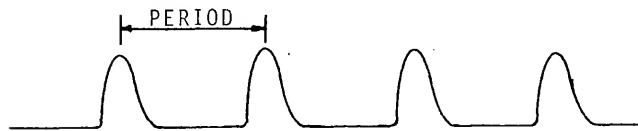
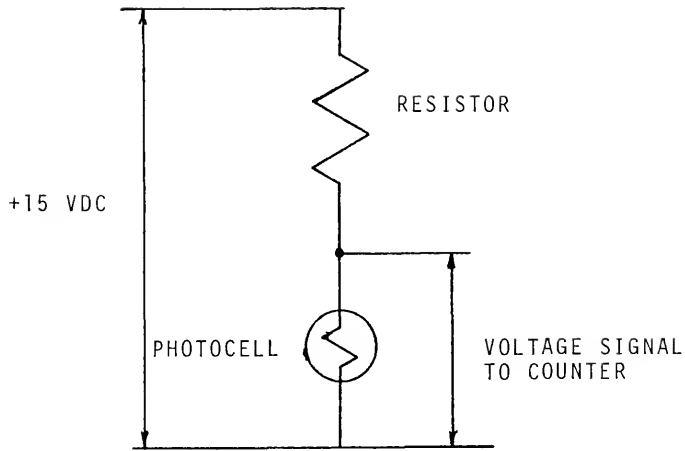
The suspended particles were illuminated using a high intensity carbon arc lamp. Two 0.0634-meter (2.5-inch) diameter condensing lenses were used to collimate the light beam and enhance the dark field illumination. By rotating a four bladed, 0.304-meter (12-inch) diameter disk

perpendicular to the axis of the light path and at the focal point between the two condensing lenses, the illumination of the suspended particles was interrupted at a constant frequency. By interrupting the light, a time scale was imposed on the photographic images obtained.

The chopping frequency was sensed with the photo-cell circuit shown in Figure 3.3. When one of the blades of the disk came between the arc and the photo cell, the illumination of the cell was reduced and its resistance to electrical current flow increased. This increase in resistance caused a corresponding increase in the voltage drop across the photo cell. The reverse occurred when the cell was illuminated. The voltage pulses generated in this manner were counted by a General Radio model 1191 counter and the corresponding period displayed.

### 3.1.3 Camera

The camera was unique in that it took 80 pictures simultaneously -- forty pictures for each view, along a 1.52-meter (5-foot) length of the flow tube. This length corresponded to 60 pipe diameters. The camera construction is shown in Figure 3.4 and is described below. Forty 0.0159-meter (5/8-inch) holes were drilled and tapped in two 0.0761-meter (3-inch) wide aluminum channels. Lenses, 0.012 meter in diameter and having a 0.138-meter focal



TYPICAL PULSE TRAIN PRODUCED  
BY LIGHT CHOPPER

Figure 3.3 Chopping Frequency Detection Circuit

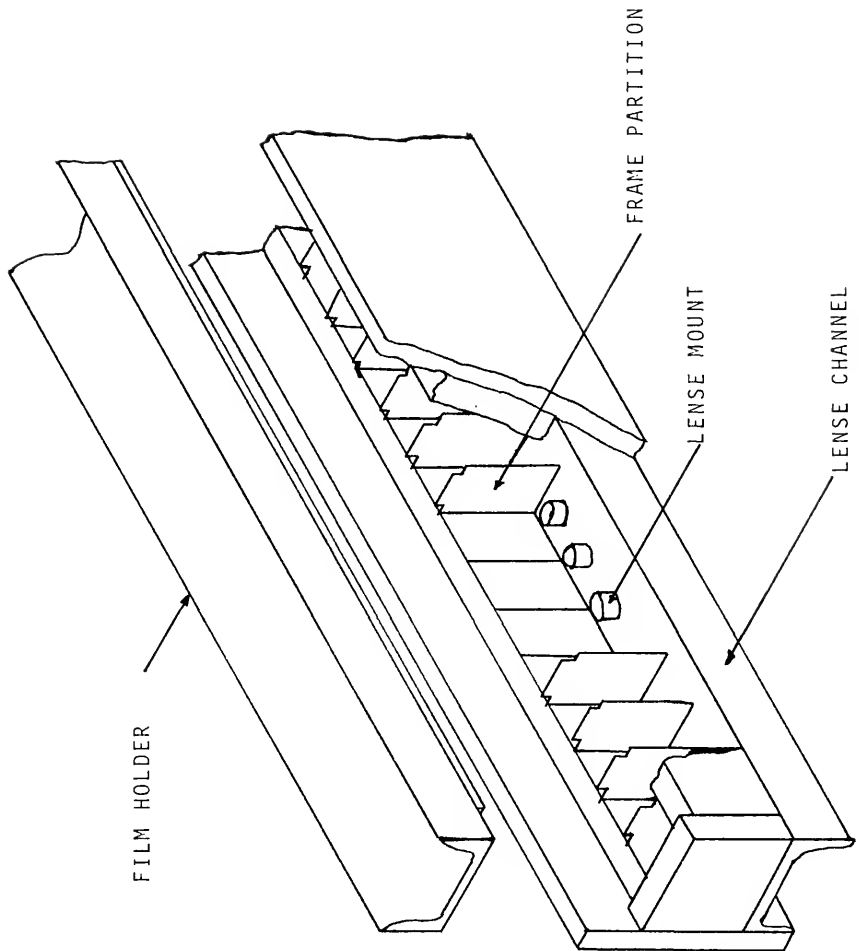


Figure 3.4 Camera Construction

length, were mounted in copper bushings and inserted in the drilled and tapped holes. In each lense mount, a disk with a central 0.00159-meter (1/16-inch) diameter hole was used as an aperture. This size aperture provided sufficient light to expose the film and resulted in good image definition for a field depth of about 0.0254 meter (1 inch). The two aluminum channels were attached to a 0.127-meter (5-inch) angle iron to establish a right angle between the two views of the flow tube and give a rigid camera construction. Each lense and aperture assembly focused a 0.038-meter (1 1/2-inch) section of the flow tube onto a corresponding frame of 35-millimeter photographic film. Each sequential section of the flow tube was photographed on a corresponding sequential frame of the film. Partitioned compartments for each lense prevented double exposure on adjacent frames. The film was mounted on two 0.0761-meter (3-inch) wide aluminum channels, one for each view and positioned 0.70 meter from the lenses, see Figure 3.5. The distance from the glass-air interface to the lenses was approximately 0.72-meter. The camera assembly was positioned over the flow tube and aligned such that the projected image of the tube was centrally located on the film. Each viewed direction was at approximately 45 degrees with the vertical, see Figure 3.2.

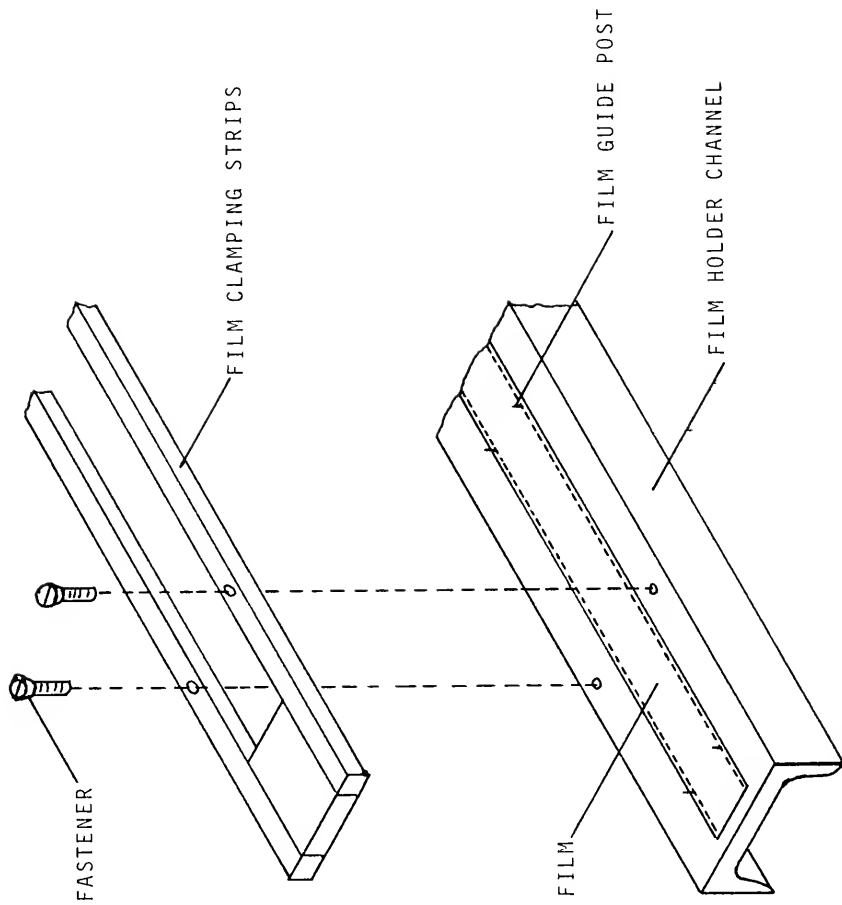


Figure 3.5 Film Mounting Arrangement

A dark room, 2.43 meters (8 feet) square by 2.43 meters (8 feet) high was constructed around the camera area of the flow loop so as to yield a darkened volume suitable for exposing the film. One shutter was installed to admit a light beam along the axis of the flow tube into the darkened room enclosing the camera.

#### 3.1.4 Procedure

The procedure used to photograph the suspended particles is given below:

- (1) The system is charged with sufficient TCE to avoid cavitation in the pump, approximately 303 liters (80 gallons).
- (2) The pump is turned on, and the system is allowed to reach thermal equilibrium at the desired flow rate.
- (3) A small 10-micron filter assembly is charged with particles by allowing TCE to flow from the pot filter through the small filter assembly. In this step, particles collected in the large pot filter are flushed to the smaller filter and reused.
- (4) By reversing the flow through the 10-micron filter assembly, particles are entrained and



directed to the glass tube for observation. The flow rate through the small filter assembly is adjusted so that approximately 10 to 20 particles are entrained per 10-second interval.

- (5) Photographic film is then clamped into place on the aluminum channel pieces and inserted into the camera.
- (6) With the shutter closed the carbon arc lamp and light chopper are turned on. When the period at which the light beam is interrupted becomes constant, the shutter is opened for approximately 7 seconds and closed again.
- (7) The flow rate, temperature, and chopping period are noted and recorded.
- (8) The light source is turned off, and light chopper is turned off.
- (9) The film holders are removed from the camera, and the film removed for processing as described in the next section.

#### 3.1.5 Processing of photographic film

High speed photographic film was used to photograph the particles. Kodak, 35-millimeter, 2475 recording film

was selected because of its availability and inexpensive cost. The ASA number rating for this film is 1600. After exposure of the film as described earlier, the film was removed from the film holder and processed in a dark room. The film was processed for 30 minutes at 65 degrees Fahrenheit in Kodak DK-50 developer. The developer solution was prepared in the manner and in the proportions given in the directions which came with the chemical. A 30-second stop bath was used to neutralize the developing chemicals. Then a 10-minute fixer step was used, followed by a 30-minute water wash step. The fixer solution was prepared as prescribed by Kodak directions. To reduce the possibility of drying stains, the film was flushed with a solution of Kodak Photo Flo 200. The film was then allowed to dry for several hours.

### 3.2 Data Analysis

Before the Lagrangian correlations could be computed, two transformations of the data were necessary. First, the two-dimensional coordinates of two perpendicular views of the same point in the flow tube were transformed into a three-dimensional Cartesian coordinate point. Secondly, the Cartesian coordinates were transformed into cylindrical coordinates. The resulting particle points were then smoothed and the Lagrangian correlations computed.

The photographed particle tracks were scanned using a PDP-11 minicomputer in conjunction with a X-Y recorder. The track images were projected into the plane of the X-Y recorder by using a photo enlarger. To obtain the coordinates of a particle's position, both parallelax and the refraction at the glass-air interface were considered. The algorithm used to collect the two-dimensional coordinates of the perpendicular views is given in Appendix A.

### 3.2.1 Transformation of photographic data

Using the laws of geometry and optics as applied to the photographing system, transformations of the image can be made to account for parallelax and refraction. In the analysis that follows, the difference in refractive index of the glass, glycerin, and the TCE is neglected. Figure 3.6 is used as a guide to the following discussion and a means of defining the nomenclature. Note that the coordinate perpendicular to  $D_1$  and  $D_2$  is measured from the centerline of the pipe in the direction of "d", i.e. perpendicular to the glass-air interface. For the present time consider "d" to be the distance from the glass-air interface to the centerline of the pipe. The analysis is started by first relating the image in the photographing plane to the virtual image in the glass-air interface. From similar triangles

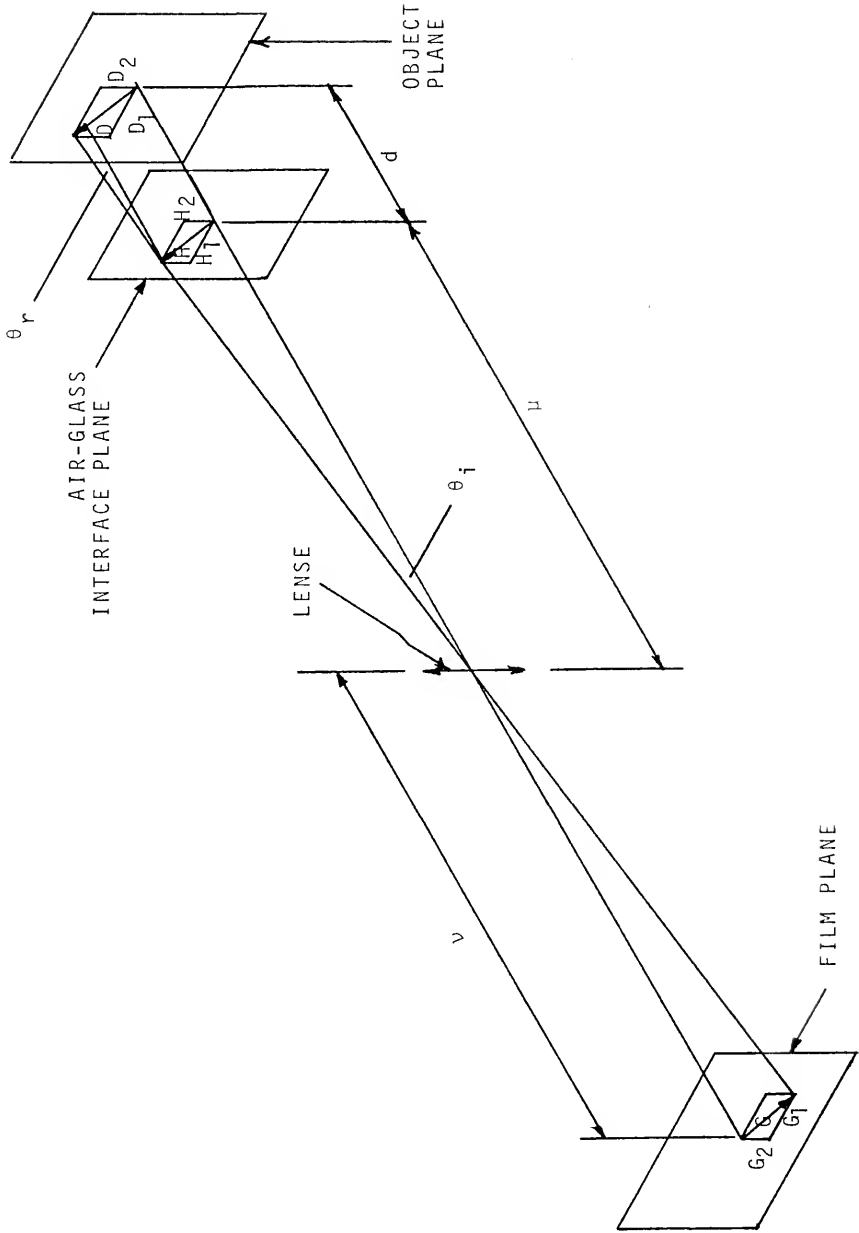


Figure 3.6 Geometry of Optics for a Typical View of the Flow Field

$$\frac{G}{v} = \frac{H}{\mu}$$

or

$$H = G \frac{\mu}{v} . \quad (3.1)$$

Also using the law of refraction,

$$n = \frac{\sin \theta_i}{\sin \theta_r} = \frac{\frac{H}{(H^2 + \mu^2)^{1/2}}}{\frac{(D-H)}{((D-H)^2 + d^2)^{1/2}}} \quad (3.2)$$

where "n" is the refractive index of the glass. From Equation (3.2), the ratio between D and H is found as

$$\frac{D}{H} = \left( 1 + \frac{d}{((n^2 - 1)H^2 + n^2\mu^2)^{1/2}} \right).$$

From Figure 3.6, it is obvious that

$$\frac{D_1}{H_1} = \frac{D_2}{H_2} = \frac{D}{H} = \left( 1 + \frac{d}{((n^2 - 1)H^2 + n^2\mu^2)^{1/2}} \right). \quad (3.3)$$

Using Equation (3.1), Equation (3.3) can be written for coordinate direction m

$$\frac{D_m}{G_m} = \frac{\mu}{v} \left( 1 + \frac{d}{\frac{\mu}{v} ((n^2 - 1)G^2 + n^2v^2)^{1/2}} \right)$$

or

$$\frac{D_m}{G_m} = \frac{\mu}{v} + \frac{d}{((n^2 - 1)G^2 + n^2v^2)^{1/2}} \quad (3.4)$$

The length of " $G_m$ ", i.e. the image height produced on the film, is projected by the photo enlarger with a magnification factor of " $M$ "; therefore, the distance " $G_m$ " on the film is magnified to a length " $C_m$ " according to

$$C_m = MG_m. \quad (3.5)$$

Using Equation (3.4) and (3.5), now the coordinate positions in the flow tube,  $(D_1, D_2)$ , can be related to the coordinates measured by the computer in the plane of the X-Y recorder,  $(C_1, C_2)$ , as

$$\frac{D_m}{C_m} = \frac{\mu}{Mv} + \frac{d}{((n^2 - 1)C^2 + n^2M^2v^2)^{1/2}} \quad (3.6)$$

The analysis given above was concerned with only one view of the particle position; however, to fix the three Cartesian coordinates of the particle position, two such perpendicular views were necessary. Let  $D_1$  be the coordinate direction corresponding the flow direction, i.e. the common coordinate of two perpendicular views. Introducing

an index "j", j = 1 or 2, to denote the two views, Equation (3.6) can be written for view "j" as

$$\frac{D_{jm}}{C_{jm}} = \frac{\mu_j}{M_j v_j} + \frac{d_j - D_{\hat{j}2}}{((n^2 - 1)C_j^2 + n^2 M_j^2 v_j^2)^{1/2}} \quad (3.7)$$

where the " $\hat{j}$ " index denotes the complement of view "j".

Note

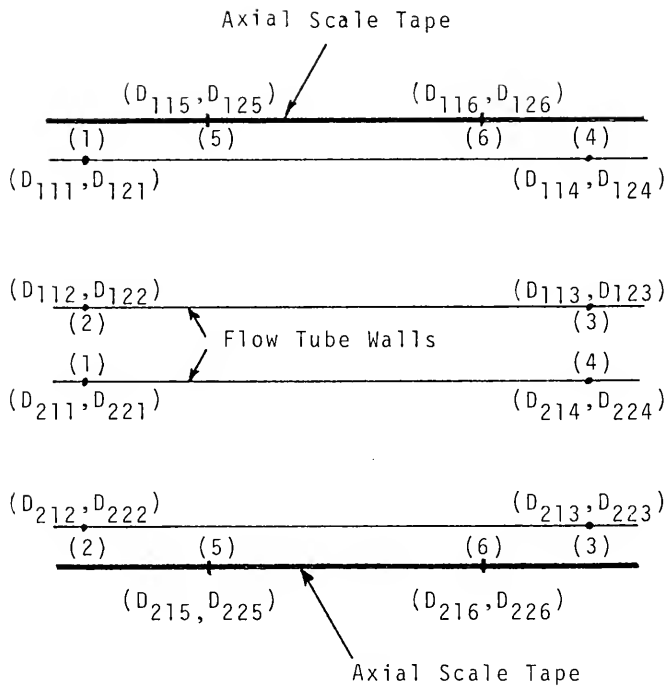
$$D_{j1} = D_{\hat{j}1} \quad \text{or} \quad D_{11} = D_{21}$$

and

$$D_{j2} \perp D_{\hat{j}2} \quad \text{or} \quad D_{12} \perp D_{22}$$

In order to align the images projected and to evaluate the terms  $\frac{\mu_j}{M_j v_j}$  and  $d_j$  of Equation (3.7), several datum points were recorded for each view of the flow tube. An alignment and scaling tape with inch markers on it was also placed within the enclosure. This tape could be photographed from both directions and thereby yield an axial scale as well as known positions within two corresponding views of a tube section. The two corresponding views of a flow tube section were projected simultaneously into the plane of the X-Y recorder. Figure 3.7 shows the arrangement of the datum points taken. Adding another index, "k", to Equation

UPPER VIEW  
(View 1)



LOWER VIEW  
(View 2)

Figure 3.7 Arrangement of Datum Points



(3.7) to denote the datum point within a view, Equation (3.7) becomes

$$\frac{D_{jmk}}{C_{jmk}} = \frac{\mu_j}{M_j v_j} + \frac{d_j - D_{j2k}}{((n^2 - 1)C_{jk}^2 + n^2 M_j^2 v_j^2)^{1/2}} \quad (3.8)$$

The value of "n" is known; however, the values of  $\frac{\mu_j}{M_j v_j}$ ,  $d_j$ , and  $D_{j2k}$  were evaluated from the datum points recorded from each view. The method used to compute these constants is discussed in Appendix B. Using Equation (3.8), all points on a track image projected in the plane of the X-Y recorder can be transformed to their corresponding Cartesian coordinates within the flow tube. The second transformation from Cartesian to cylindrical coordinates is straightforward and can be obtained from any elementary algebra text.

### 3.2.2 Computation of particle velocity

The velocity of the suspended particle was obtained from smoothed particle position data. A fourth-order polynomial was used to represent the particle's trajectory over a short distance. This order polynomial allows for second order variations in the particle's acceleration. The polynomial form is

$$x_i = c_1 + c_2 t_i + c_3 t_i^2 + c_4 t_i^3 + c_5 t_i^4 \quad (3.9)$$

where  $i$  designates the time coordinate number. Differentiating Equation (3.9) gives the velocity as

$$V_i = c_2 + 2c_3t_i + 3c_4t_i^2 + 4c_5t_i^3. \quad (3.10)$$

The coefficients of Equation (3.9) can be evaluated using a least-squares fit over a short length of the particle track which spans the point being smoothed. The coefficients found in this manner can now be used to compute the velocity via Equation (3.10).

### 3.2.3 Computation of Lagrangian correlations

The statistical properties of the random motion of a single fluid particle can be used to effectively evaluate the dispersion of a scalar property within a turbulent flow field. Particle position and velocity with respect to time is a starting point from which certain statistical correlations can be generated that help describe turbulent dispersion. The flow field of particular interest in this study is that of turbulent shear pipe flow. Consider a fluid particle starting at time  $t_0$  from a point  $\underline{x}_0$  within the flow field. At any time during the particle's flight, its velocity,  $\underline{V}(t|t_0, \underline{x}_0)$ , is equal to the Eulerian velocity,  $\underline{U}(t, \underline{x})$ , at the point  $\underline{x}$  which is the point at which the fluid particle is located at time  $t$ .

Therefore

$$\underline{V}(t|t_0, \underline{x}_0) = \underline{U}(t, \underline{x}) \quad (3.11)$$

or, expressing the velocity as a mean plus a deviation

$$\underline{V}(t|t_0, \underline{x}_0) = \langle \underline{U}(t, \underline{x}) \rangle + \underline{u}'(t, \underline{x}). \quad (3.12)$$

Note that the deviation in the fluid particle's velocity from the local mean velocity of the field is

$$\underline{V}'(t|t_0, \underline{x}_0) = \underline{V}(t|t_0, \underline{x}_0) - \langle \underline{U}(t, \underline{x}) \rangle = \underline{u}'(t, \underline{x}). \quad (3.13)$$

Let

$$\underline{X}'(t|t_0, \underline{x}_0) = \int_{t_0}^t \underline{V}'(t_1|t_0, \underline{x}_0) dt_1 \quad (3.14)$$

or

$$\begin{aligned} \underline{X}'(t|t_0, \underline{x}_0) = & \int_{t_0}^t \underline{V}(t_1|t_0, \underline{x}_0) dt_1 \\ & - \int_{t_0}^t \langle \underline{U}(t_1, \underline{x}) \rangle dt_1 \end{aligned} \quad (3.15)$$

be the deviation of the fluid particle's position after an elapsed time  $t-t_0$  from the position it would have had had it been moved only by the local mean velocity.

The transport of a scalar quantity within a steady nonhomogeneous flow field has not been theoretically derived

at the present time. However, from the studies of isotropic homogeneous turbulent flow by Taylor (1921) and Batchelor (1949) respectively, a functional relationship between the eddy diffusivity tensor and the Lagrangian correlations apparently exists. From the results of these studies, it was shown that the eddy diffusivity tensor is

$$E_{ij}(t) = \frac{1}{2} \frac{d}{dt} \langle X_i'(t) X_j'(t) \rangle \quad (3.16)$$

or

$$E_{ij}(t) = \frac{1}{2} (\langle X_i'(t) V_j'(t) \rangle + \langle V_i'(t) X_j'(t) \rangle). \quad (3.17)$$

From the statistical analysis of single-particle trajectories, the above Lagrangian correlations can be obtained, i.e.

$\langle X_i'(t) X_j'(t) \rangle$  and  $\langle X_i'(t) V_j'(t) \rangle$ . Other correlations such as  $\langle V_i'(t_0) V_j'(t) \rangle$  and  $\langle V_i'(t) V_j'(t) \rangle$  can be computed easily from the data on the particle's position and velocity at discrete time intervals.

In the case of cylindrical coordinates, the computation of displacements and velocities needs further explanation. The application of Equations (3.13) and (3.15) is straightforward for the axial and radial directions, i.e.

$$V_z'(t|t_0, \underline{x}_0) = U_z(t|t_0, \underline{x}_0) - \langle U_z(t, \underline{x}) \rangle \quad (3.18)$$

$$V_r'(t|t_0, \underline{x}_0) = V_r(t|t_0, \underline{x}_0) \quad (3.19)$$

$$z'(t|t_0, \underline{x}_0) = \int_{t_0}^t U_z(t_1|t_0, \underline{x}_0) dt_1 - \int_{t_0}^t \langle U_z(t_1, \underline{x}) \rangle dt_1 \quad (3.20)$$

and

$$r'(t|t_0, \underline{x}_0) = \int_{t_0}^t V_r(t_1|t_0, \underline{x}_0) dt_1. \quad (3.21)$$

The displacement and velocity deviation in the angular direction needs additional interpretation. In reference to the starting point or origin,  $\underline{x}_0$ , of a given particle, the angular velocity is defined as

$$V_\theta'(t|t_0, \underline{x}_0) = r_0 \frac{d\theta(t|t_0, \underline{x}_0)}{dt} \quad (3.22)$$

and the angular displacement follows from Equation (3.15) as

$$r_{0\theta}'(t|t_0, \underline{x}_0) = \int_{t_0}^t V_\theta'(t_1|t_0, \underline{x}_0) dt_1 \quad (3.23)$$

where  $r_0$  is the value of the radius at time  $t = t_0$ . Note that if the angular velocity is defined using  $r(t|t_0, \underline{x}_0)$ , then when Equation (3.15) is used to compute the angular displacement, the displacement would not necessarily have the proper value of zero for a closed path. Using the above definitions for displacements and deviations in velocity, the elements of the eddy diffusivity tensor,  $\underline{\underline{E}}$ , are consistent with Equation (2.49) where

$$\underline{\nabla}\Gamma = \frac{\partial\Gamma}{\partial r} \underline{i}_r + \frac{1}{r} \frac{\partial\Gamma}{\partial\theta} \underline{i}_\theta + \frac{\partial\Gamma}{\partial z} \underline{i}_z \quad (3.24)$$

for cylindrical coordinates, and

$\underline{i}_r$  is the unit vector in the radial direction

$\underline{i}_\theta$  is the unit vector in the angular direction

$\underline{i}_z$  is the unit vector in the axial direction.

## CHAPTER 4

### RESULTS AND DISCUSSION

Paths of suspended particles were photographed over large distances, and the turbulent intensities and Lagrangian correlations were computed from the paths observed in a 0.0254 meter (1 inch) I.D. diameter pipe. The Reynolds number at which the observations were made was 110,000. Particle paths were observed for elapsed times as great as 1.2 seconds, corresponding to an axial distance of 1.32 meters (4.33 feet). Seven particle tracks were examined with a total of 1600 time intervals recorded. The time period of the observations was  $6.16 \times 10^{-3}$  seconds. The direction of the particle paths varied very little over this interval of time, so that the images of the paths were nearly straight lines with very little curvature.

#### 4.1 Results

The particle track data were used to compute both turbulent intensities and Lagrangian correlations. These variables were computed for five radial intervals. The annular zones formed by the radial intervals are shown in Figure 4.28. In view of the frequent use of homogeneous

models for turbulent pipe flow and the relatively small sample size, the overall averages of the correlations for the five zones were computed.

#### 4.1.1 Turbulent intensities and shear stresses

The computed relative turbulent intensities are shown in Table 4.1, and the relative shear stresses are given in Table 4.2. The relative turbulent intensities agree with those given by Patterson and Zakin (1967) for organic solvents using hot-film anemometry. However, the radial variations are not in agreement. This lack of agreement probably stems from the relatively small number of points available to form ensemble averages for the five radial zones. The relative radial turbulent intensities are also in fair agreement with published values by Laufer (1954) for air and by Cermak and Baldwin (1964) for water. The relative turbulent shear stress,  $\langle V'_z(t_0)V'_r(t_0) \rangle / U_{z,MAX}^2$ , is in good agreement with published data. The relative shear stress,  $\langle V'_r(t_0)V'_\theta(t_0) \rangle / U_{z,MAX}^2$ , appears to be zero as expected. However, the nonzero results for  $\langle V'_z(t_0)V'_\theta(t_0) \rangle / U_{z,MAX}^2$  cannot be explained. Both shear stresses  $\langle V'_z(t_0)V'_\theta(t_0) \rangle$  and  $\langle V'_r(t_0)V'_\theta(t_0) \rangle$  should be zero since there is symmetry in the tangential direction.

#### 4.1.2 Lagrangian correlations

The computed correlations for fully developed turbulent pipe flow are shown in Figures 4.1 through 4.27. Figures



Table 4.1 Relative Turbulent Intensities

Radial Interval, $2r/D_o$	Axial $\frac{v_r'^2(t_o)^{1/2}}{U_{z,MAX}}$	Radial $\frac{v_r'^2(t_o)^{1/2}}{U_{z,MAX}}$	Tangential $\frac{v_\theta'^2(t_o)^{1/2}}{U_{z,MAX}}$
0.0 to 0.2	0.0927	0.0295	0.0367
0.2 to 0.4	0.0799	0.0315	0.0378
0.4 to 0.6	0.0695	0.0351	0.0400
0.6 to 0.8	0.0869	0.0397	0.0470
0.8 to 1.0	0.0879	0.0344	0.0451
Overall	0.0819	0.0359	0.0429

Table 4.2 Relative Turbulent Shear Stresses

Radial Interval, $2r/D_o$	$\frac{v_z'(t_o)v_r'(t_o)}{U_{z,MAX}^2}$	$\frac{v_z'(t_o)v_\theta'(t_o)}{U_{z,MAX}^2}$	$\frac{v_r'(t_o)v_\theta'(t_o)}{U_{z,MAX}^2}$
0.0 to 0.2	0.000592	0.000543	-0.000160
0.2 to 0.4	0.000562	-0.000204	0.000240
0.4 to 0.6	0.000537	0.000387	-0.000013
0.6 to 0.8	0.001015	0.000851	0.000044
0.8 to 1.0	0.000709	0.000581	-0.000447
Overall	0.000740	0.000521	-0.000035

4.1 to 4.3 give a representative sample of the results obtained for the 5 radial zones. However, since the sample size is relatively small, only the overall correlations given in Figures 4.4 through 4.27 will be discussed. Specific observations about the correlations are made below.

The time period between observations is an adjusted  $3.08 \times 10^{-3}$  seconds or 0.145 dimensionless time units. One dimensionless time unit,  $t^* = 1$ , corresponds to the time required to traverse the pipe diameter at a velocity equal to the maximum centerline velocity.

Displacement-displacement correlations,  $\langle X_i'(t)X_j'(t) \rangle$ .  
The overall displacement-displacement correlations are given in Figures 4.4 to 4.9. These correlations are normalized to the pipe diameter,  $D_0$ . The correlations form a symmetric second-order tensor; therefore, only the six elements presented need to be considered. The diagonal component for the axial direction,  $\langle z'^2(t) \rangle$ , is at least an order of magnitude greater than the other components, except for the diagonal component for the tangential direction,  $\langle (r_0\theta'(t))^2 \rangle$ .

The shape of the correlations of the diagonal components of the above tensor are the form expected. The correlation for the spread in the axial direction, Figure 4.4, does not contain the time linear portion predicted by Equation (2.51); however, the correlation apparently does tend towards an inclined straight line for large elapsed times.

The shape of the curve is similar to that reported by Gielow (1972) for shear flow between parallel plates. For the radial diagonal correlation,  $\langle r'^2(t) \rangle$  in Figure 4.5, the effect of the confining pipe wall is evident for the larger elapsed times. There is an asymptotic limit for the radial displacement correlation because of the confining walls of the system. This limit is found by assuming a random dispersion of the particles from an initial radial position,  $r_0$ , i.e. the mean square displacement from  $r_0$  at infinite time is

$$\frac{2\pi \int_0^{\frac{D_0}{2}} (r - r_0)^2 r dr}{2\pi \int_0^{\frac{D_0}{2}} r dr} = \frac{D_0^2}{8} - \frac{2D_0 r_0}{3} + r_0^2. \quad (4.1)$$

For the overall correlation, the particle may start at any radius; therefore, the asymptotic limit is

$$\frac{2\pi \int_0^{\frac{D_0}{2}} \left( \frac{D_0^2}{8} - \frac{2D_0 r_0}{3} + r_0^2 \right) r_0 dr_0}{2\pi \int_0^{\frac{D_0}{2}} r_0 dr_0} = \frac{D_0^2}{36}. \quad (4.2)$$

Since the ordinate of Figure 4.5 is normalized relative to  $D_0^2$ , the asymptotic limit for the ordinate of the figure is  $1/36$  or  $0.0278$ .

The off-diagonal components of the tensor are given in Figures 4.7 to 4.9. These correlations are of the same order of magnitude as the radial diagonal correlation. The positive value of the correlation between the axial and radial components of the fluid particle displacement vector,  $\langle z'(t)r'(t) \rangle$  in Figure 4.7, is to be expected. Due to the mean velocity profile, if a fluid particle has a positive displacement in the radial direction, it has moved to a flow region of lower mean axial velocity. Consequently, the average effect would be a positive axial deviation in the particle's displacement. Similarly, a negative radial displacement leads to a negative axial displacement, on the average. The product of the two displacement combinations is positive, thereby resulting in a positive correlation. The two remaining correlations are expected to be zero because of angular symmetry in the pipe. This appears to be the case for the correlation between the radial and tangential components of the fluid particle displacement vector,  $\langle r'(t)r_0\theta'(t) \rangle$  in Figure 4.9. However, the correlation between the axial and tangential components,  $\langle z'(t)r_0\theta'(t) \rangle$  in Figure 4.8, has a significant positive nature. This probably occurs because of the relatively small number of samples present in the correlation. If numerous samples had been taken, the effect of multiple crossings of the starting angular position could reduce the magnitude of the correlation.

Displacement-velocity correlations,  $\langle x'_i(t) v'_j(t) \rangle$ .

The correlations between displacement and velocity deviations are presented in Figures 4.10 through 4.18. These correlations are the components of the eddy diffusivity tensor for various mixing length theories. In addition, the symmetric off-diagonal components of the eddy diffusivity tensor suggested by Batchelor (1949), see Equation (2.45), are presented in Figures 4.19 to 4.21. Both of these types of correlations are normalized relative to the product of the pipe diameter,  $D_0$ , and the maximum mean axial velocity at the centerline,  $U_{z,MAX}$ . Again the diagonal component of the tensor for the axial direction,  $\langle z'(t) v'_z(t) \rangle$ , is an order of magnitude greater than the other components.

The diagonal components of the eddy diffusivity tensor behave very much as expected. In Figure 4.10, the axial component,  $\langle z'(t) v'_z(t) \rangle$ , shows a gradual increase and appears to be approaching a constant value. The change in direction near a dimensionless time of 9 is probably due to decreasing statistical accuracy since the sample size diminished with increases in the time coordinate. After a rapid initial increase, the radial component reaches a plateau and begins to decline. The approach of the axial component to its asymptotic value appears to be more gradual. The assumption of a constant eddy diffusivity coefficient for the radial direction, often used in modeling

dispersion in pipe flow, seems appropriate for a portion of the dispersion time. As seen in Figure 4.14, the radial diagonal component could be approximated by a constant. Of course, for large times, the correlation is expected to go to zero since the radial spread is bounded by the pipe walls. The behavior of the tangential component,  $\langle r_0 \theta'(t) V_\theta'(t) \rangle$  in Figure 4.18, seems to be more akin to the behavior of the axial component than the radial component. The rapid decrease in the tangential correlation after a dimensionless time of 5 is probably due to poor statistics.

Figures 4.11, 4.13, and 4.19 give the correlations between the axial and radial deviations. The correlations  $\langle z'(t) V_r'(t) \rangle$  and  $\langle r'(t) V_z'(t) \rangle$ , Figures 4.11 and 4.13 respectively, have similar shapes which suggest that the eddy diffusivity tensor is symmetric. Using the eddy diffusivity components as given by Batchelor (1949) symmetry is imposed by definition, see Equation (2.45). Figure 4.19 gives the axial-radial component of Batchelor's definition of the eddy diffusivity tensor.

Because of symmetry in the tangential direction, the remaining off-diagonal components are normally assumed to be zero. Since the data were readily available, these correlations were computed also. The correlations between the radial and tangential directions are apparently zero as indicated in Figures 4.15, 4.17, and 4.21. Figure 4.12

suggests that  $\langle z'(t)V'_\theta(t) \rangle$  is also zero. However, the correlation  $\langle r'_0\theta'(t)V'_z(t) \rangle$ , Figure 4.16, does not show a tendency toward zero. It appears to be increasing. The axial-tangential component as defined by Batchelor also shows a continuing increase with time. This is only a reflection of  $\langle r'_0\theta'(t)V'_z(t) \rangle$  since

$$\frac{d}{dt} \langle z'(t)r'_0\theta'(t) \rangle = \langle z'(t)V'_\theta(t) \rangle + \langle r'_0\theta'(t)V'_z(t) \rangle .$$

Considering the tangential symmetry, for any  $V'_z(t)$  it would be equally likely that the tangential displacement could be positive or negative. This would result in a zero correlation. The problem of a positive correlation appears to be in the data. Perhaps, since the sample size was relatively small, there was not sufficient crossing of the initial angular position. The portion of the particle path remaining after the last crossing could cause an excessive positive contribution to  $\langle r'_0\theta'(t)V'_z(t) \rangle$ . With a sufficiently large sample size, these correlations should approach zero for all times.

Velocity-velocity correlations,  $\langle V'_i(t_0)V'_j(t) \rangle$ . The correlations between the velocity deviations at the initial time  $t_0$  and elapsed times  $t-t_0$  are given in Figures 4.22 to 4.27. These correlations are the Lagrangian double velocity correlation coefficients defined by Equation (2.32). Because

of the manner by which the correlations were generated from the particle path data, the Lagrangian double velocity correlation tensor is symmetric. In view of this, only six of the nine components of the tensor are presented.

The diagonal components of the tensor, Figures 4.22 to 4.24, start at one, as required, and decrease toward zero for large times. All three correlations are identical for elapsed dimensionless times less than 0.5; after which, the radial correlation,  $\langle V_r(t_0)V_r(t) \rangle$  in Figure 4.23, decreases most rapidly. Since the diagonal components of the eddy diffusivity tensor are proportional to the integrals of the respective diagonal components of the Lagrangian double velocity correlations, the most rapid increase in the radial eddy diffusivity coefficient is consistent with the above observation. Also from the integral relationship between the two radial components, the radial Lagrangian velocity correlation would be expected to decrease to negative values and then return to zero. This behavior is expected since the radial eddy diffusivity coefficient should decrease from its relatively constant value to a zero value at large times. Similarly, since the axial and tangential diagonal components of the diffusivity tensor,  $\langle z'(t)V_z'(t) \rangle$  and  $\langle r_\theta'(t)V_\theta'(t) \rangle$ , tend to a constant value for large times, the respective Lagrangian double velocity correlations should monotonically decrease to zero for large times. This appears to be the case for the



axial Lagrangian correlation, but not so for the tangential correlation  $\langle V'_\theta(t_0)V'_\theta(t) \rangle$  in Figure 4.24. Again there seems to be a statistical problem related to the tangential element of the data.

Off-diagonal components of the Lagrangian double velocity correlation tensor are given in Figures 4.25 to 4.27. The correlation between the radial and tangential velocity deviations,  $\langle V'_r(t_0)V'_\theta(t) \rangle$ , is zero as expected, Figure 4.27. The correlation between the axial and tangential velocity deviations,  $\langle V'_z(t_0)V'_\theta(t) \rangle$  in Figure 4.26, is not zero as would be expected from symmetry. Figure 4.25 gives the correlation between the axial and radial velocity deviations,  $\langle V'_z(t_0)V'_r(t) \rangle$ . The correlation begins at a positive value and decreases to zero for large times. This behavior can be explained as follows. If the radial velocity is positive the fluid particle would enter a flow region of lower mean axial velocity. Consequently, the axial velocity deviations would on the average be positive, resulting in a positive product of the velocity deviations. A similar argument applies for a negative radial velocity deviation.

The interrelationships between the three different types of correlations do appear to be satisfied from a detailed study of Figures 4.4 through 4.27. This can be viewed as a confirmation of the internal consistency of the computer program used to generate the various correlations.

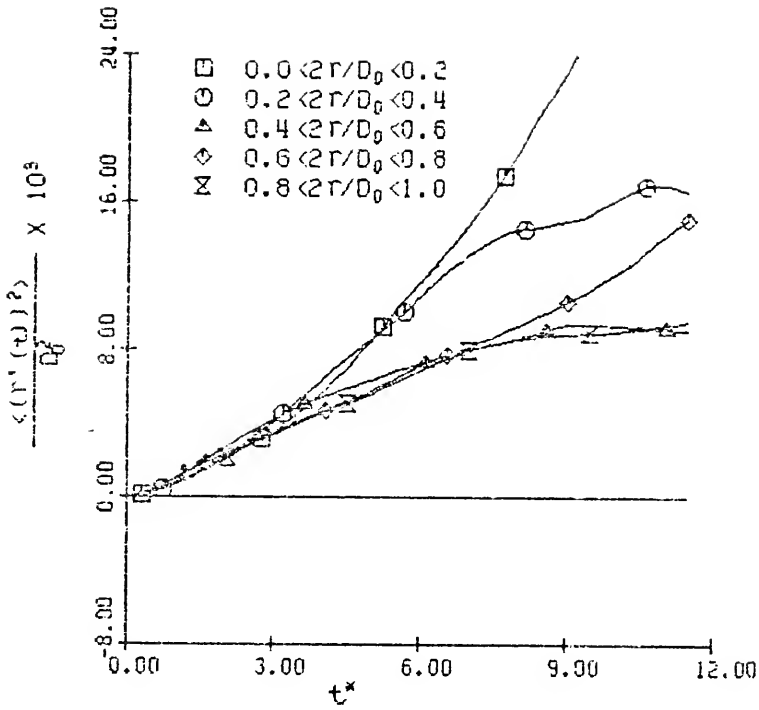


Figure 4.1  $\frac{\langle r^2(t) \rangle}{D_0^2}$  Versus  $t^*$

for All Radial Zones

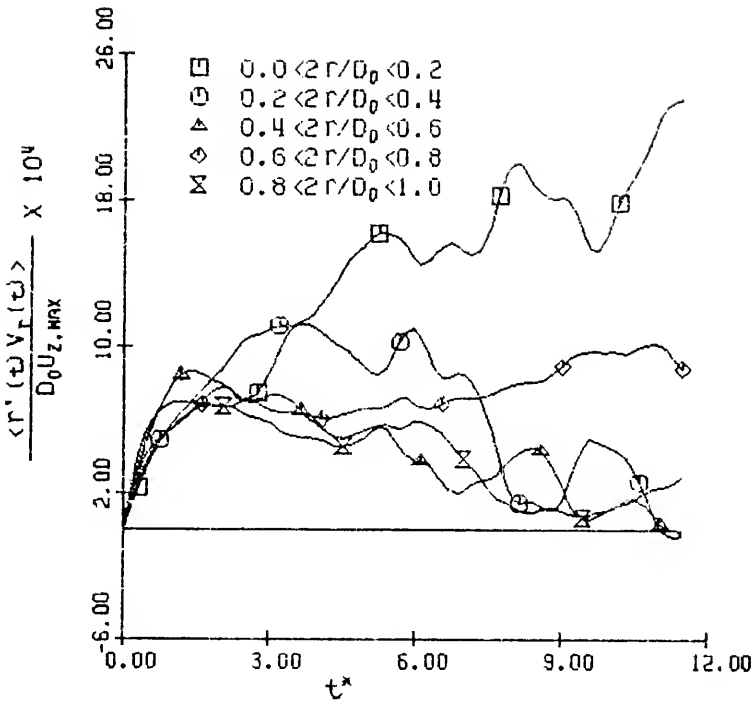


Figure 4.2  $\frac{\langle r'(\tau) v_r(\tau) \rangle}{D_0 u_{z, \max}}$  Versus  $t^*$

for All Radial Zones

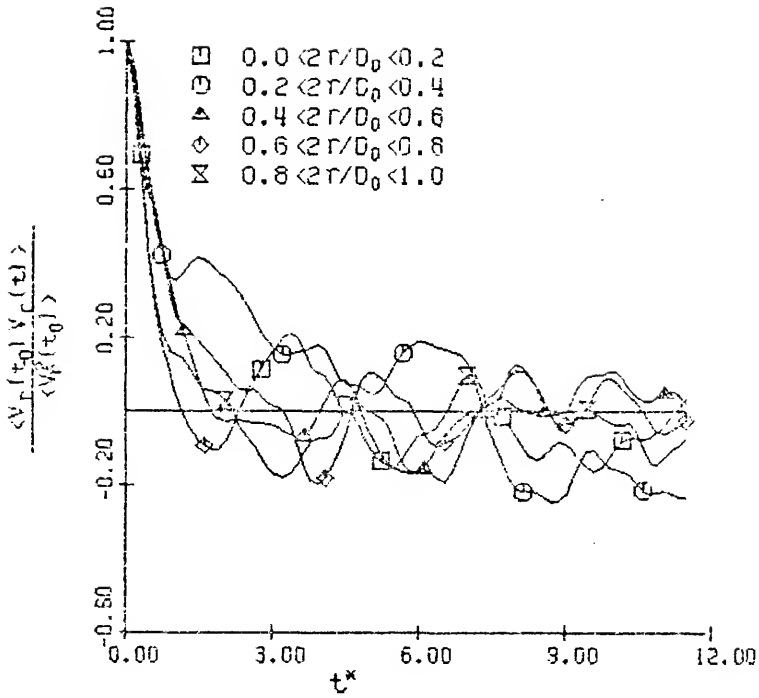


Figure 4.3  $\frac{\langle V_r(t_0) V_r(t) \rangle}{\langle V_r^2(t_0) \rangle}$  Versus  $t^*$   
for All Radial Zones

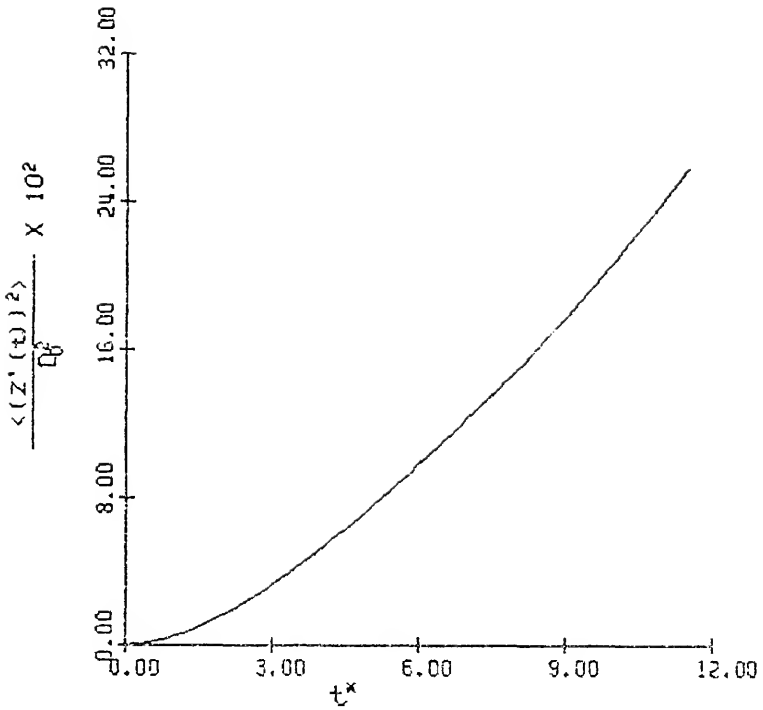


Figure 4.4  $\frac{\langle (Z'(t))^2 \rangle}{D_0^2}$  Versus  $t^*$

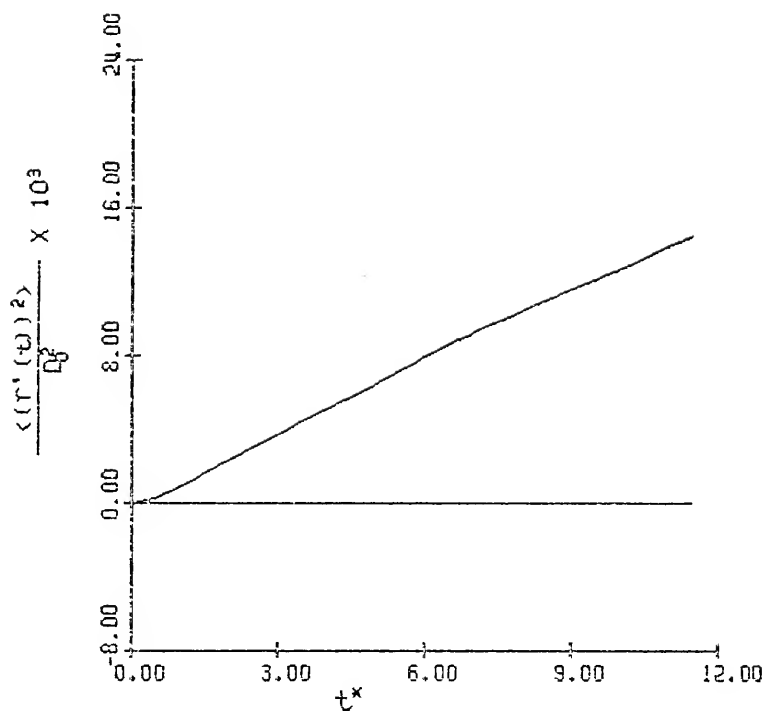


Figure 4.5  $\frac{\langle (r^*(t))^2 \rangle}{l_0^2}$  Versus  $t^*$

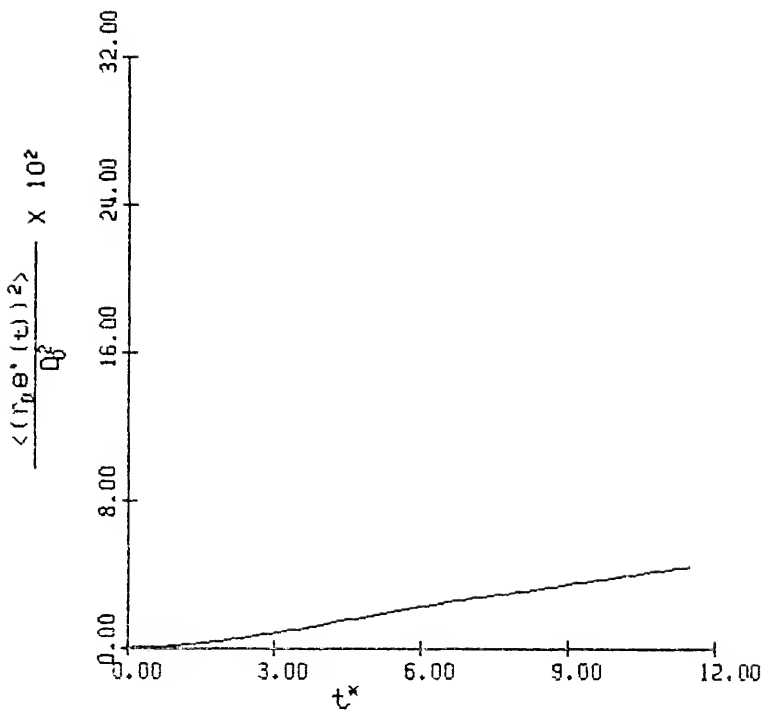


Figure 4.6  $\frac{\langle (\bar{r}_0 \Theta^*(t))^2 \rangle}{Q_0^2}$  Versus  $t^*$

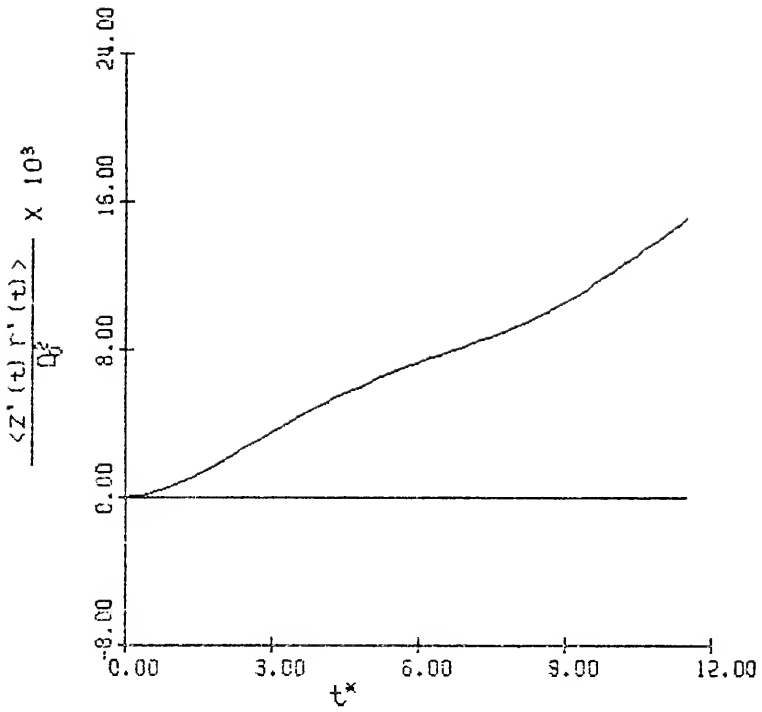


Figure 4.7  $\frac{\langle Z'(t) r'(t) \rangle}{Q_0^2}$  Versus  $t^*$



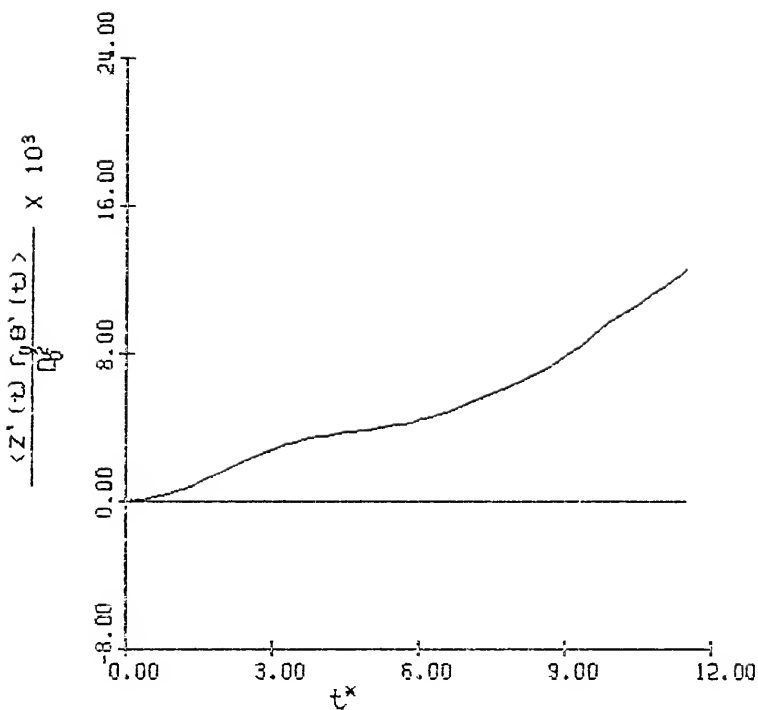


Figure 4.8  $\frac{\langle Z^*(t) r_{\beta} \theta^*(t) \rangle}{Q_0^2}$  Versus  $t^*$

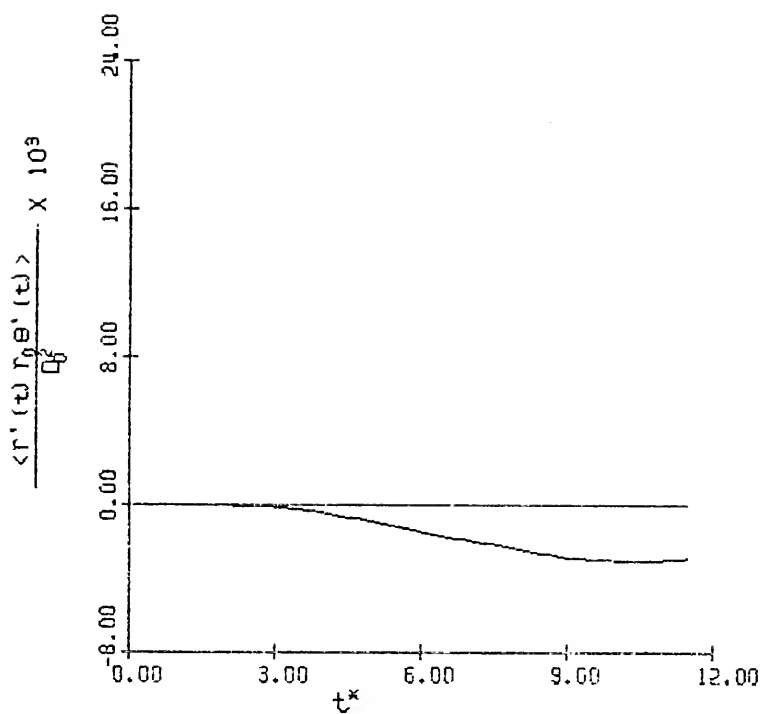


Figure 4.9  $\frac{\langle r^*(t) r_s^*(t) \rangle}{Q_0^2}$  Versus  $t^*$

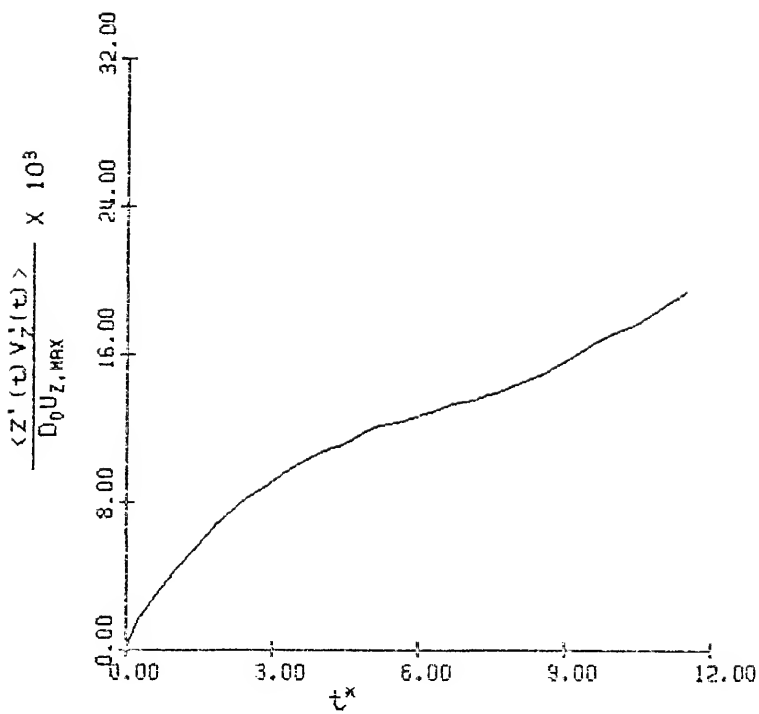


Figure 4.10  $\frac{\langle Z^*(t) V_z^*(t) \rangle}{D_0 U_{z, \text{MAX}}}$  Versus  $t^*$

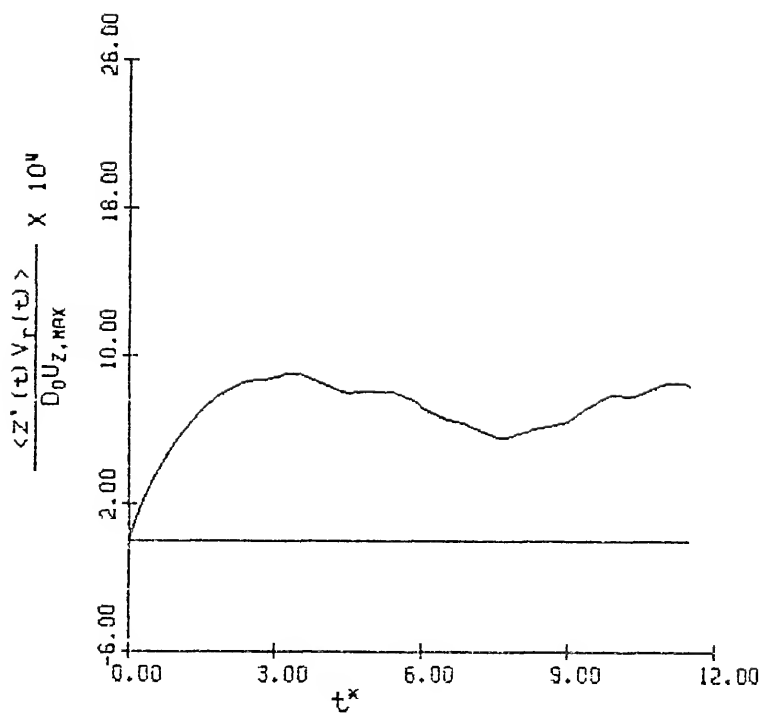


Figure 4.11  $\frac{\langle Z^*(t) V_r(t) \rangle}{D_0 U_{Z, \text{MAX}}}$  Versus  $t^*$

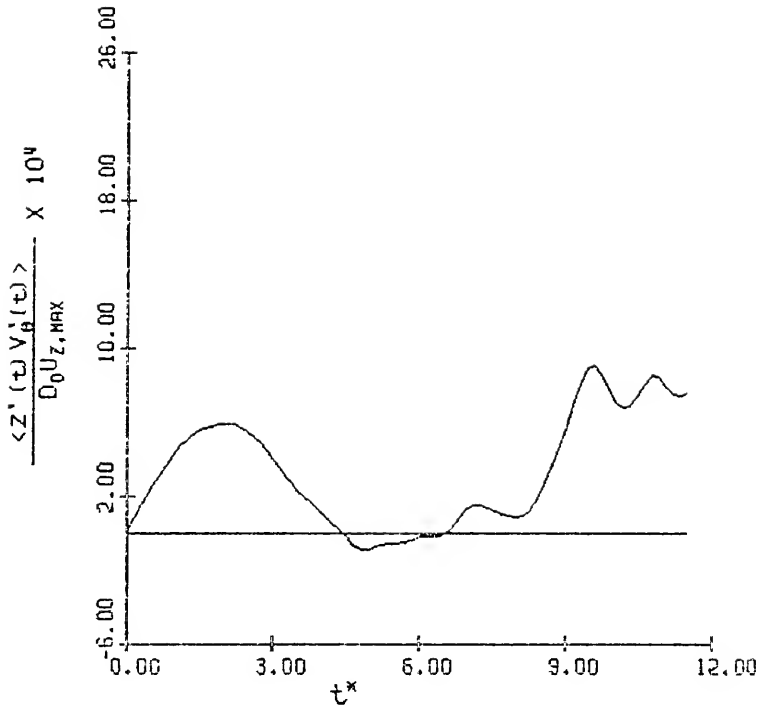


Figure 4.12  $\frac{\langle Z^*(t) V_6^*(t) \rangle}{D_0 U_{Z, \text{MAX}}}$  Versus  $t^*$

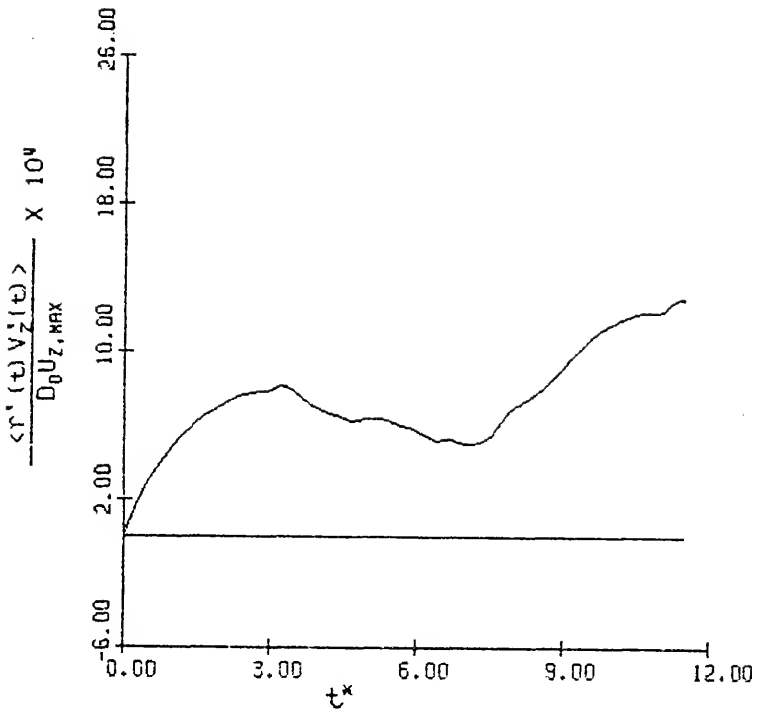


Figure 4.13

$$\frac{\langle v'_1(t)v'_2(t) \rangle}{D_0 U_{Z,MAX}} \text{ Versus } t^*$$

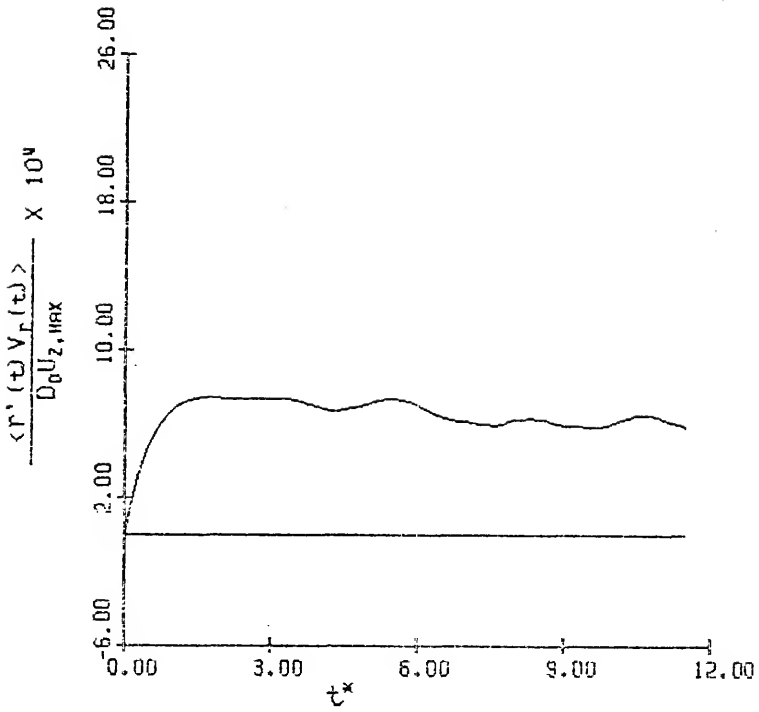


Figure 4.14  $\frac{\langle r'(\tau) v_r(\tau) \rangle}{D_0 U_{z, \max}}$  Versus  $\tau^*$

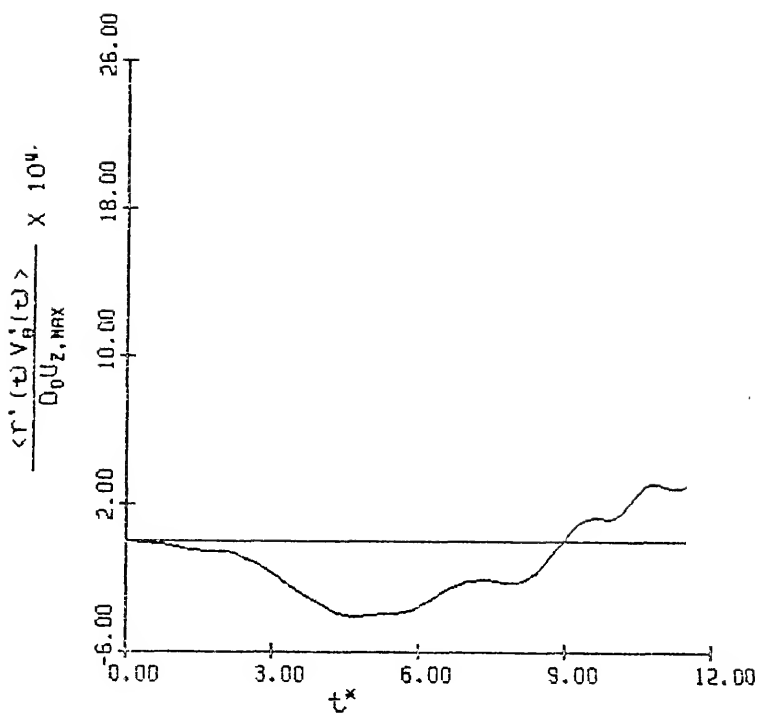


Figure 4.15

$$\frac{\langle r^*(t) V_a^*(t) \rangle}{D_0 U_{Z,MAX}}$$

Versus  $t^*$



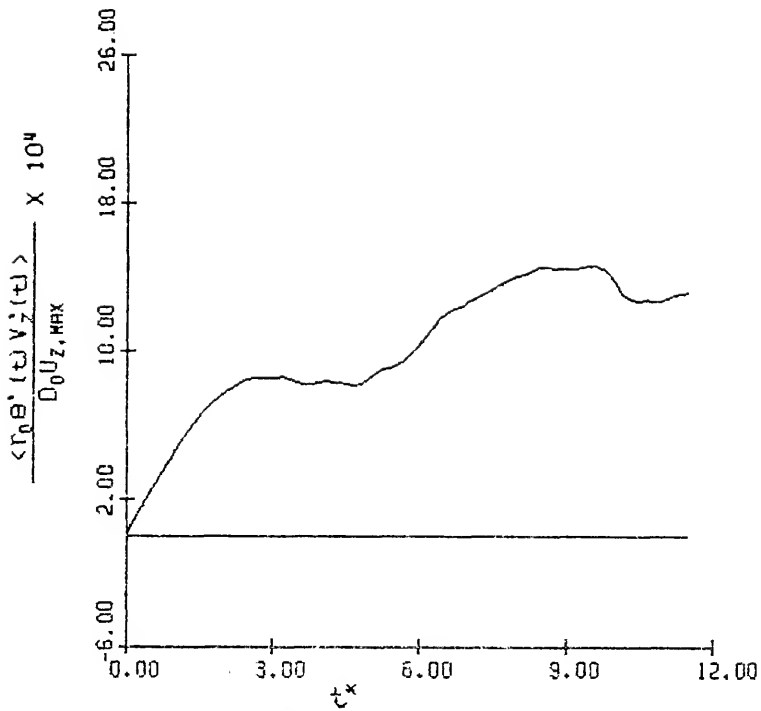


Figure 4.16  $\frac{\langle r_0 s'(t) v_z'(t) \rangle}{D_0 U_{z, \text{MAX}}}$  Versus  $t^*$

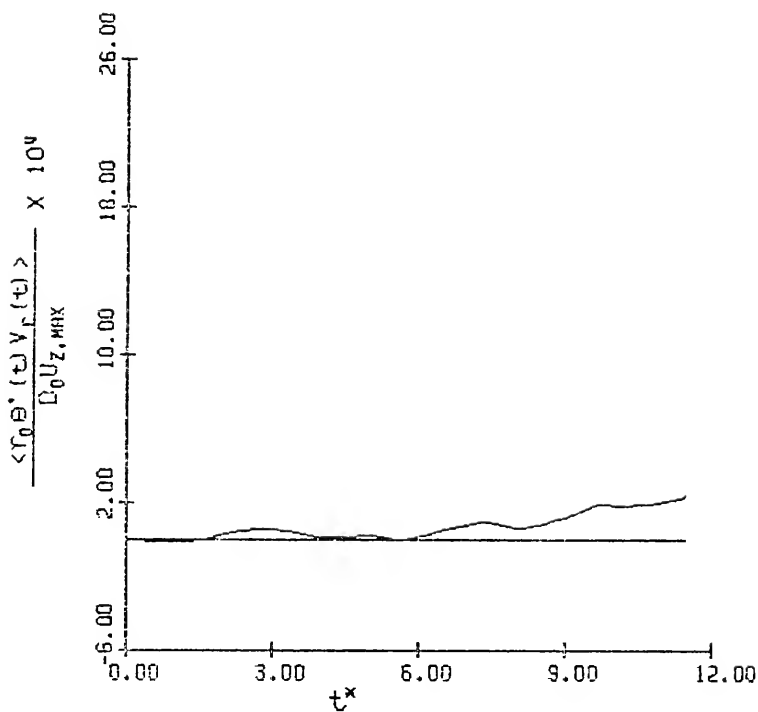


Figure 4.17  $\frac{\langle r_0 \theta' (t) v_r (t) \rangle}{U_0 U_{z, \max}}$  Versus  $t^*$

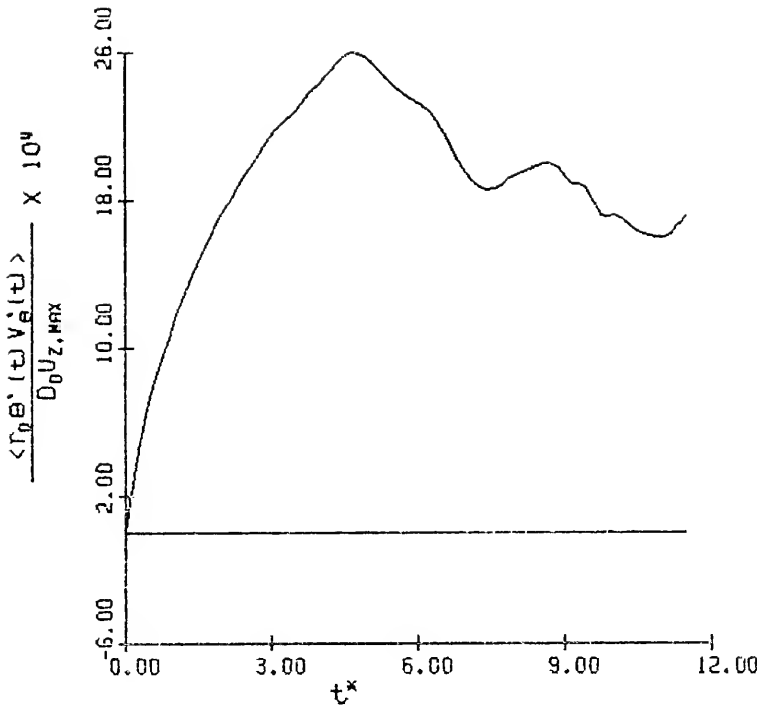


Figure 4.18  $\frac{\langle \Gamma_0 \Theta'(t) V_0'(t) \rangle}{D_0 U_{Z, \text{MAX}}}$  Versus  $t^*$

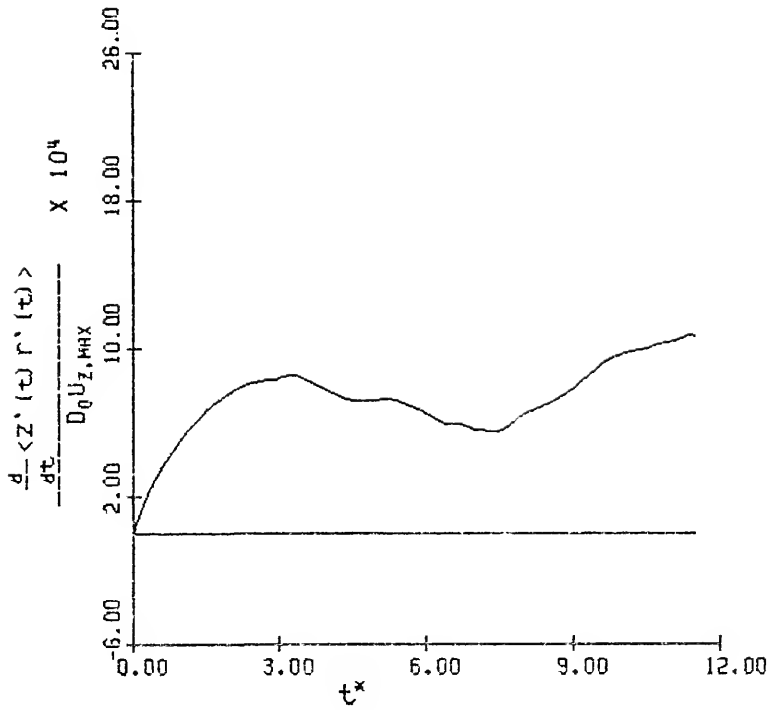


Figure 4.19  $\frac{d}{dt} \langle z'(t) r'(t) \rangle \frac{1}{D_0 U_{z, MAX}}$  Versus  $t^*$

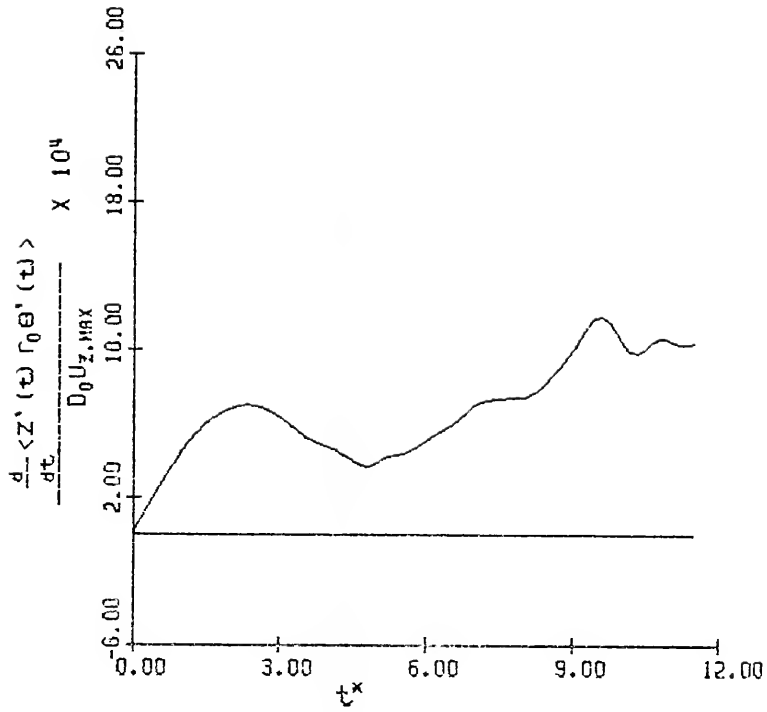


Figure 4.20  $\frac{\frac{d}{dt} \langle Z'(t) r_0 \Theta'(t) \rangle}{D_0 U_{Z,MAX}}$  Versus  $t^*$

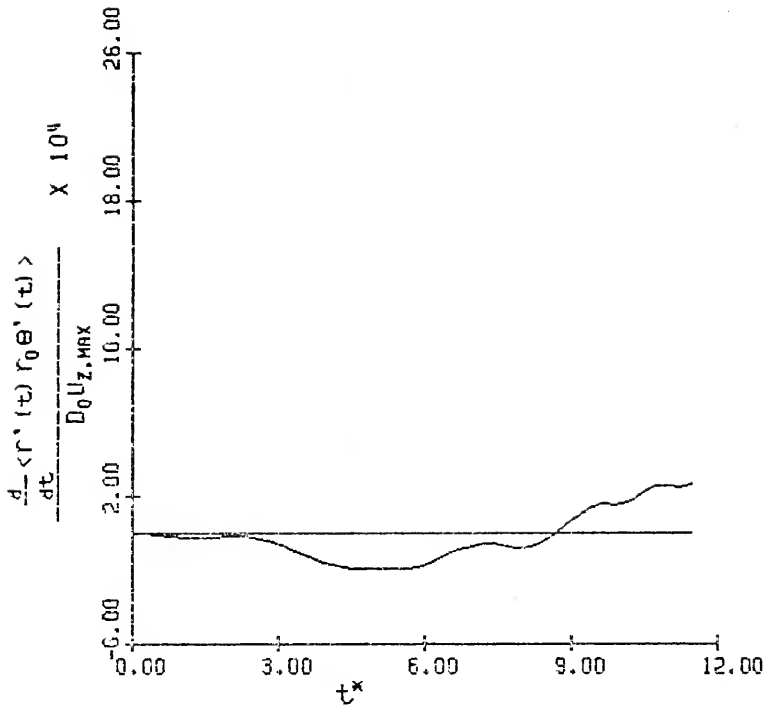


Figure 4.21  $\frac{d}{dt} \langle r^*(t) r_0 \theta^*(t) \rangle$  Versus  $t^*$   
 $D_0 U_{z, \text{MAX}}$

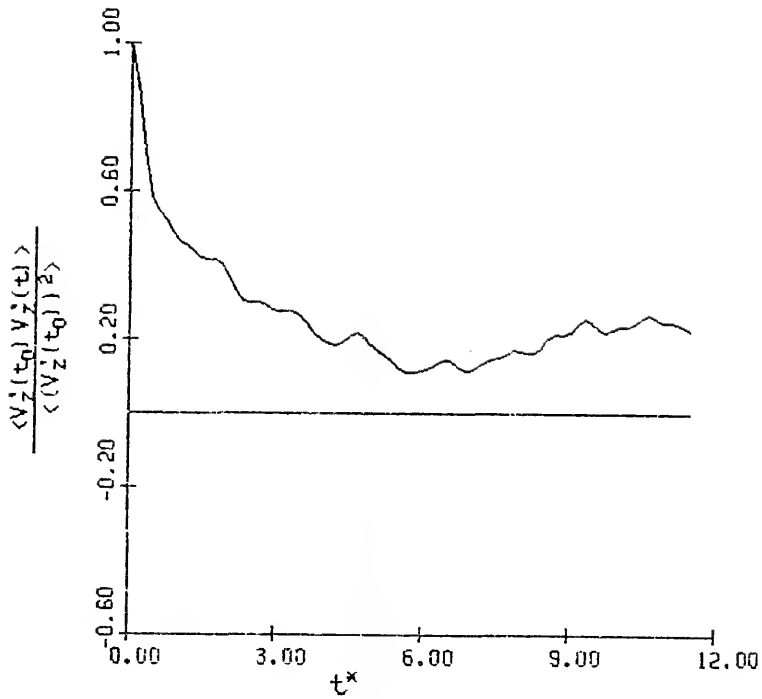


Figure 4.22  $\frac{\langle V_z^2(t_0) V_z^2(t) \rangle}{\langle (V_z^2(t_0))^2 \rangle}$  Versus  $t^*$

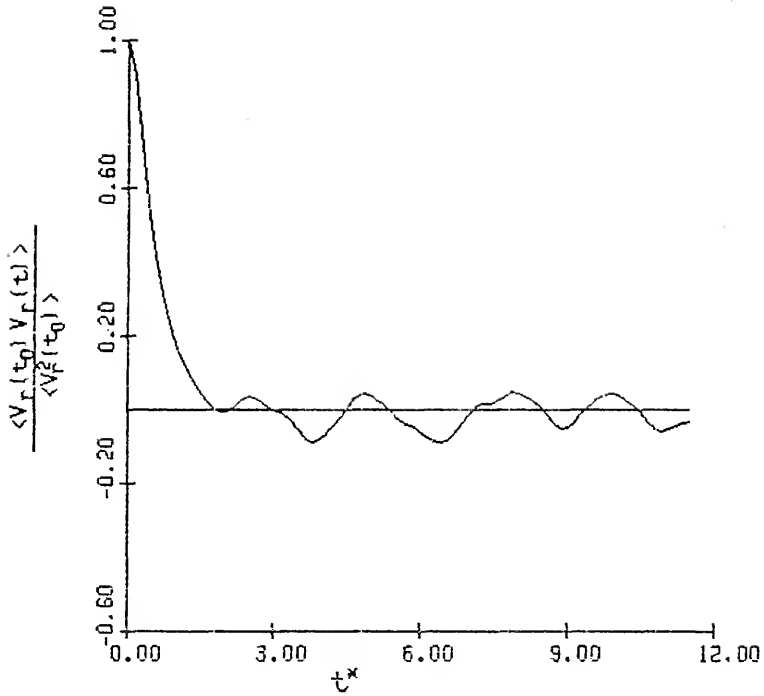


Figure 4.23  $\frac{\langle V_r(t_0) V_r(t) \rangle}{\langle V_r^2(t_0) \rangle}$  Versus  $t^*$



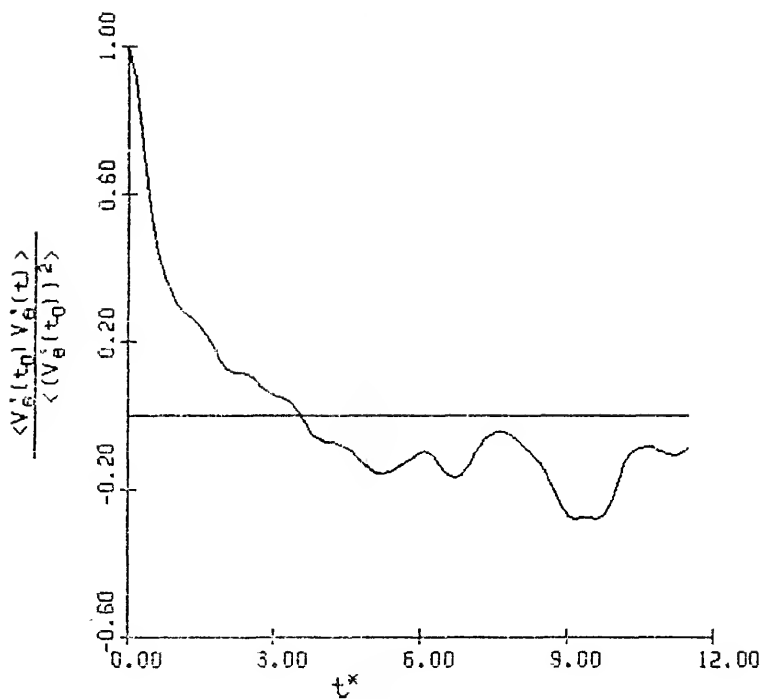


Figure 4.24

$$\frac{\langle V_a^i(t_0) V_a^i(t) \rangle}{\langle (V_a^i(t_0))^2 \rangle} \text{ Versus } t^*$$

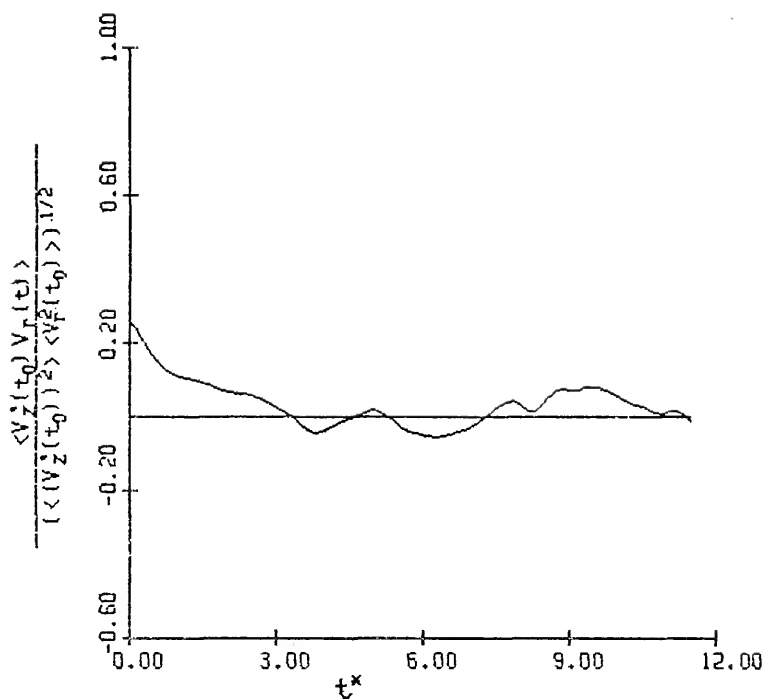


Figure 4.25  $\frac{\langle V_z^2(t_0) V_r(t) \rangle}{(\langle V_z^2(t_0) \rangle^2 \langle V_r^2(t_0) \rangle)^{1/2}}$  Versus  $t^*$

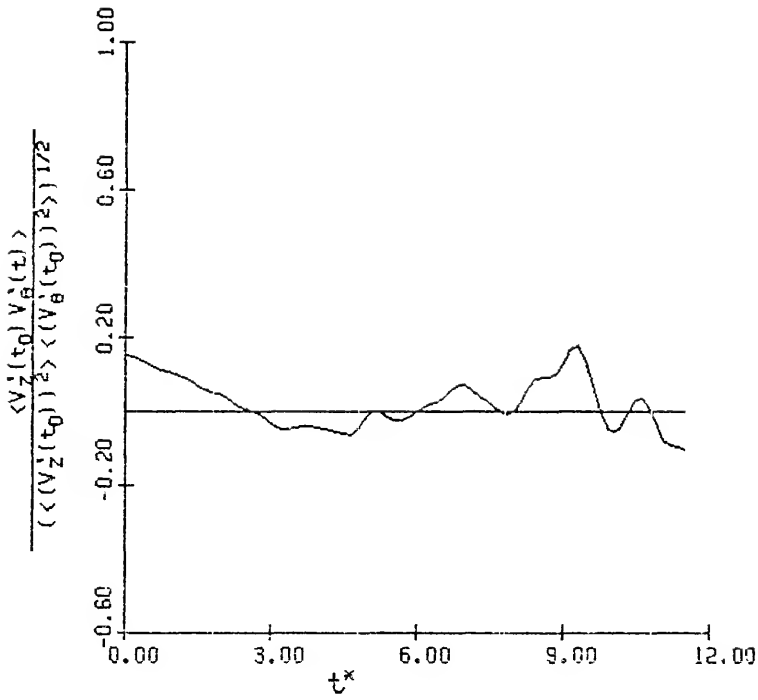


Figure 4.26  $\frac{\langle V_z^*(t_0) V_\theta^*(t) \rangle}{(\langle V_z^*(t_0) \rangle^2 \langle V_\theta^*(t_0) \rangle^2)^{1/2}}$  Versus  $t^*$

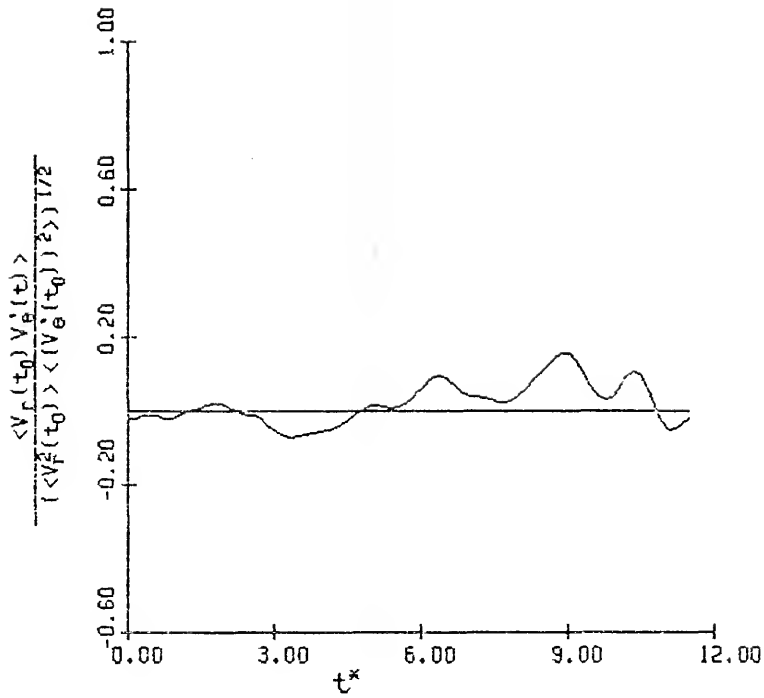


Figure 4.27

$$\frac{\langle V_r(t_0) V_b^*(t) \rangle}{(\langle V_r^2(t_0) \rangle \langle V_b^2(t_0) \rangle)^{1/2}} \text{ Versus } t^*$$

## 4.2 Equipment and Procedure

The equipment and procedure were effective in obtaining the desired data. Turbulent conditions were generated in the flow loop without abnormal or distorted flow patterns. The suspended particles were photographed and their positions were accurately determined from the photographs. Even though the quality of the photographs was not as good as desired, a particle could be followed continuously over tens of diameters of the flow tube.

Operation of the flow loop was satisfactory, and it is felt that fully developed turbulence was established within the observation section. No abnormal bulk flow characteristics were indicated from a close examination of the particle path data. In addition, visual observations of the overall flow of the illuminated particles revealed no abnormal flow patterns within the observation section. The flow rate was determined using a rotameter calibrated with the process fluid, trichloroethylene. The temperature was also measured to within  $\pm 1^\circ\text{F}$ . The measured flow rate was  $0.52 \pm 0.01$  liter/sec ( $8.3 \pm 0.2$  GPM) which corresponds to an average velocity of  $1.04 \pm 0.03$  meters/sec ( $3.41 \pm 0.06$  ft/sec). Using an equation form developed by Pai (1953) for the mean velocity profile, a least-squares fit to the particle velocity data yielded an average velocity of 0.969 meter/sec (3.18 ft/sec). The exact equation used

for the mean velocity profile will be discussed later. The Reynolds number computed from the above data is 110,000, a flow condition well within the turbulent region of fluid flow.

Steady flow conditions were maintained during the photographing of the suspended particle motion. Because the flow system was closed, the heat generated from pumping caused an increase in fluid temperature relative to the room temperature. Sufficient time was allowed in order to reach a steady fluid temperature. After the flow rate was adjusted, the rotameter float position varied only slightly corresponding to a flow rate difference of  $\pm 0.01$  liters/sec ( $\pm 0.2$  GPM). The particle injection rate was adjusted so that approximately 10 to 20 particles visibly passed through the observation section within a 10-second period. After due preparation, the film was loaded into the camera and the shutter opened for approximately seven seconds to expose the film. The 7-second exposure time was sufficient to obtain an image of the pipe without over-exposing the film. Images of the pipe walls were possible because of the light being scattered from dirt particles on the pipe wall and slight differences between the refractive indices of the TCE, glass pipe, and the glycerin surrounding the pipe (see Section 3.1.1 for a description of the pipe enclosure).

The combined optical geometry and the photographing technique provided photographs from which consistent data were obtained. Care was taken during the construction of the camera and camera support to obtain a trueness of the optical geometry. The angle between the glass plates of the pipe enclosure was adjusted so that the glass plates coincided with the edges of a squaring tool. Also the right angle of the angle-iron on which the lense assemblies were mounted was checked for squareness. In support of the trueness of the optical geometry, no distortions were noticed in the images registered on the film.

The photographic quality of the particle images was not as good as was hoped. A fully automated tracking algorithm using a PDP-11 minicomputer was tried but was abandoned because the approach required excessive time. Extraneous images and a varying background light intensity required time-consuming scans by the algorithm to establish the particle track position. Consequently, an algorithm was employed using the minicomputer to data-log coordinate positions which were located manually. The extraneous images were present because of scratches on the glass pipe and dirt and dust particles which were ever present in the work area and would settle on the glass plates of the enclosure. The light intensity available for forming track images on the film varied because of forward scattering of

light from the hollow glass beads. Within any given frame of film, the particle images were the darkest at positions nearest the light source. For many of the particle tracks photographed, the images of the particle paths were not detectable over a sufficient length of the frames to match up tracks on the adjacent frames. If the above two problems could be eliminated, a less time-consuming computer data collection algorithm could be implemented. The extraneous images could be reduced by polishing the surface of the glass pipe to remove scratches and by moving the apparatus into a more controlled environment. The particle images can be enhanced in several ways; increased light intensity, use of a more reflective particle, and use of a more harsh developer. The latter two are probably the more promising. A possible reflective particle which was not tested is titanium oxide. Other Kodak developers which could be tested are HC-110 and D-19.

#### 4.3 Data Collection and Analysis

Reliable coordinate data on particle positions in time were extracted from two photographed views of the flow loop using a PDP-11 minicomputer. The coordinate data collected from the two views for a given particle track were merged together to yield the three-dimensional Cartesian coordinate points of the particle path. These



coordinate points were then converted to cylindrical coordinates from which the Lagrangian correlations were generated.

As was mentioned earlier, since the quality of the photographic images was not as good as desired, a manual data-logging algorithm was used. The projected image from the photo-enlarger yielded a total magnification varying from 2.9 to 3.7. The objects which were farthest from the glass-air interface were magnified the least. The voltage from the D/A unit of the PDP-11 minicomputer ranged from -10 volts to +10 volts with a resolution of 1/1024 volts. The calibration of the X-Y recorder was set at 2 volts/inch. This combination of image magnification, volt resolution, and voltage scale provided a length resolution of  $\pm 0.0001$  meter ( $\pm 0.005$  inch). However, due to hysteresis in the recorder carriage positioning mechanism and errors in manual positioning, the accuracy of the position data was about  $\pm 0.0002$  meter ( $\pm 0.01$  inch). A particle path's image was a dashed line in which the dash was about three times longer than the space between dashes, i.e. about 0.768 fraction of the track was visible. This fraction was computed from the blade area of the light chopping disk. Since corresponding views of a given segment of the flow tube were projected simultaneously, corresponding points on a given track could be measured at the same time. All measured points from

corresponding frames, along with datum points, were stored on punched paper tape, and then the data were transferred to magnetic tape for use with an IBM/370 computer. The larger IBM/370 computer was used to transform the two 2-dimensional views of the flow tube into a 3-dimensional cylindrical coordinate system. The coefficients of the transforming equations for each frame were computed as discussed in Section 3.2.1. These equations were then used to compute the coordinates of the desired points on the particle paths. The longitudinal distance was taken as the average obtained from the two views. The standard deviation of the differences between the corresponding longitudinal distances computed from the two views is 0.0002 meter (0.01 inch). Position and time coordinates for a section of a typical particle path are given in Table 4.3. Also in Figure 4.28,  $r-\theta$  data for all the tracks are presented graphically. As can be seen from Figure 4.28 even though the particles are less dense than the trichloroethylene, they do not tend to collect at the top of the pipe.

The data were smoothed to give a uniform time period and to generate velocity data. Smoothing was accomplished using a least-square fit of eight points of a particle path to a fourth-order polynomial. The eight points were centered around the point to be smoothed.

Top of Pipe

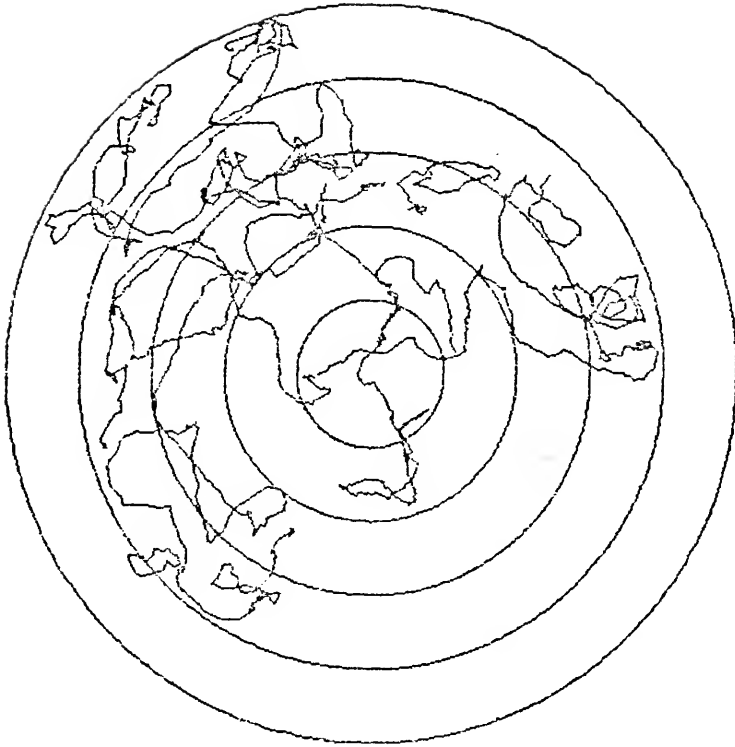


Figure 4.28      Projection of the Particle Paths onto  
the  $r$ - $\theta$  Plane

Table 4.3 Typical Particle Path Coordinates

Time, msec	Coordinates of Particle Position		
	Radial, inch	Tangential, radians	Axial, inch
0.00	0.407	1.359	3.551
4.72	0.406	1.367	3.636
6.16	0.395	1.333	3.790
10.88	0.390	1.317	3.837
12.32	0.377	1.242	3.992
17.04	0.374	1.218	4.042
18.48	0.363	1.161	4.218
23.20	0.359	1.155	4.269
24.64	0.342	1.151	4.430
29.36	0.337	1.146	4.479
30.80	0.319	1.111	4.642
35.52	0.312	1.099	4.693
36.96	0.290	1.036	4.870
41.68	0.286	1.019	4.926
43.12	0.283	0.983	5.117
47.84	0.283	0.977	5.175
49.28	0.282	0.958	5.365

Since the points of the particle paths were taken as the end points of the dashed segments of the particle's image on the film, these points were not distributed uniformly in time. Therefore during the smoothing step, the particle positions were computed for a uniform time period of 3.08 milliseconds, i.e. half the time period of the dashes. The velocities of the particles were also computed for each time using the derivative of the fourth-order polynomial generated from the least-square fitting.

Using a discrete fast Fourier transform of the data, the equivalent convolution function,  $g(t)$ , for the least-square smoothing technique was examined. The effective convolution function is shown in Figure 4.29. The function shown in the figure was computed from the data of one track, but it is typical of the functions examined for each of the tracks. As would be expected, the shape of the curve indicates that only those points near the point being smoothed contribute to the smoothing. Since eight time intervals were used in the smoothing and they were centered around the point being smoothed, the function is expected to have a zero value for times greater than four time intervals. From Figure 4.29 the function goes to zero after three time intervals. This indicates that the smoothing technique placed nearing all the weight on only five time intervals, the point itself and two points on each side of it. Figure

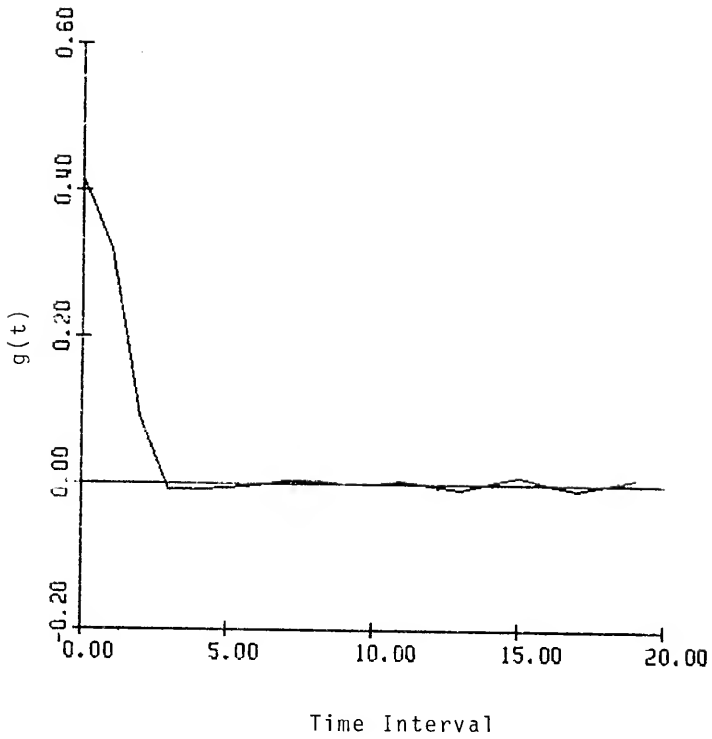


Figure 4.29      Equivalent Convolution Function for the  
Least-Square Smoothing

4.30 shows the discrete Fourier transform of the function,  $G(f)$ , where  $f$  is the frequency. Note that the smoothing reduces the high frequency content of the data. This was not considered detrimental in the analysis since the particle path images were slow varying curves and better estimates of the particle velocities were obtained than by finite differencing of the experimental position data. Also, the smoothing enhanced the manipulation of the data by making it possible to compute the position of the particles with a uniform time interval.

The deviation of the axial velocity was computed as the difference between the actual velocity and a mean velocity determined from a mean velocity profile equation. The mean axial velocity profile was established using an equation form suggested by Pai (1953). A least-square fit of the instantaneous axial velocities to the following equation form

$$\frac{U}{U_{z,MAX}} = 1 + a_1 \left(\frac{r}{r_0}\right)^2 + a_2 \left(\frac{r}{r_0}\right)^{2m} \quad (4.1)$$

yielded the following parameters

$$a_1 = -0.3626$$

$$a_2 = -0.6374$$

$$m = 75$$

$$U_{z,MAX} = 1.20 \text{ meters/sec (3.93 feet/sec)}$$

$$U_{z,AVE} = 0.969 \text{ meter/sec (3.18 feet/sec)}$$

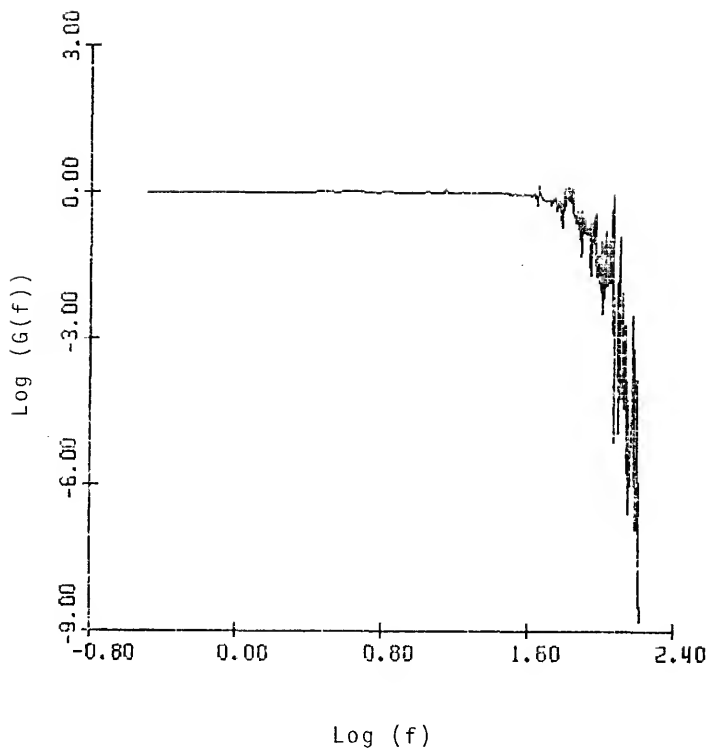


Figure 4.30      Energy Spectra Function for the Equivalent  
Convolution Function



Averaged velocities for 50 equally spaced radial intervals are plotted in Figure 4.31 along with the fitted equation.

From a statistical viewpoint, the correlations obtained in this study should be viewed cautiously since a minimal of data were used in generating the correlations. However, even though only seven particle tracks were examined, approximately 1600 particle positions were used in the correlations. The number of paths used in the correlations is not the sole consideration in examining the statistical accuracy of the data. Jenkins and Watts (1969) note that the covariance function of a stochastic process may be estimated with arbitrarily small error from a single, sufficiently long record. For the covariance function, the average over one infinite record is equivalent to an ensemble average, and hence the covariance function is said to be ergodic.

As seen in Figures 4.22 through 4.24, the period over which the velocity deviations are correlated is rather small, about 3 dimensionless time units. This time corresponds to 20 time intervals of the experiment. In a rough statistical interpretation, the 1600 particle positions may be considered equivalent to 80 independent particle paths having a 20-time-interval length. As the path length is increased, the number of equivalent, independent paths decreases. In view of this, the values of

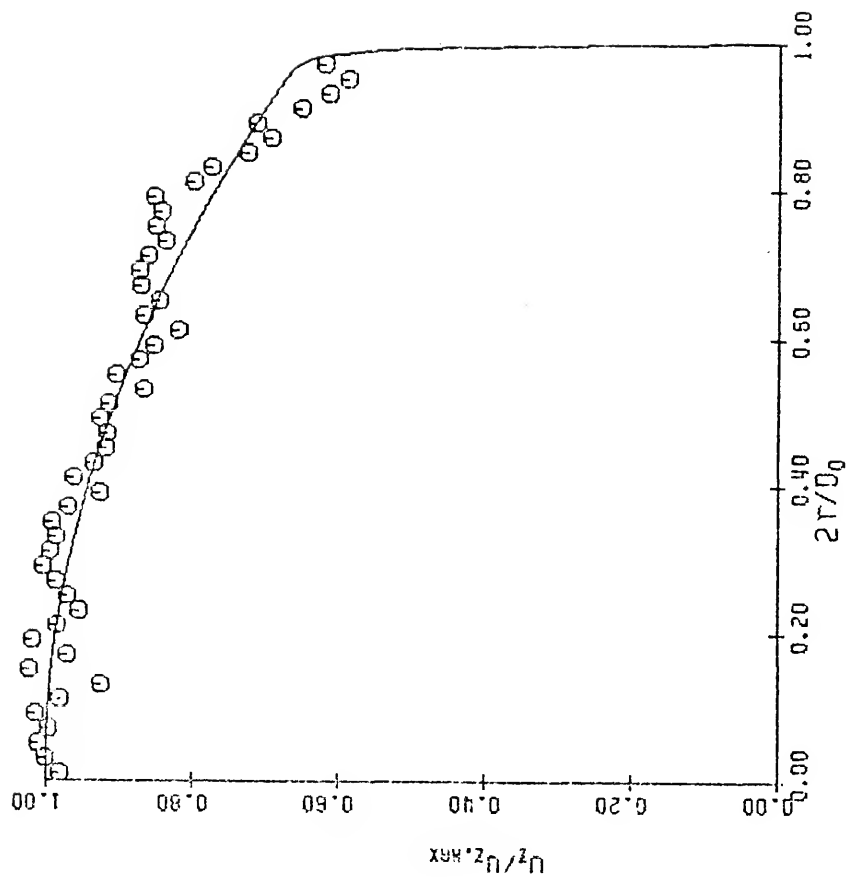


Figure 4.31 Mean Axial Velocity Profile

the correlations are most reliable near time zero and become less and less credible as the value of the time argument increases. This is also indicated by the number of contributions to the correlations for the different times, see Table 4.4.

In order to estimate the statistical error involved in the correlations, consider the following analysis of the axial dispersion correlation. For naturally occurring random variables, the normal distribution can be used to approximate the statistical distribution of their values (Jenkins and Watts, 1969). This fact can be explained by the central limit theorem, which states that the p.d.f. of the sum of  $N$  random variables tends very quickly to the normal form as  $N$  increases. This theorem applies to any form of the p.d.f. for the individual random variables. Therefore, assume the random variable  $z'(t)$  to be normally distributed with zero mean and  $\sigma^2$  variance. Note that  $\langle z'^2(t) \rangle$  is the sample variance of  $N$  measurements of  $z'(t)$ . Under these conditions, the random variable  $N\langle z'^2(t) \rangle / \sigma^2$  has a chi-square distribution with  $N-1$  degrees of freedom (Hogg and Craig, 1965). For large  $N$ , the distribution of  $(N\langle z'^2(t) \rangle / \sigma^2 - N) / \sqrt{2N}$  approaches a normal distribution with zero mean and unity variance. Now the probability that

$$-1.96 \leq (N\langle z'^2(t) \rangle / \sigma^2 - N) / \sqrt{2N} \leq 1.96 \quad (4.2)$$

Table 4.4 Number of Contributions to the Correlations

<u>Time, t*</u>	<u>Sample Size</u>	<u>Time, t*</u>	<u>Sample Size</u>
0.145	3186	5.809	2636
0.726	3126	6.535	2566
1.452	3056	7.261	2500
2.178	2986	7.987	2440
2.904	2916	8.713	2380
3.631	3846	9.439	2320
4.357	2776	10.166	2260
4.083	2706	10.892	2200

is 0.95. Equation (4.2) implies that

$$\sigma^2(1 - 2.77/\sqrt{N}) \leq \langle z'^2(t) \rangle \leq \sigma^2(1 + 2.77/\sqrt{N}) \quad (4.3)$$

is the 95% confidence interval for the axial variance. Approximating  $\sigma^2$  with the variance of the axial spread, i.e.  $\langle z'^2(t) \rangle$ , an estimated statistical error can be computed. The upper and lower bounds as estimated from the above analysis are shown in Figure 4.32 for  $\langle z'^2(t) \rangle$ .

As given in Section 2.1.1 for a time stationary process, the Lagrangian correlation tensor is symmetric about the zero elapsed time. Figure 4.33 through 4.36 show the Lagrangian double velocity correlations for selected components of the tensor for the fourth radial zone from the center of the pipe. This radial zone was selected because it contained the most contributions to its correlations. Symmetry for small elapsed times is expected because of the manner in which the correlations were computed from the data. However, symmetry of the diagonal components is quite noticeable even for large times. The off-diagonal component  $\langle V'_z(t_0) V_r(t) \rangle$ , shown in Figure 4.36 does not demonstrate the expected symmetry. If either of the curves were shifted vertically, the symmetry would be excellent. The reason for the offset is not apparent from a review of the path data.

The power spectra were computed for the three principal directions using a discrete fast Fourier transform

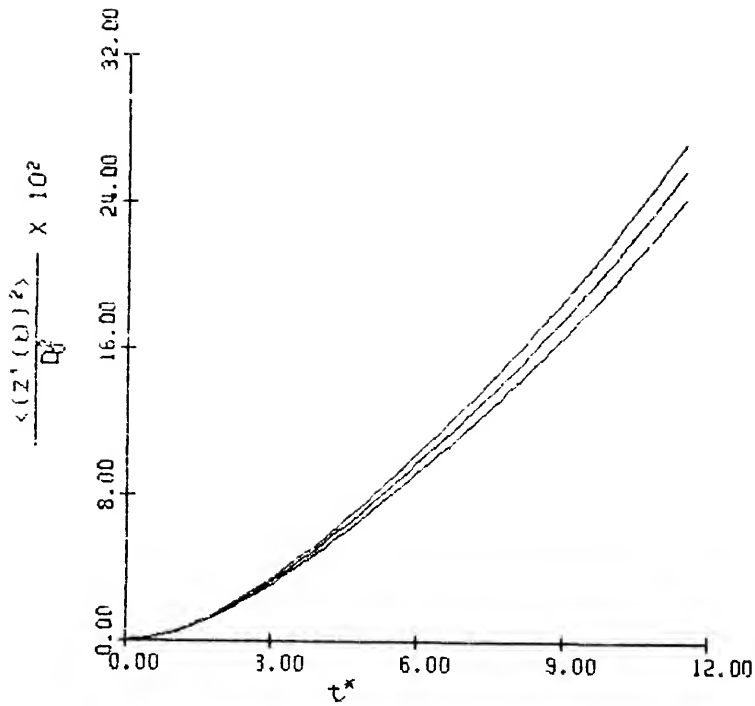


Figure 4.32 An Estimate of the Statistical Error  
for  $\langle (z'(t))^2 \rangle / D_0^2$

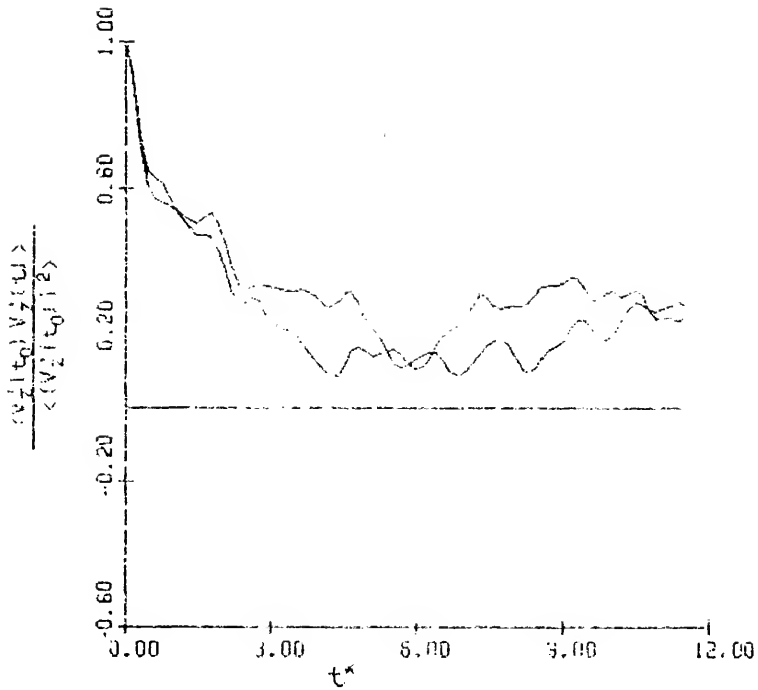


Figure 4.33 Time Symmetry in  $\frac{\langle V'_z(t_0)V'_z(t) \rangle}{\langle (V'_z(t))^2 \rangle}$  for the Fourth Radial Zone from Center of Pipe

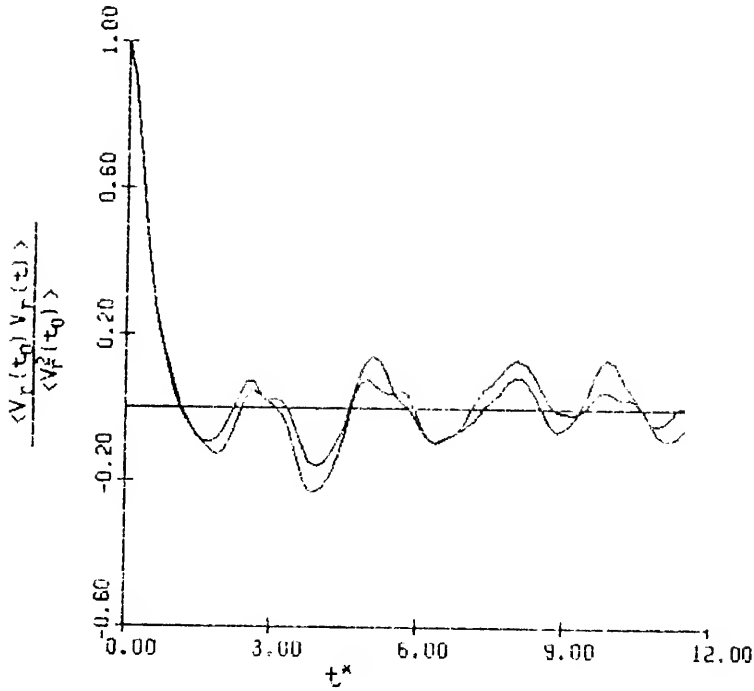


Figure 4.34 Time Symmetry in  $\frac{\langle V_r(t_0) V_r(t) \rangle}{\langle V_r^2(t_0) \rangle}$  for the Fourth Radial Zone from Center of Pipe



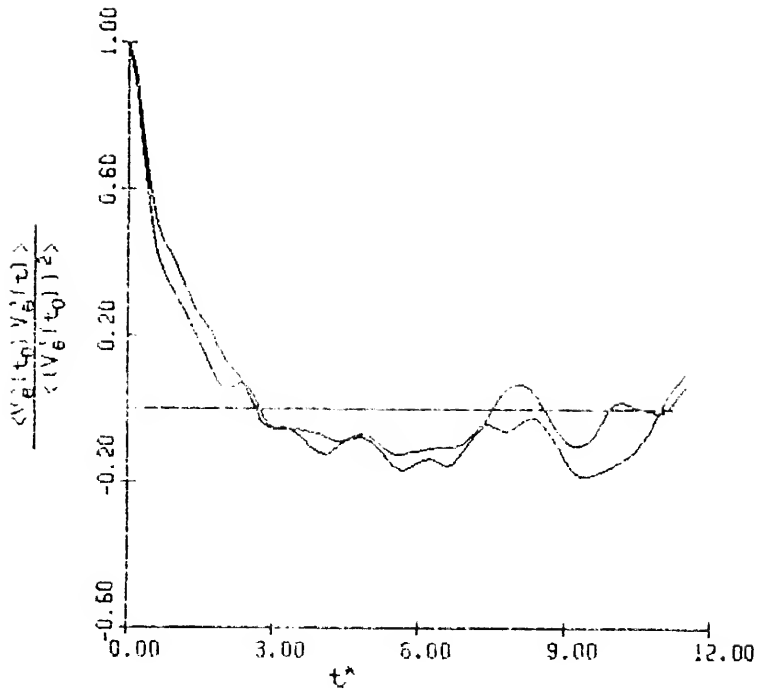


Figure 4.35 Time Symmetry in  $\frac{\langle v'_\theta(t_0) v'_\theta(t) \rangle}{\langle (v'_\theta(t))^2 \rangle}$  for the Fourth Radial Zone from Center of Pipe

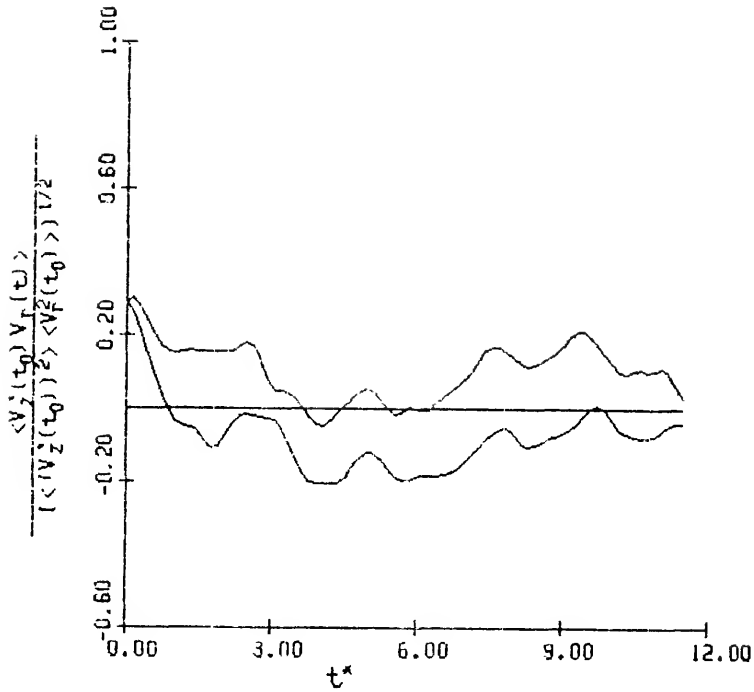


Figure 4.36 Time Symmetry in  $\frac{\langle v_z'(t_0) v_r(t) \rangle}{(\langle v_z'^2(t_0) \rangle \langle v_r^2(t_0) \rangle)^{1/2}}$   
for the Fourth Radial Zone from Center  
of Pipe

algorithm. The spectra were computed using the velocity data which were obtained from the smoothed particle position data. When applying the Fourier transform, the data are treated as though it were from a homogeneous process. As a consequence, detection of radial variations in the spectra is not possible. The energy functions for the three coordinate directions,  $F_z(f)$ ,  $F_r(f)$ , and  $F_\theta(f)$ , are shown in Figures 4.37 to 4.39 respectively, where "f" symbolizes the frequency. There is an appreciable amount of variation in the spectra which is probably because of the relatively small sample size. However, overall characteristics can be noted. From Figure 4.30, the contributions from frequencies above 100 cps would be drastically reduced by the smoothing technique. The Nyquist frequency for this data is 162 cps. A close examination of the power spectra shows that at 100 cps, the power function has decreased to about 0.01 of its original value. The power is distributed similarly for each of the principal directions. Decreases in the power of 4 orders of magnitude occur over a 2 decade change in frequency.

As shown in Hinze (1959), the velocity autocorrelation functions,  $R_z^{(F)}(t)$ ,  $R_r^{(F)}(t)$ , and  $R_\theta^{(F)}(t)$  are related to the energy spectra functions  $F_z$ ,  $F_r$ , and  $F_\theta$  respectively. The autocorrelation functions were computed by taking the inverse Fourier transforms of the energy spectra functions.

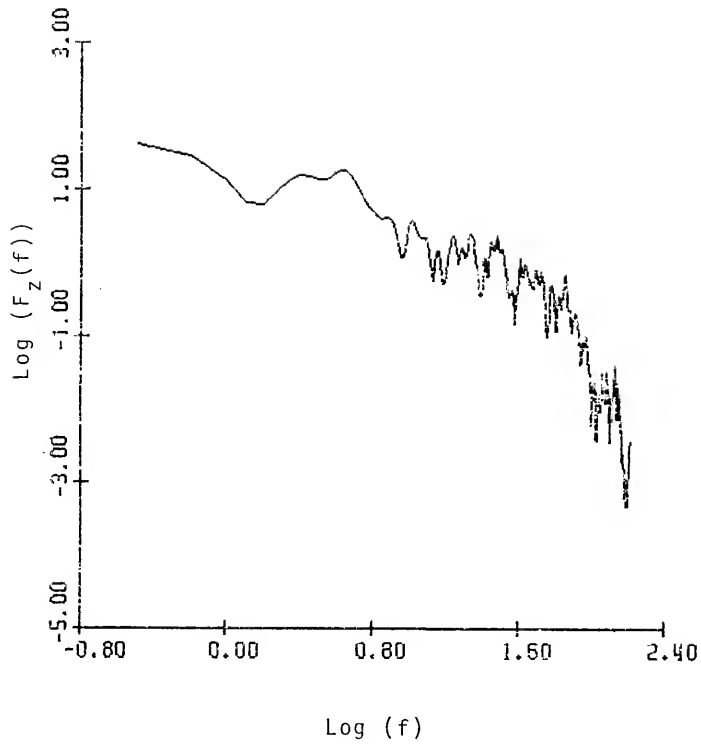


Figure 4.37      Axial Energy Spectra Function

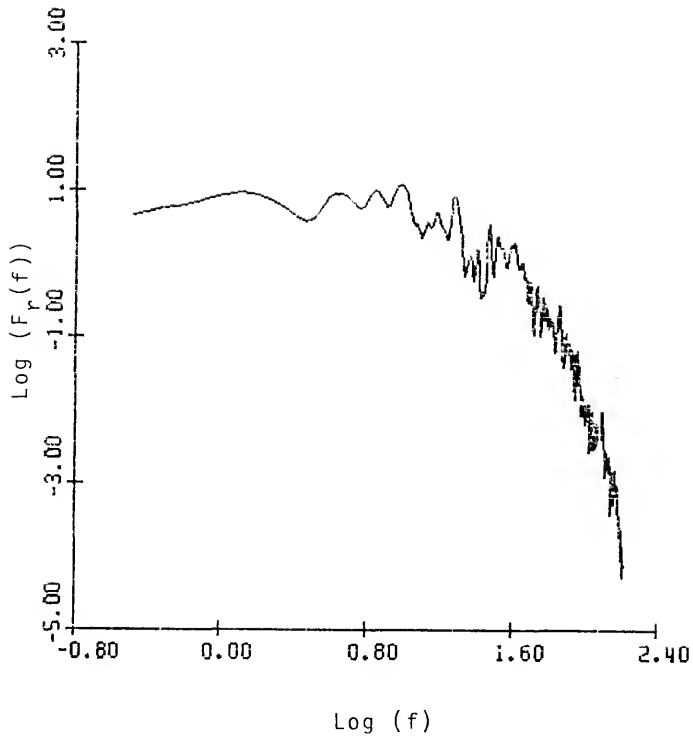


Figure 4.38 Radial Energy Spectra Function

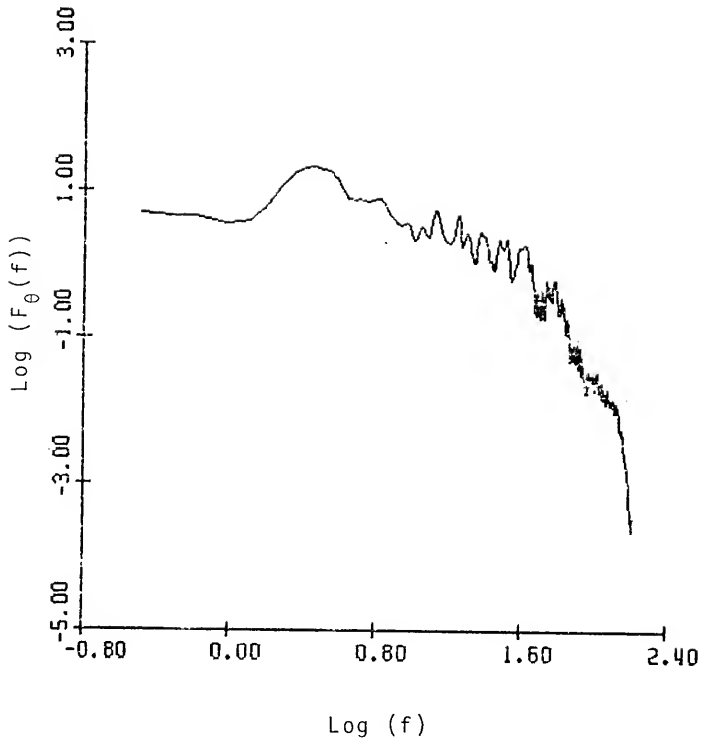


Figure 4.39 Tangential Energy Spectra Function

They are shown in Figures 4.40 through 4.42. In comparing these correlations with those computed with ensemble averages, Figures 4.22 through 4.24, excellent agreement is found. This is expected since in both methods the flow was considered to be homogeneous.

It has been noted in the results that most of the correlations involving the tangential direction have behaved unexpectedly. These correlations are the  $\langle z'(t)r_0\theta'(t) \rangle$ ,  $\langle r_0\theta'(t)V_z'(t) \rangle$ ,  $\langle r_0\theta'(t)V_\theta'(t) \rangle$ , and  $\langle V_z'(t_0)V_\theta'(t) \rangle$  given in Figures 4.8, 4.16, 4.18, and 4.26 respectively. The common reason given for this behavior was that the sample size was relatively small. Additional insight may be found for this behavior in the nature of the tangential displacement for particle paths passing near the center of the pipe. In particular, consider the tangential displacement for a particle path which coincides with a diameter of the pipe. The tangential displacement will be zero until the particle passes over the center of the pipe. After passing through the center, the displacement becomes  $2\pi r_0$ , where  $r_0$  is the starting radius for the path. Similar behavior in the tangential displacement would occur for particles which pass near the center. One such particle track was obtained from the experiment. If the positive contributions of this path to the above-mentioned correlations is not countered by equal negative contributions, the observed behavior could occur.

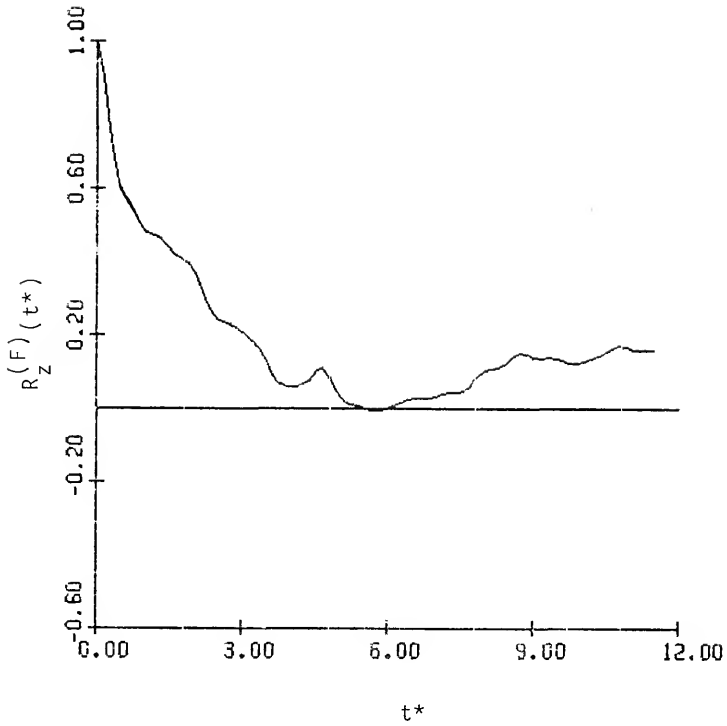


Figure 4.40      Axial Autocorrelation Function  
Obtained from the Axial Energy  
Spectra Function



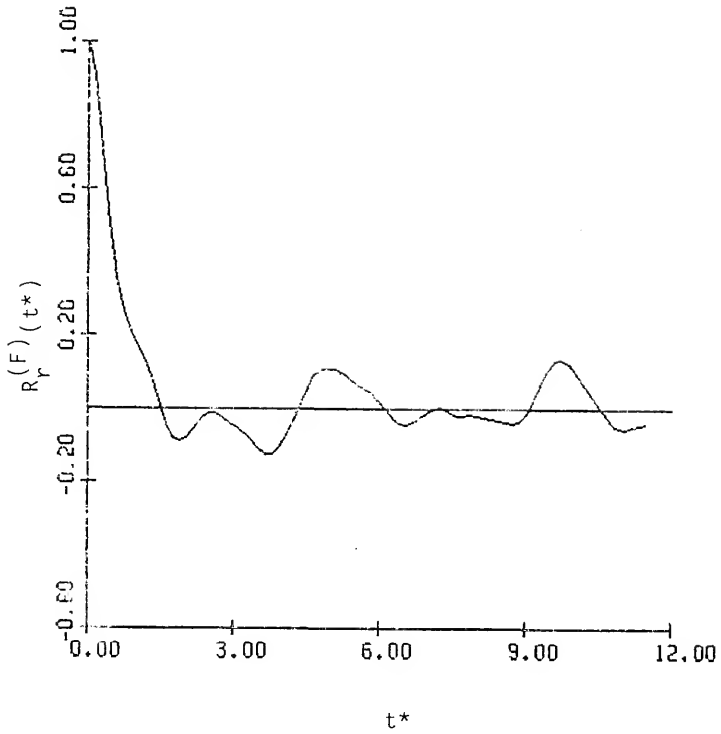


Figure 4.41 Radial Autocorrelation Function  
Obtained from the Radial Energy  
Spectra Function

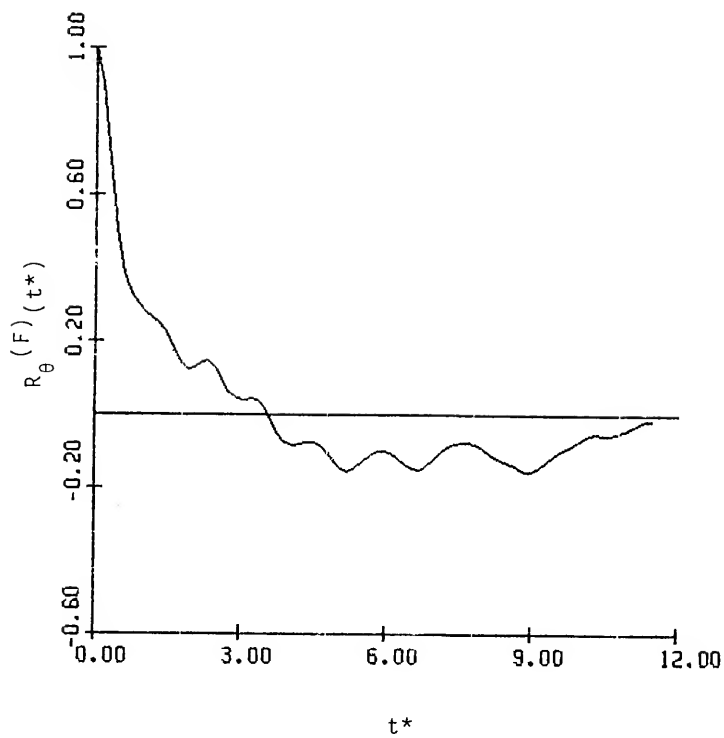


Figure 4.42      Tangential Autocorrelation Function  
Obtained from the Tangential Energy  
Spectra Function

It should also be noted at this time that the smoothed velocities for the tangential direction differed significantly from the tangential velocities computed by differencing consecutive time intervals of the particle tracks. The magnitude of the velocities computed from the smoothed data was several times larger than those velocities computed by differences. The correspondence between the smoothed and measured angles was excellent. Also velocities computed by the two methods for the other two directions were in good agreement. In view of the fair agreement between the two methods for the axial and radial directions, it was decided to use the smoothing technique to compute all the velocity components. The larger magnitude of the tangential velocities computed from the smoothed data would be expected to only increase the positive or negative values of the non-zero correlations.

In this chapter the various Lagrangian characteristics of turbulent pipe flow have been presented in the context of the results of the experiment. The overall results support and enforce certain concepts of the Lagrangian aspects of the flow field. The photographing technique developed in this investigation could be used with some improvements to generate additional particle path data with more ease. With additional studies of this type, a larger sample size could be accumulated; and consequently, the

statistical errors and uncertainties could be reduced. Lagrangian characteristics for a range of flow conditions could also be established. With minor changes in the equipment, drag reduction could be studied too.

## CHAPTER 5

### SUMMARY AND CONCLUSIONS

1. The motion of suspended particles in fully-developed turbulent pipe flow was experimentally observed. From a close examination of the images of the particle paths and visual observations of the flow, fully-developed turbulence appeared to be present in the flow loop at a Reynolds' number of 110,000.

2. A photographing technique was developed using black background illumination which enabled the photographing of the motion of suspended particles over large distances. Photographic images of particle paths were obtained for tens of pipe diameters. Even though photographic quality was not as good as desired, particle path images were contrasting enough to establish the particles 3-dimensional coordinate positions in time. The interrupted illumination of the particles was an effective method for embedding a time scale into the particle path images.

3. Lagrangian time correlations were computed from displacement and velocity deviations obtained from the particle trajectory data. Displacement-displacement, displacement-velocity, and velocity-velocity correlations were obtained.

4. The time dependence of the various correlations is apparent from close examination of the plotted correlations. The effect of a confining wall on the radial dispersion was visible at large times. Even though the radial eddy diffusivity coefficient is time-dependent, the rate of change of the correlation is small after a rapid initial increase from zero. Consequently, it appears the radial dispersion can be effectively modeled with a constant radial diffusivity coefficient.

## APPENDIX A

### DATA COLLECTION ALGORITHM

This appendix discusses the equipment used in obtaining data from the photographs and the algorithm for collecting the data. A general purpose real time BASIC, CHE BASIC, was developed and used for controlling the data collection equipment. A brief introduction will be given later to the computer language CHE BASIC. The form of the experimental data was photographs of paths of solid particles suspended in turbulent pipe flow. The form of the data needed for computational purposes was the coordinate positions of the suspended particles at sequential intervals of time. The particle paths were photographed from two perpendicular views in order to obtain the 3-dimensional coordinate position, see Figure 3.2.

Data were collected through the use of three pieces of equipment. A Digital Equipment Corp. PDP-11/20 mini-computer was used in conjunction with a Biesler photo-enlarger and a Moseley model 2D-2 X-Y recorder. The photo-enlarger was used to simultaneously project two photographic images of the perpendicular views. The images were focused

onto a plane surface of a board mounted on the pen carriage of the X-Y recorder. A visible point marked on the board will be called the congruent-point hereafter. The congruent-point could be moved at will by varying the input voltages to the X-Y recorder, thereby making it possible to match any point on a particle path segment.

In order to control the X-Y recorder and to measure the position of the congruent-point on the pen board of the recorder, an interface panel between the minicomputer and recorder was constructed. A schematic of the interface panel is given in Figure A.1. Both analog and digital signals were used to control the X-Y recorder. The position of the congruent-point could be controlled by analog signals, either manually from the interface panel or remotely from the minicomputer. With the toggle switch on the panel positioned at remote, a digital signal from the minicomputer was used to select the mode of operation. An "OFF" signal established manual mode and an "ON" signal established remote mode. If the toggle switch was in the manual position only manual operation was possible. The recorder pen position, up or down, was also controlled by a digital signal from the minicomputer, "OFF" for pen up and "ON" for pen down. A digital signal compatible with the digital input channels of the minicomputer could also be generated from the interface panel.

To ease the task of controlling the X-Y recorder with the analog and digital signals, a general purpose real-time



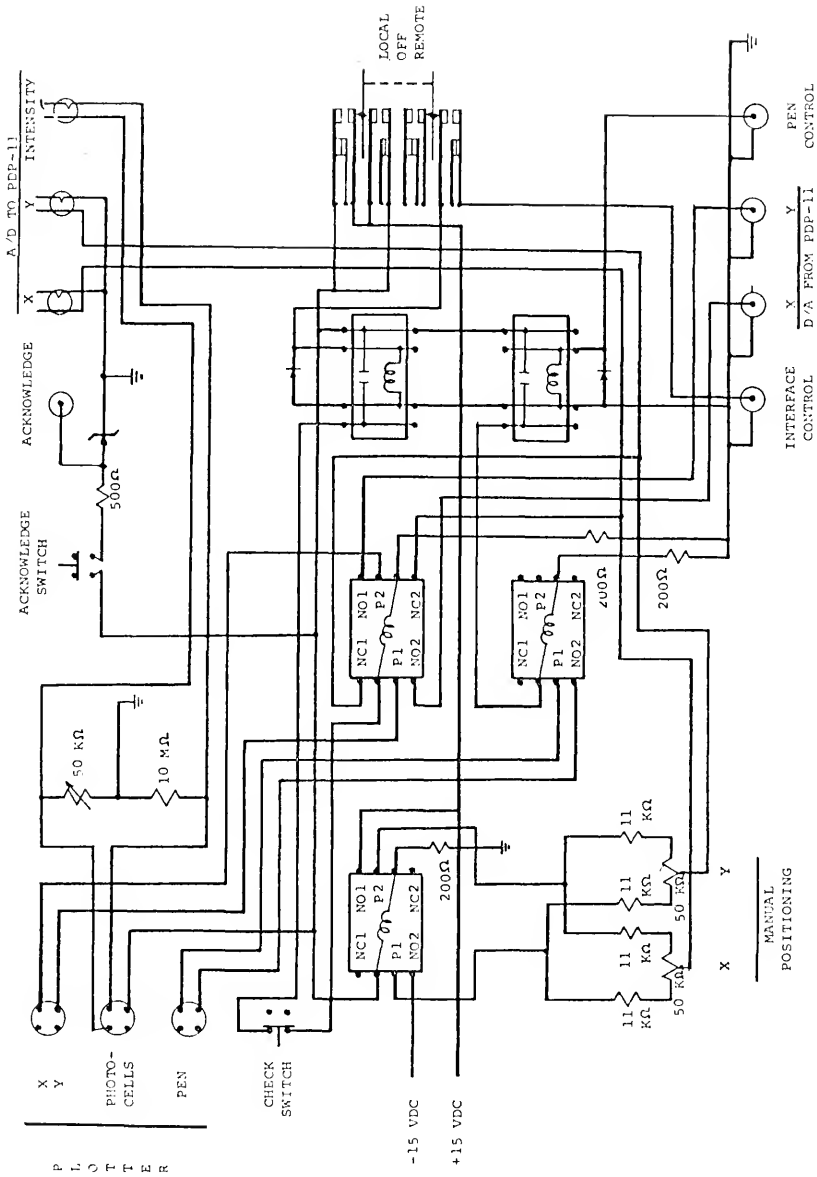


Figure A.1 Electrical Schematic of Interface between the PDP-11 Minicomputer and the Mosely X-Y Recorder

BASIC computer language was developed. Six new statements and five new functions were added to the PDP-11 1 of 8 USER BASIC so that BASIC programs could be written to input and output analog and digital signals to and from the computer. The additions were modeled after similar statements and functions in the Fischer Controls  $pc^2$  language. The language thus created is referred to as CHE BASIC. A programmer's manual has been prepared for easy user application of a real-time computer system.

The algorithm used for collecting the data not only incorporated the use of the above-mentioned equipment but also a CHE BASIC computer program listed at the end of this appendix. The computer program used two analog output channels, and one digital input channel. This program used only part of the total number of channels available on the PDP-11 computer. Initial attempts were made to automate the data collection algorithm using a photocell mounted on the pen board to detect the light intensity of the image. In order to establish the position of the track, excessive scanning of the image was required. In view of the relatively slow response of the equipment, the collection of data was very slow using a fully automated algorithm. Because of the slowness of the automated procedure, a more operator-oriented algorithm was used to collect the data. A flow diagram of the algorithm used is given in Figure A.2. A description of the algorithm follows:

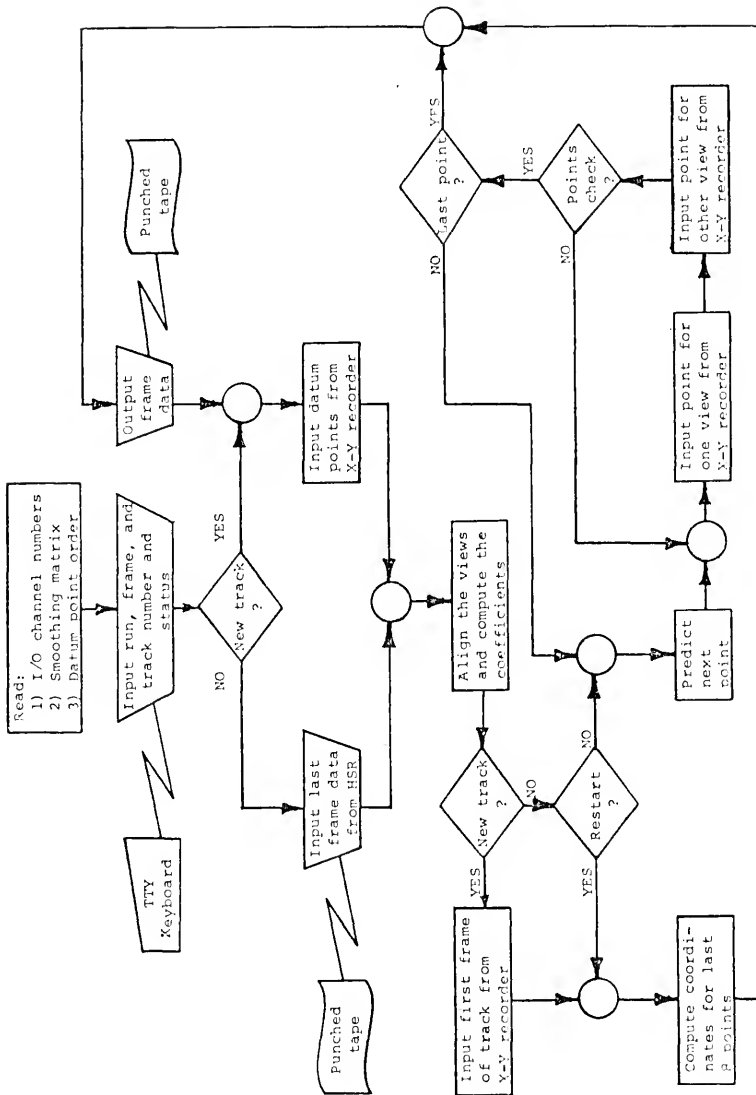


Figure A.2 Flow Diagram for Data Collection Algorithm

- (1) The following variables are read into the program;
  - a) Input/Output channel numbers for the analog and digital signals.
  - b) Correlating matrix for least-square fitting of data points.
  - c) Number sequence for order in which the datum points are to be read.
- (2) The program requests the following input from the keyboard of the teletype;
  - a) Run, Frame, and Track number
  - b) Status: 0 for new track, 1 for restart of old track
- (3) If starting a new track go to (6).
- (4) Input datum points and track points from previous frame. Use the high speed paper tape reader for input of data from previous frame.
- (5) Go to (7).
- (6) Datum points are input for current frame by positioning the congruent-point manually and pressing the acknowledge button. This is done for all 14 datum points shown in Figure 3.7.
- (7) From the datum point data align the views and compute the coefficients of Equation (3.7).
- (8) If not starting a new track go to (12).

- (9) Set switch register switch 1 of PDP-11 console to zero (down position). Position the congruent-point manually to correspond with a point of the new track in top view. When the acknowledge button is pressed, the coordinates of the point are read into the computer. The program then requests the corresponding point from the bottom view. At this point the program reads the position and computes the X position to correspond with the X position read for the top view and moves the carriage accordingly. By manually adjusting the vertical position, all possible vertical positions in the bottom view can be scanned. The X position can also be adjusted within a 2 inch span. When the appropriate point is found, press the acknowledge button. This point is read in and the program checks for agreement in the X coordinates read. If the X positions for the points of the two views do not agree within 0.015 inch, another point from the bottom view is requested. The first 4 track points are sequentially read into the computer in this manner. The remaining track points for the frame are predicted from the previous 2 points, displayed on the X-Y recorder, and manually adjusted to correspond to the projected points in the images. Pressing the acknowledge button initiates the reading of the adjusted point and the display of the predicted point for the other view. The

program will display the predicted point in alternate views for a given point until a change in the position of switch register switch 0 on the console is observed. At this time the program predicts and displays the next point unless switch register switch 1 is set to 1 (up position) in which case the reading in of points for the current frame is discontinued.

(10) Compute the coordinates in inches of the last 8 points of the current frame to be used to predict the first point of the track in the next frame.

(11) Go to (18)

(12) If a restart is in progress go to (10).

(13) Predict next point using correlating matrix and last 7 points.

(14) Display point on X-Y recorder in top view. Position switch register switch 1 to down position. Manually adjust position of congruent-point to match image.

(15) Press acknowledge button to initiate reading of point. If position of switch register switch 0 has changed go to (17).

(16) Display point on X-Y recorder in other view. Manually adjust position of congruent-point to match image.

Change position of switch register switch 0 if points of the views agree. If it is the last point of frame

position switch register switch 1 to 1 (up position).

Go to (15).

(17) If position of switch register switch 1 is down, go to (13).

(18) Output datum points and track point data for current frame on the low speed punch. Go to (6).

The BASIC computer program of the data collection algorithm is listed on the following pages.

```

1 REMARK *** THIS PROGRAM WAS WRITTEN TO COLLECT DATA
2 REM      DISPLAYED ON A X-Y RECORDER. THE PEN CARRIAGE
3 REM      POSITION OF THE RECORDER IS CONTROL BY VOLTAGE
4 REM      SIGNALS FROM THE PDP-11 MINICOMPUTER,
5 REM      D/A CHANNELS Y1 AND Z1
101 REMARK *** A1  A2  A3  D1  D2  D3  Y1  Z1
102 DATA      1,   2,   0,   0,   1,   0,   1,   0
105 REMARK *** CORRELATING MATRIX
106 DATA -.01458767, .06793961, -.01815699, -.1073415
107 DATA -.02588002, .4729543, .5910213 .03589145
108 DATA .002071306, -.01449972, .01055905, .01685078
109 DATA -.007939577, -.03570045, .03539776, .5991604
115 REMARK *** ORDER OF DATUM POINTS
116 DATA 2,3,6,5,4,0,1,0,1,4,5,6,2,3
150 REMARK *** DEFINITION OF FUNCTIONS USED IN PROGRAM
151 DEF FNA(J)=D(J,K+1-2)+D(J,K+1-1)-D(J,K+1-3)
152 DEF FND(K)=2*K-4*INT(K/2)-1
153 DEF FNC(I)=F(L,1)/FND(FNR(I))
154 DEF FND(X)=SQP(1.19*X+20)
155 DEF FNE(X)=X+2-B*INT((X+2)/8)
158 DEF FNI(I)=2*INT((I-1)/2)+1
168 DEF FNR(I)=(F(K-1,1)*F(K-1,1)+F(K,1)*F(K,1))*C(J,6)
169 DEF FNS(K)=(A(0,K)*A(0,K)+A(1,K)*A(1,K))*C(0,6)
170 DEF FNT(K)=(A(2,K)*A(2,K)+A(3,K)*A(3,K))*C(1,6)
200 DIM A(3,1),B(1,5),C(1,9),D(3,30),DO(3,30)
201 DIM F(7,6),T(1,7),X(2,9),Y0(J),N(1),E(1,5)
209 REMARK *** READ I/O CHANNEL NUMBERS
210 READ A1,A2,A3,D1,D2,D3,Y1,Z1
211 REMARK *** READ CORRELATING MATRIX
212 FOR I=0 TO 1
214 FOR J=0 TO 7: READ T(1,J): NEXT J: NEXT I
219 REMARK *** READ ORDER OF DATUM POINTS
220 FOR I=0 TO 1
222 FOR J=0 TO 6: READ E(1,J): NEXT J: NEXT I
224 REMARK *** REQUEST RUN, FRAME,
225 REM      AND TRACK NUMBER, AND STATUS
226 PRINT "INPUT FRAME DATA: R0,F0,J0,I0";
227 INPUT R0,F0,J0,I0
228 PRINT: IF I0 GO TO 700
230 REMARK *** INPUT FRAME DATUM POINTS FROM X-Y RECORDER
231 PRINT "DATUM POINTS FOR FRAME";F0;
232 PRINT ", RUN";R0; ", TRACK";J0; "."
233 CONTACT D1 TO 0: CONTACT D2 TO 1
234 FOR J=2 TO 0 STEP -2
236 FOR K=0 TO 6: GOSUB 1100
238 LET F(J,E(J/2,K))=Z: LET F(J+1,E(J/2,K))=Y: GOSUB 1005
240 NEXT K: PRINT: PRINT: NEXT J
250 REMARK *** ALIGN THE VIEWS, I.E. ROTATE AXIS AND CENTER
252 FOR J=0 TO 2 STEP 2: LET Y0(J)=0: LET Y0(J+1)=0
254 LET Z0=ATN((F(J+1,3)-F(J+1,0))/(F(J,3)-F(J,0)))
256 LET C(J/2,7)=ATN((F(J+1,2)-F(J+1,1))/(F(J,2)-F(J,1)))
257 LET C(J/2,7)=(Z0+C(J/2,7))/2
258 FOR K=0 TO 6: LET S1=-C(J/2,7)

```



```

260 LET Z=F(J,K): LET Y=F(J+1,K): GOSUB 1200
262 LET F(J+4,K)=Z: LET F(J+5,K)=Y: IF K>3 GO TO 270
268 LET Y0(J)=Y0(J)+F(J+4,K): LET Y0(J+1)=Y0(J+1)+F(J+5,K)
270 NEXT K
272 LET Y0(J)=Y0(J)/4: LET Y0(J+1)=Y0(J+1)/4
274 FOR K=0 TO 6: LET F(J+4,K)=F(J+4,K)-Y0(J)
276 LET F(J+5,K)=F(J+5,K)-Y0(J+1): NEXT K: NEXT J
278 REMARK *** COMPUTE THE COEFFICIENTS OF THE COORDINATE
279 REM          TRANSFORMATION EQUATIONS.
280 FOR J=0 TO 1: LET K=2*J+5: LET L=K
282 LET C(J,0)=(F(K,0)+F(K,3)-F(K,1)-F(K,2))/2
283 LET C(J,6)=1/C(J,0)/2
284 LET C(J,1)=(FNC(0)+FNC(3)-FNC(1)-FNC(2))/2
286 LET C(J,4)=(2*J-1)*F(K,6): LET C(J,5)=(2*J-1)*FNC(6)
288 LET L=K-1: LET C(J,2)=F(L,6)-F(L,4)
290 LET C(J,3)=FNC(6)-FNC(4): NEXT J
291 FOR J=0 TO 1: LET B(J,2)=1/C(J,1)-1/C(J,3)
292 LET B(J,0)=C(J,0)/C(J,1)-C(J,2)/C(J,3)+C(1-J,5)/C(1-J,3)
294 LET B(J,1)=C(J,4)-C(J,2)*C(J,5)/C(J,3): NEXT J
300 FOR J=0 TO 1: LET K=2*J+4
302 LET B(J,3)=B(0,0)*L(1,0)-B(J,1)*B(J,2)+B(1-J,1)*B(1-J,2)
304 LET B(J,4)=B(J,3)*B(J,3)+4*B(0,0)*B(1,0)*B(J,1)*B(J,2)
305 LET B(J,4)=SQR(B(J,4))
306 LET C(J,2)=(B(J,4)-B(J,3))/(2*B(J,0)*B(J,1))
308 LET C(J,4)=B(J,1)*C(J,2)+C(J,5)/C(J,3)
310 LET C(J,3)=(1/C(J,2)-C(J,0))/C(J,1)
312 LET C(J,0)=(2*J-1)*(C(J,4)*F(K,6)/F(K+1,6))
314 LET C(J,5)=10*C(J,2)/C(0,2): LET K=2*J
316 LET C(J,3)=(F(K+1,0)-F(K+1,1)-F(K,6)+F(K,4))
318 LET C(J,9)=F(K+1,0)-F(K+1,1)-(F(3-K,0)+F(3-K,1))*C(J,9)
317 LET C(J,9)=F(K+1,0)-F(K+1,1)-(F(3-K,0)+F(3-K,1))*C(J,9)
318 LET C(J,8)=2*C(J,3): NEXT J
320 LET Z2=INT(1.5*F0+1.25): LET B0=10: IF I0 GO TO 390
321 REMARK *** INPUT TRACK POINTS FOR 1ST FRAME
322 PRINT "INPUT 1ST 4 POINTS": LET Z3=F: LET Y2=0: LET Y3=0
324 FOR K=0 TO 2 STEP 2: LET J2=0
326 FOR J=0 TO 1: LET Z=Z3: LET Y=Y2: GOSUB 1010
328 LET M=SWR(1): LET L=2*M: LET Z3=Z: LET Y2=Y
330 LET D(L,K+J)=Z: LET D(L+1,K+J)=Y
332 LET Y=Y3: GOSUB 1210
334 LET D(2-L,K+J)=Z: LET D(3-L,K+J)=Y: LET Y3=Y: GOSUB 1050
336 LET X0=A(L,J): LET X1=A(3-L,J)
337 LET X2=A(L+1,J): GOSUB 1150
338 LET X0=A(L,J)-A(2-L,J): PRINT X0,
339 IF ABS(X0)>0.015 GOTO 332
340 PRINT: NEXT J: NEXT K: PRINT
346 PRINT "TRACK END POINTS": REMARK *** NOW GET 'EM ALL
348 PRINT: PRINT "UPPER FRAME", "LOWER FRAME"
350 FOR K=0 TO 30 STEP 2
352 FOR I=0 TO 1: IF K GE 4 GO TO 358
354 GOSUB 1262
356 GO TO 360
358 FOR J=0 TO 3: LET D0(J,0)=FNA(J): NEXT J: GOSUB 1250

```

```

360 NEXT I: GOSUB 1050
362 FOR I=0 TO 1: PRINT A(0,I);A(2,I);A(1,I);A(3,I): NEXT I
364 IF NOT(SWR(2) AND (K LT 6)) GOTO 386
365 PRINT CHR$(7);: WAIT 1000: GOTO 384
366 IF SWR(2)=0 THEN NEXT K
370 REMARK *** COMPUTE COORDS IN INCHES OF LAST 8 POINTS
371 REM      OF FRAME
372 LET K0=FNI(K+1): LET J2=0: LET J1=4: LET J3=3
374 FOR K=K0-7 TO K0 STEP 2: GOSUB 1050
376 LET J2=J2+2: NEXT K
378 LET J2=6: IF I0 GO TO 570
380 LET K=K0: GO TO 530
390 LET K=K0: IF I0>0 GO TO 372
400 REMARK *** NOW FIND POINTS ON FRAME
402 PRINT "TRACK END POINTS"
404 PRINT: PRINT "UPPER FRAME",,"LOWER FRAME"
410 FOR K=0 TO 30 STEP 2
412 REMARK *** PREDICT NEXT POINT
414 LET J1=FNE(J1): LET J2=FNE(J2): LET J3=FNE(J3)
420 FOR I=0 TO 2: LET X0=X(I,J1+1)-X(I,J3)
422 FOR J=0 TO 1: LET X(I,J2+J)=X(I,J1+J)+X0: NEXT J: NEXT I
426 FOR I=0 TO 1: LET X0=0: LET X1=0
427 LET X2=0: LET X3=INT(X)
429 FOR J=0 TO 7: LET J4=FNE(J2+J)
429 LET X0=X0+T(I,J)*(X(0,J4)-X3)
430 LET X1=X1-T(I,J)*X(1,J4): LET X2=X2+T(I,J)*X(2,J4)
431 NEXT J
432 LET X0=X0+X3
433 REMARK *** CONVERT TO RECORDER COORDS AND GET POINT
434 FOR J=0 TO 1: GOSUB 1150
440 LET A4=M0: LET Z0=X2: LET X2=-X1: LET X1=Z0
442 LET D0(2*J,0)=Z: LET D0(2*J+1,0)=Y: NEXT J: GOSUB 1250
444 NEXT I: GOSUB 1050
486 REMARK *** LIST THE PAIR OF POINTS
487 FOR I=0 TO 1: PRINT A(0,I);A(2,I);A(1,I);A(3,I): NEXT I
489 IF SWR(2)=0 THEN NEXT K
490 LET K=K+1
500 REMARK *** OUTPUT DATA: FIRST LIST THE "C" MATRIX
501 PRINT: PRINT "C MATRIX"
502 FOR I=0 TO 1: PRINT: PRINT I;
503 FOR J=0 TO 7: PRINT C(I,J);: NEXT J: NEXT I
505 PRINT: PRINT: PRINT "PREPARE FOR OUTPUT.";: GOSUB 1190
510 LET C0=255: GOSUB 1000
514 REMARK *** PUNCH TITLE OF DATA BLOCK
515 PRINT "RUN NO";R0;". FRAME NO";F0;". TRACK NO";J0;".
516 GOSUB 1000
520 LET C0=0: GOSUB 1000
523 REMARK *** PUNCH RUN, FRAME, AND TRACK NUMBER AND
524 REM      NUMBER OF POINTS TAKEN FROM FRAME
525 PRINT R0;". ";F0;". ";J0;". ";K:CHR$(13);
529 REMARK *** PUNCH DATUM POINTS
530 FOR J=0 TO 3
535 FOR I=0 TO 5: PRINT P(J,I);CHR$(13);: NEXT I: NEXT J

```

```

540 LET I1=SGN(D(0,0)-C(0,K)): LET K0=0: LET K1=K
542 IF I1<0 THEN LET K0=K: LET K1=0
544 REMARK *** PUNCH TRACK POINTS
545 FOR J=0 TO 3
550 FOR I=K0 TO K1 STEP I1: PRINT INT(D(J,I)+0.5);CHR$(13);
560 NEXT I: NEXT J: GOSUB 1000
565 GOSUB 1190
570 PRINT: PRINT: PRINT: LET F0=F0+I1: LET I0=-1: GO TO 230
700 REMARK *** RESTART WITH LAST FRAME
701 LET I1=SGN(I0): LET K0=0
702 OPEN "PR:" AS FILE 2: INPUT #2,F1,F1,J1,K1
703 IF (R1 NE R0) GOTO 706
704 IF (F0 EQ (F1+I1) AND (J1 EQ J0) GO TO 710
706 PRINT : PRINT "FRAME DATA DO NOT MATCH.": CLOSE 2: STOP
710 FOR J=0 TO 3
712 FOR K=0 TO 6: INPUT #2,F(J,K): NEXT K: NEXT J
714 IF I1<0 THEN LET K0=K1: LET K1=0
720 FOR J=0 TO 3
722 FOR K=K0 TO K1 STEP I1:INPUT #2,D(J,K): NEXT K: NEXT J
724 IF K0=0 THEN LET K0=K1
726 CLOSE 2: LET F0=F1: LET I0=1: GO TO 250

```

```
1000 REMARK *** PRINT 20 CHR$(C0)'S
1001 FOR I=1 TO 20: PRINT CHR$(C0);: NEXT I: RETURN
```

```
1004 REMARK *** LIST AND MARK RECORDER COORD POINT
1005 PRINT " (";INT(Z);";";INT(Y);";)",
1006 CONTACT D1 TO 1: WAIT 200: CONTACT D1 TO 0: WAIT 200
1007 IF 2*INT((K+1)/2)=K+1 THEN PRINT
1009 RETURN
```

```
1010 REMARK *** READ RECORDER COORD POINTS - FINE
1012 SET Z1 TO Z+AIN(A1)/B0: SET Y1 TO Y+AIN(A2)/B0
1014 IF ABS(AIN(A1))>1000 THEN LET Z=Z+5*SGN(AIN(A1))
1016 IF ABS(AIN(A2))>1000 THEN LET Y=Y+5*SGN(AIN(A2))
1018 IF DIN(D3)=0 GO TO 1012
1020 IF DIN(D3)=1 GO TO 1020
1022 LET Z=Z+AIN(A1)/B0: LET Y=Y+AIN(A2)/B0: RETURN
```

```
1050 REMARK*** CONVERT 2 POINTS AT A TIME
1052 FOR J=0 TO 1: GOSUB 1060
1054 NEXT J: RETURN
```

```
1060 REMARK *** CONVERT COORDS TO INCHES
1062 FOR I=0 TO 2 STEP 2: LET S1=-C(I/2,7)
1064 LET Z=D(I,K+J): LET Y=D(I+1,K+J): GOSUB 1200
1066 LET A(I,J)=Z-Y0(I): LET A(I+1,J)=Y-Y0(I+1): NEXT I
1070 LET X1=FND(FNS(J)): LET X2=FND(FNT(J))
1072 LET Z0=1+C(0,2)*C(1,2)*A(1,J)*A(3,J)/(X1*X2)
1074 LET A4=(C(0,3)-C(1,2)*A(3,J)*(1+C(1,3)/X2))/X1
1076 LET A(1,J)=-A(1,J)*C(0,2)*(1+A4)/Z0
1078 FOR I=2 TO 3
1080 LET A(1,J)=C(1,2)*A(I,J)*(1+(C(1,3)-A(1,J))/X2): NEXT I
1082 LET A(0,J)=C(0,2)*A(0,J)*(1+(C(0,3)-A(3,J))/X1)
1094 LET A(0,J)=Z2-A(0,J)+C(0,0)
1096 LET A(2,J)=Z2-A(2,J)+C(1,0)
1098 LET X(1,J+J2)=A(1,J): LET X(2,J+J2)=A(3,J)
1088 LET X(0,J+J2)=(A(0,J)+A(2,J))/2: RETURN
```

```

1100 REMARK *** READ RECORDER COORD POINTS - COARSE
1102 PRINT K;
1110 LET Z=AIN(A1): LET Z=AIN(A1): SET Z1 TO Z
1115 LET Y=AIN(A2): LET Y=AIN(A2): SET Y1 TO Y
1120 IF DIN(D3)=0 GO TO 1110
1130 IF DIN(D3)=1 GO TO 1130
1140 RETURN

```

```

1150 REMARK *** CONVERT FOR RECORDER COORDS
1152 LET Z0=Z2-X0+C(J,0): LET S1=C(J,7)
1154 LET M0=C(J,2)*(1+(C(J,3)-X2)/FND(Z0*X0+X1*X1))
1156 LET Z=Z0/M0+Y0(2*J): LET Y=X1/M0+Y0(2*J+1): GOSUB 1200
1158 RETURN

```

```

1190 REMARK *** WAIT FOR ACKNOWLEDGEMENT
1192 IF DIN(D3)=0 GO TO 1192
1194 IF DIN(D3)=1 GO TO 1194
1196 RETURN

```

```

1200 REMARK ** ROTATE THE COORD. AXIS
1201 LET R1=SQR(Z*Z+Y*Y)
1202 IF Z=0 THEN LET A4=3.14159*SGN(Y)+S1: GJ TO 1206
1203 LET A4=ATN(Y/Z)
1204 LET A4=A4+1.57079*SGN(A4)*(SGN(Z)-1)+S1
1206 LET Z=R1*COS(A4): LET Y=R1*SIN(A4): RETURN

```

```

1210 REMARK *** READ ONE OF FIRST FOUR FOR 1ST FRAME
1212 LET X2=C(M,3)*D(2*M+1,K+J)+C(M,9)
1214 LET X0=Y+AIN(A2)/B0: SET Y1 TO X0
1216 LET X1=C(1-M,8)*X0+C(1-M,9)
1218 LET Z=(D(2*M,K+J)-F(2*M,6))*X2/X1+F(2-2*M,6)
1220 IF ABS(AIN(A2))>1000 THEN LET Y=Y+5*SGN(AIN(A2))
1222 SET Z1 TO Z+AIN(A1)/B0: IF DIN(D3)=0 GO TO 1214
1224 GO TO 1020
1250 REMARK *** GET NEXT POINT
1252 LET J=0: LET Z0=SWP(0)
1254 LET Z=D0(J,0): LET Y=D0(J+1,0)
1256 SET Z1 TO Z: SET Y1 TO Y: LET B0=C(J/2,5): GOSUB 1010
1258 LET D(J,K+1)=Z: LET D(J+1,K+1)=Y
1259 IF SWP(0) NE Z0 GO TO 1262
1260 LET J=2-J: GO TO 1254
1262 FOR J=0 TO 2 STEP 2: PRINT K+I;
1264 LET Z=D(J,K+1): LET Y=D(J+1,K+1)
1266 SET Z1 TO Z: SET Y1 TO Y: WAIT 500: GOSUB 1005
1268 NEXT J: PRINT: RETURN

```

## APPENDIX B

### SOLUTION FOR COEFFICIENT TO X-Y RECORDER COORDINATE TRANSFORMATION EQUATION

The coordinates as read from the plane of the X-Y recorder must be transformed to the Cartesian coordinates of the flow tube in order to fix the position of a particle. The equation for such transformation is by Equation (3.8) of Chapter 3 as

$$\frac{D_{jmk}}{C_{jmk}} = \frac{\mu_j}{M_j v_j} + \frac{d_j - D_{j2k}}{((n^2 - 1)C_{jk}^2 + n^2 M_j^2 v_j^2)^{1/2}} \quad (B.1)$$

where the nomenclature is given in said chapter. Equation (B.1) is rearranged to give

$$\frac{D_{jmk}}{C_{jmk}} = \frac{\mu_j}{M_j v_j} \left( 1 + \frac{d_j - D_{j2k}}{((n^2 - 1)\left(\frac{\mu_j}{M_j v_j}\right)^2 C_{jk}^2 + n^2 \mu_j^2)^{1/2}} \right). \quad (B.2)$$

The values of  $\frac{\mu_j}{M_j v_j}$  and  $d_j$  for each view of a tube section are needed to compute  $D_{j1k}$  and  $D_{j2k}$ , Cartesian coordinates within the flow tube. To accomplish this, first express the known distances between certain datum points in terms

of these unknown parameters. Since the inside diameter of the tube is one inch, then for points (1) and (2) on Figure 3.7,

$$C_{i21}m_i\left(1 + \frac{d_i}{\lambda_{i1}}\right) - C_{i22}m_i\left(1 + \frac{d_i}{\lambda_{i2}}\right) = 1 \quad (B.3)$$

and for points (3) and (4)

$$C_{i24}m_i\left(1 + \frac{d_i}{\lambda_{i4}}\right) - C_{i23}m_i\left(1 + \frac{d_i}{\lambda_{i3}}\right) = 1 \quad (B.4)$$

where

$$m_i = \frac{\mu_i}{M_i v_i} \quad (B.5)$$

$$\lambda_{ij} = ((n^2 - 1)m_i^2 C_{ij}^2 + n^2 \mu_i^2)^{1/2}. \quad (B.6)$$

Note that

$$D_{i21} = D_{i22} = D_{i23} = D_{i24} = 0 \quad (B.7)$$

for  $i = 1, 2$ . Averaging these two equations and rearranging the resulting equation yields

$$(C_{i21} + C_{i24} - C_{i23} - C_{i22})\frac{m_i}{2} + \left(\frac{C_{i21}}{\lambda_{i1}} + \frac{C_{i24}}{\lambda_{i4}} - \frac{C_{i23}}{\lambda_{i2}} - \frac{C_{i22}}{\lambda_{i2}}\right)\frac{m_i d_i}{2} = 1. \quad (B.8)$$

Similarly, the distance between inch markers on the tape is one inch, so that for points (5) and (6)

$$(C_{i16} - C_{i15})m_i + \left(\frac{C_{i16}}{\lambda_{i6}} - \frac{C_{i15}}{\lambda_{i5}}\right)m_i(d_i - D_{i25}) = 1. \quad (B.9)$$

A third equation can be written to relate  $D_{i25}$  to  $d_i$  and  $m_i$  as

$$(-1)^i C_{i25}m_i + (-1)^i \frac{C_{i25}}{\lambda_{i5}}m_i(d_i - D_{i25}) = D_{i25}. \quad (B.10)$$

The factor  $(-1)^i$  is required because view 1 is inverted. Each of these equations apply to both views, so there are six equations and six unknowns. These equations are non-linear since  $\lambda_{ij}$  is a function of  $m_i$ . Before attempting a solution, write the equations in a more compact form, for  $i = 1, 2$

$$A_{i1}m_i + A_{i2}m_id_i = 1 \quad (B.11)$$

$$A_{i3}m_i + A_{i4}m_i(d_i - D_{i25}) = 1 \quad (B.12)$$

$$A_{i5}m_i + A_{i6}m_i(d_i - D_{i25}) = D_{i25} \quad (B.13)$$

$$\text{where } A_{i1} = \frac{(C_{i31} + C_{i24} - C_{i23} - C_{i22})}{2} \quad (B.14)$$

$$A_{i2} = \frac{1}{2}\left(\frac{C_{i21}}{\lambda_{i1}} + \frac{C_{i24}}{\lambda_{i4}} - \frac{C_{i23}}{\lambda_{i3}} - \frac{C_{i22}}{\lambda_{i2}}\right) \quad (B.15)$$



$$A_{i3} = C_{i16} - C_{i15} \quad (B.16)$$

$$A_{i4} = \frac{C_{i16}}{\lambda_{i6}} - \frac{C_{i15}}{\lambda_{i5}} \quad (B.17)$$

$$A_{i5} = (-1)^i C_{i25} \quad (B.18)$$

$$A_{i6} = (-1)^i \frac{C_{i25}}{\lambda_{i5}} . \quad (B.19)$$

Because the equations are nonlinear, an iterative method is employed. By assuming a value for  $m_i$  the function  $\lambda_{ij}$  can be evaluated and by assuming a value for  $D_{i25}$ , Equations (B.11) and (B.12) can be solved for  $m_i$  and  $d_i$ . Equation (B.13) yields a new approximation for  $D_{i25}$  and  $D_{225}$ . This procedure can be repeated until values of  $m_i$ ,  $d_i$ , and  $D_{i25}$  have converged. Once  $m_i$  and  $d_i$  are known for a given tube section, all points photographed within that section of tube can be transformed to their corresponding Cartesian coordinates of the flow tube.

## APPENDIX C

### COMPUTER PROGRAM FOR COMPUTING THE CYLINDRICAL COORDINATES OF PARTICLE PATHS

The theory and use of this program is found in Section 3.2.1 and Appendix B. Documentation is also included within the program.

```

C -----
C| THIS PROGRAM COMPUTES THE CYLINDRICAL COORDINATES OF |
C| PARTICLE POSITIONS FROM THE TWO 2-DIMENSIONAL VIEWS. |
C| DEFINITION OF MAJOR VARIABLES IN THE PROGRAM FOLLOW: |
C|     TO      --- TIME PERIOD OF TACK, SECOND. |
C|     NUMTRK  --- EXPERIMENTAL TRACK NUMJER. |
C|     NUMFRM  --- NUMBER OF PHOTO FRAMES WITH DATA. |
C|     INITF   --- FIRST FRAME ON WHICH PARTICLE PATH IS |
C|              VIEWED. |
C|     NUMRUN  --- EXPERIMENT RUN NUMBER. |
C|     NOFRM   --- FRAME NUMBER. |
C|     NOTRK   --- EXPERIMENT TRACK NUMBER. |
C|     NUMSG1  --- NUMBER OF SEGMENTS OF PARTICLE PATH |
C|              VIEWED IN FRAME. |
C|     F       --- ARRAY OF DATUM POINTS FOR FRAME. |
C|     C       --- ARRAY OF COEFFICIENTS FOR TRANSFORMA- |
C|              TION EQUATION. |
C|     D       --- ARRAY OF PARTICLE PATH DATA FOR THE |
C|              TWO 2-DIMENSIONAL VIEWS OF THE FRAME. |
C|     X       --- ARRAY OF COMPUTED CYLINDRICAL COOR- |
C|              DINATES. |
C|     V       --- ARRAY OF COMPUTED VELOCITIES. |
C|     VZAVG   --- ARRAY OF AVERAGE VELOCITIES FOR THE |
C|              FIVE RADIAL ZONES. |
C|     N       --- ARRAY OF THE TOTAL NUMBER OF SEGMENTS |
C|              IN THE PARTICLE TRACKS. |
C| -----

```

```

      DIMENSION A(4,2),C(2,10),D(4,25),F(8,7),B(2,6)
      .      ,X(7,2,3,210),V(7,2,3,210),XAVG(4),XNF(7)
      .      ,VZAVG(2,5),N(10)
      DATA TO/0.00616/,VZAVG/10*0.0/
      M1=1

```

C

C \*\*\* READ IN TRACK DATA

C

```

      1 READ(1) NUMTRK,NUMFRM,INITF
      M=0
      2 READ(1) NUMRUN,NOFRM,NOTRK,NUMSG1,F,C
      READ(1) D

```

C

C

C

ALIGN FRAMES

```

      DO 11 I=1,4,2
      XAVG(I)=0
      XAVG(I+1)=0
      C((I+1)/2,7)=(ATAN2(F(I+1,4)-F(I+1,1),F(I,4)-F(I,1))
      .      +ATAN2(F(I+1,3)-F(I+1,2),F(I,3)-F(I,2)))/2
      DO 10 J=1,7
      CALL ROTAX(F(I,J),F(I+1,J),-C((I+1)/2,7),
      .      F(I+4,J),F(I+5,J))
      IF (J .GT. 4) GOTO 10
      XAVG(I)=XAVG(I)+F(I+4,J)/4
      XAVG(I+1)=XAVG(I+1)+F(I+5,J)/4

```

```

10 CONTINUE
   DO 11 J=1,7
      F(I+4,J)=F(I+4,J)-XAVG(I)
11 F(I+5,J)=F(I+5,J)-XAVG(I+1)
C
C *** COMPUTE COEFF FOR EQUATION TO ADJUST COORDS
C
   DO 12 I=1,2
      K=2*(I-1)+6
      C(I,1)=(F(K,1)+F(K,4)-F(K,3)-F(K,2))/2
      XNF(I)=1/C(I,1)
      C(I,5)=(2*I-3)*F(K,5)
      B(I,3)=(2*I-3)*F(K,5)/(F(K-1,7)-F(K-1,5))
12 CONTINUE
31 DO 13 I=1,2
      K=2*(I-1)+6
      C(I,2)=(FUNC(F(K,1),F(K-1,1),XNF(I))
      +FUNC(F(K,4),F(K-1,4),XNF(I))
      -FUNC(F(K,3),F(K-1,3),XNF(I))
      -FUNC(F(K,2),F(K-1,2),XNF(I)))/2
      C(I,4)=FUNC(F(K-1,7),F(K,7),XNF(I))
      -FUNC(F(K-1,5),F(K,5),XNF(I))
      C(I,6)=(2*I-3)*FUNC(F(K,5),F(K-1,5),XNF(I))
      C(I,3)=F(K-1,7)-F(K-1,5)-C(I,4)*B(3-I,3)
13 CONTINUE
   DO 14 I=1,2
      A1=C(I,1)*C(I,4)-C(I,2)*C(I,3)
      B(I,1)=(C(I,4)-C(I,2))/A1
      B(I,2)=(C(I,1)-C(I,3))/(A1*B(I,1))
      K=2*I+3
      C(I,10)=B(I,1)*(F(K,7)+(B(I,2)-B(3-I,3))
      *FUNC(F(K,7),F(K+1,7),XNF(I)))
14 CONTINUE
   IF(ABS((XNF(I)-B(I,1))/XNF(I)),LT,0.0001) GOTO 20
   DO 30 I=1,2
      XNF(I)=B(I,1)
      B(I,3)=B(I,1)*(C(I,5)+C(I,6)*(B(I,2)-B(3-I,3)))
30 CONTINUE
   GOTO 31
20 IPDS=1.5*NDPRM+1.25
C
C *** CONVERT DATA TO CYLINDRICAL COORDS.
C
   DO 15 I=1,NUMSG1,2
      DO 16 J=1,2
         DO 17 K=1,4,2
            CALL RDTAX(D(K,I+J/2),D(K+1,I+J/2),
            -C((K+1)/2,7),A(K,J),A(K+1,J))
            A(K,J)=A(K,J)-XAVG(K)
17 A(K+1,J)=A(K+1,J)-XAVG(K+1)
      DUM1=XNF(1)*XNF(1)
      DUM2=XNF(2)*XNF(2)
      DUM1=SQRT(1.19*(A(1,J)*A(1,J)+A(2,J)*A(2,J))*DUM1+16)

```

```

DUM2=SQRT(1.19*(A(3,J)*A(3,J)+A(4,J)*A(4,J))*DUM2+16)
DUM3=A(4,J)*B(2,1)*(1+B(2,2)/DUM2)
A(2,J)=-A(2,J)*3(1,1)*1+(B(1,2)-DUM3)/DUM1)
      /(1+A(2,J)*A(4,J)*B(1,1)*B(2,1)/(DUM1*DUM2))
DO 18 K=3,4
19 A(K,J)=A(K,J)*B(2,1)*(1+(B(2,2)-A(2,J))/DUM2)
A(1,J)=A(1,J)*B(1,1)*(1+(B(1,2)-A(4,J))/DUM1)
A(1,J)=IPDS-A(1,J)+C(1,10)
16 A(3,J)=IPDS-A(3,J)+C(2,10)
M=M+1
DO 15 J=1,2
X(41,J,1,M)=(A(1,J)+A(3,J))/2
X(41,J,2,M)=SQRT(A(2,J)*A(2,J)+A(4,J)*A(4,J))
X(41,J,3,M)=ATAN2(A(4,J),A(2,J))
IF(M.NE. 1) GOTO 27
DO 25 L=1,3
26 V(41,J,L,M)=0
GOTO 15
27 DO 22 L=1,3
V(41,J,L,M)=(X(41,J,L,M)-X(41,J,L,M-1))/T0
IF(L.NE. 3) GOTO 23
IF(ABS(T0*V(41,J,3,M)).GT. 5.5) V(41,J,3,M)=
9 V(41,J,3,M)-SIGN(6.283182/T0,V(41,J,3,M))
V(41,J,L,M)=V(41,J,L,M)*X(41,J,2,M)
23 IF(L.NE. 2) GOTO 22
IRAD=X(41,J,2,M)/0.1+1
IF(IRAD.GT. 5) IPAD=5
24 VZAVG(1,IRAD)=VZAVG(1,IPAD)+V(41,J,1,M)
VZAVG(2,IRAD)=VZAVG(2,IPAD)+1
22 CONTINUE
15 CONTINUE
C
C *** LIST DATUM POINT DATA
C
WRITE(6,120) NOFRM,NJTRK,NUMRUN
120 FORMAT('1','FRAME ',I2,10X,'TRACK',I3,10X,'RUN',I3,
. ///,1X,'FRAME DATUM POINTS :',/,1X,5('===='),
. ///,11X,'UPPER VIEW LOWER VIEW',/,
. 2X,'POS',2X,2(2X,'====='),/,
. 2X,'NUM Z1 X Z2 Y',/,
. 1X,'===== ',4(2X,'====='))
WRITE(6,102) (I,(F(J,I),J=1,4),I=1,7)
102 FORMAT(1X,I3,2X,4F9.0)
C
C *** LIST SEGMENT END POINT DATA FROM DATA COLLECTION,
C CYLINDRICAL COORDINATE DATA, AND VELOCITIES COMPUTED
C BY DIFFERENCE.
C
WRITE(6,121)
121 FORMAT(///,1X,'SEGMENT END POINTS :',/,1X,5('===='),
. ///,1X,'TIM',6X,
. 'TIM ',6X,'UPPER VIEW LOWER VIEW',
. 13X,'CYLINDRICAL COORDINATES',20X,

```

```

      'VELOCITIES, DIA/SEC',/,1X,
      'INT      D1      D2      D3      D4',
      13X,'Z,DIA',5X,'R,DIA',5X,'THETA',14X,
      'VZ',12X,'VR',10X,'VTHETA',
      /,1X,'-----',4('-----'),5X,
      J('-----'),4X,3('-----'))
      L=M-(NUMSG1-1)/2
      DO 19 J=1,NUMSG1,2
      DO 19 K=1,2
      K1=J+K/2+2*(L-1)
19  WRITE(6,101) K1,(D(I,J+K/2),I=1,4),
      (X(M1,K,I,L+J/2),I=1,3)
      , (V(M1,K,I,L+J/2),I=1,3)
101  FORMAT(1X,I3,1X,4F9.0,6X,3F10.3,6X,1P3E14.3)
      IF (NOFORM .LT. NUMFORM) GOTO 2
      N(M1)=M
      M1=M1+1
      IF (M1 .LE. 7) GO TO 1
      M1=M1-1
      DO 25 I=1,5
      IF(VZAVG(2,I) .EQ. 0) GOTO 25
      VZAVG(1,I)=VZAVG(1,I)/VZAVG(2,I)
25  CONTINUE
C
C *** SAVE CYLINDRICAL COORDINATE DATA FOR PARTICLE POSI-
C     TIONS
C
      WRITE(2) M1,N,VZAVG
      DO 60 I=1,M1
      DO 60 K=1,3
      WRITE(2) ((X(I,J,K,L),J=1,2),L=1,210)
      WRITE(2) ((V(I,J,K,L),J=1,2),L=1,210)
60  CONTINUE
      END FILE 2
      STOP
      END

```

```

C-----
C| THIS FUNCTION ROUTINE COMPUTES THE LAMBDA FUNCTION OF
C| TRANSFORMATION EQUATIONS
C|-----

```

```

FUNCTION FUNC(X,Y,D)
FUNC=X/SQRT(1.19*(X*X+Y*Y)*D*D+16)
RETURN
END

```

```

C-----
C| THIS FUNCTION ADJUSTS THE ANGLE
C|-----

```

```

FUNCTION ANGLE(A)
ANGLE=A-SIGN(6.283186,A)
RETURN
END

```

```

C-----
C| SUBROUTINE TO ROTATE COORD AXIS
C|-----

```

```

SUBROUTINE ROTAX(X,Y,A,XNEW,YNEW)
A1=ATAN2(Y,X)+A
R1=SQRT(X*X+Y*Y)
XNEW=R1*COS(A1)
YNEW=R1*SIN(A1)
RETURN
END

```

## APPENDIX D

### COMPUTER PROGRAM FOR THE COMPUTATION OF THE LAGRANGIAN TIME CORRELATION

The theory of this program is found in Section

3.2.2. Documentation is also included within the program.



```

C-----
C| THIS PROGRAM COMPUTES THE LAGRANGIAN CORRELATIONS AND
C| TURBULENT INTENSITIES FROM PARTICLE DATA RELATING
C| POSITION OF PARTICLE IN TIME. CORRELATIONS FOR BOTH
C| POSITIVE AND NEGATIVE TIMES ARE COMPUTED FOR FIVE
C| ANNULAR ZONES OF A ONE INCH DIAMETER PIPE. DEFINI-
C| TIONS OF THE MAJOR VARIABLES IN THE PROGRAM FOLLOW:
C|     CORREL(I,J,K,L) *** THE J-TH CORRELATION FOR THE
C|                          L-TH TIME INTERVAL OF THE K-TH
C|                          RADIAL INTERVAL. I=1 FOR
C|                          NEGATIVE TIMES, AND I=2 FOR
C|                          POSITIVE TIMES.
C|     NCON(I,J,K)      *** NUMBER OF CONTRIBUTIONS TO J-TH
C|                          CORELATION AT TIME INTERVAL
C|                          K. I=1 FOR NEGATIVE TIME, AND
C|                          I=2 FOR POSITIVE TIME.
C|     X(I,J,K)         *** THE J-TH COORDINATE OF THE
C|                          PARTICLE POSITION FOR TIME
C|                          INTERVAL K. I=2 FOR RAW DATA,
C|                          AND I=1 FOR SMOOTHED DATA.
C|                          J=1 FOR Z COORDINATE J=2 FOR
C|                          R COORDINATE, J=3 FOR THETA
C|                          COORDINATE.
C|     V(I,J,K)         *** THE J-TH VELOCITY COMPONENT OF
C|                          PARTICLE AT TIME INTERVAL K.
C|     T1               *** MATRIX FOR SMOOTHING PARTICLE
C|                          POSITION COORDINATES.
C|     T2               *** MATRIX FOR SMOOTHING VELOCITY
C|                          COMPONENTS.
C|     T0               *** TIME INTERVAL OF PARTICLE
C|                          POSITIONS, SECONDS.
C|     M1               *** NUMBER OF PARTICLE TRACKS.
C|     N(I)             *** NUMBER OF INTERVALS FOR PARTI-
C|                          CLE TRACK I.
C|     ZSTAR            *** MEAN Z POSITION OF PARTICLE.
C| THE CORRELATIONS ARE NUMBERED AS FOLLOW:
C|     1: <Z'(T)*Z'(T)>      2: <Z'(T)*R'(T)>
C|     3: <Z'(T)*THETA'(T)>  4: <R'(T)*R'(T)>
C|     5: <R'(T)*THETA'(T)>  6: <THETA'(T)*THETA'(T)>
C|     7: <Z'(T)*VZ'(T)>     8: <Z'(T)*VR'(T)>
C|     9: <Z'(T)*VTHETA'(T)> 10: <R'(T)*VZ'(T)>
C|    11: <R'(T)*VR'(T)>     12: <R'(T)*VTHETA'(T)>
C|    13: <THETA'(T)*VZ'(T)>  14: <THETA'(T)*VR'(T)>
C|    15: <THETA'(T)*VTHETA'(T)> 16: <VZ'(T0)*VZ'(T)>
C|    17: <VZ'(T0)*VR'(T)>   18: <VZ'(T0)*VTHETA'(T)>
C|    19: <VR'(T0)*VZ'(T)>   20: <VR'(T0)*VTHETA'(T)>
C|    21: <VR'(T0)*VTHETA'(T)> 22: <VTHETA'(T0)*VZ'(T)>
C|    23: <VTHETA'(T0)*VR'(T)>
C|    24: <VTHETA'(T0)*VTHETA'(T)>
C| WHERE Z' = Z DISPLACEMENT FROM MEAN PATH
C|        R' = R DISPLACEMENT FROM INITIAL ORIGIN
C|        THETA' = (INITIAL RADIUS)*(THETA DISPLACEMENT)

```

```

C|          VZ'      = DEVIATION OF Z VELOCITY COMPONENT      |
C|          VR       = R VELOCITY COMPONENT                   |
C|          VTHETA' = (INITIAL RADIUS)*(TIME RATE OF CHANGE   |
C|                      THETA DISPLACEMENT)                  |
C|-----|
      DIMENSION T1(21,21),T2(21,21),PINT(10),N(10)
      COMMON X(2,3,420),V(2,3,420),CORREL(2,24,5,210)
      .      ,ARG(9),NCOR(2,5,210),IRAD,ZSTAR
      DATA PINT/0.0,2*0.2,2*0.4,2*0.6,2*0.8,1.0/
      DO 10 I=1,2
      DO 10 J=1,5
      DO 10 K=1,210
      NCOR(I,J,K)=0
      DO 10 L=1,24
      CORREL(I,L,J,K)=0
10  CONTINUE
      NPT=8
      T0=0.00016

C
C *** READ IN SMOOTHING MATRIX
C
      READ(5,101) ((T1(I,J),I=1,NPT),J=1,NPT)
      READ(5,101) ((T2(I,J),I=1,NPT),J=1,NPT)
101  FORMAT(5F15.9)

C
C *** READ IN NUMBER OF TRACKS, M1, AND NUMBER OF TIME
C      INTERVALS IN EACH PARTICLE TRACK
C
      READ(3) M1,N,(DUMMY,I=1,10)
      PI2=6.283186
      DO 15 I=1,M1
      N1=2*N(I5)
      DO 17 K=1,3
      READ(3) (X(2,K,L),L=1,420)
      READ(3) (V(2,K,L),L=1,420)
      IF (K .NE. 3) GOTO 17
      DO 16 L=1,N1
      IF (X(2,K,L) .LT. -2.7) X(2,K,L)=PI2+X(2,K,L)
16  CONTINUE
17  CONTINUE

C
C *** SMOOTH PARTICLE POSITION DATA AND COMPUTE VELOCITIES
C      FROM SMOOTHED DATA
C
      DO 31 K=1,3
      DO 31 L=1,N1
      INTX=X(2,K,L)
      X0=INTX
      V0=0
      M2=2*(L/2)-4
      M3=L-2*(L/2)+4
      IF ((L .GT. 3) .AND. (L .LT. N1-2)) GOTO 22
      M2=0

```

```

      M3=L
      IF (L .LT. 4) GOTO 22
      M2=N1-3
      M3=L-M2
22   DO 20 M=1,NPT
      X0=X0+(X(2,K,M2+M)-INTX)*T1(M3,M)
      V0=V0+X(2,K,M2+M)*T2(M3,M)
20   CONTINUE
      X(1,K,L)=X0
      V(1,K,L)=V0/T0
31   CONTINUE

C
C *** COMPUTE THE CORRELATIONS
C
      DO 35 K=1,N1
      N2=K+1
      N3=N1
      IRAD=X(1,2,K)/0.1+1
      IF (IRAD .GT. 5) IRAD=5
      ARG(7)=V(1,1,K)-VEL(X(1,2,K))
      ARG(8)=V(1,2,K)
      ARG(9)=V(1,3,K)*X(1,2,K)
      ZSTAR=X(1,1,K)

C
C *** FOR NEGATIVE TIMES
C
      DO 28 M=1,K
      M2=K-M+1
      IF (K-M2 .GT. 209) GOTO 28
      CALL COPLAT(K,M2)
      ZSTAR=ZSTAR-T0*VEL(X(1,2,M2))/2
28   CONTINUE

C
C *** FOR POSITIVE TIMES
C
      ZSTAR=X(1,1,K)
      IF (N2 .GT. N3) GOTO 36
      DO 29 M=N2,N3
      IF (M-K .GT. 209) GOTO 36
      ZSTAR=ZSTAR+T0*VEL(X(1,2,M))/2
      CALL COPLAT(K,M)
29   CONTINUE
36   CONTINUE
15   CONTINUE
      DO 38 L=1,2
      DO 38 J=1,5
      DO 38 I=1,210
      IF (NCOR(L,J,I) .EQ. 0) GOTO 38
      DO 37 K=1,24
37   CORREL(L,K,J,I)=CORREL(L,K,J,I)/NCOR(L,J,I)
39   CONTINUE

```

```

C
C *** SAVE TURBULENT INTENSITIES
C
      WRITE(1) ((CORREL(1,I,J,1),J=1,5),I=16,24)
C
C *** LIST TURBULENT INTENSITIES
C
      WRITE(6,142)
142  FORMAT(/,1X,'TURBULENT INTENSITIES')
      WRITE(6,135) (RINT(I),I=1,10)
135  FORMAT(////////,48X,'RADIAL INTERVAL',/,3X,'      ',6X,
.      89('='),/,3X,'NUM ',2X,5(F9.1,'<R/R0<',F3.1),
.      /,1X,9('='),2X,5(1X,'===== '))
      DO 34 I=16,24
34   *WRITE(6,132) I,(CORREL(1,I,J,1),NCOR(1,J,1),J=1,5)
132  FORMAT(1X,I8,1X,5(1PE13.4,'/',14))
C
C *** NORMALIZE DOUBLE VELOCITY CORRELATIONS
C
      DO 40 L=1,2
      DO 40 J=1,5
      DO 40 I=16,24
      I1=16+4*((I-16)/3)
      C1=CORREL(1,I1,J,1)
      C2=CORREL(1,I1+4*(I-I1),J,1)
      IF ((C1 .EQ. 0) .OR. (C2 .EQ. 0)) GOTO 40
      C3=SQRT(C1)*SQRT(C2)
      DO 41 K=1,210
      IF (CORREL(L,I,J,K) .EQ. 0) GOTO 41
      IF ((K .EQ. 1) .AND. (4*(1/4) .EQ. 1)) GOTO 41
      CORREL(L,I,J,K)=CORREL(L,I,J,K)/C3
41  CONTINUE
40  CONTINUE
      DO 50 L=1,2
      DO 51 J=1,5
      DO 51 M=16,24,4
      CORREL(L,4,J,1)=1.0
51  CONTINUE
C
C *** LIST CORRELATIONS
C
      DO 50 J=1,24
      IC=72
      DO 52 M=1,210
      C1=0
      DO 49 K=1,5
49  C1=C1+ABS(CORREL(L,J,K,M))
      IF ((C1 .EQ. 0) .AND. (M .NE. 1)) GOTO 53
      IF (IC .LE. 70) GOTO 53
      WRITE(6,130) J,(RINT(I),I=1,10)
130  FORMAT('1','CORRELATION',I3,' / NUMBER',/,/,
.      48X,'RADIAL INTERVAL',/,3X,'TIME',6X,89('='),/,
.      3X,'MSEC',2X,5(F9.1,'<R/R0<',F3.1),/,1X,

```

```

      .          9('=',2X,5(1X,'===== '))
      IC=1
53  A2=500*T0*(M-1)
      IC=IC+1
52  WRITE(6,131) A2,(CORREL(L,J,K,M),NCOR(L,K,M),K=1,5)
131  FORMAT(1X,F8.2,1X,5(1PE13.4,'/',I4))
50  CONTINUE

C
C *** SAVE CORRELATIONS AND NUMBER OF CONTRIBUTIONS TO EACH
C      CORRELATION
C
      DO 61 I=1,24
      DO 61 J=1,5
61  WRITE(1) ((CORREL(L,I,J,K),K=1,210),L=1,2)
      DO 62 J=1,5
62  WRITE(1) ((NCOR(L,J,K),K=1,210),L=1,2)
      END FILE 1
      STOP
      END

```

```

C-----
C| SUBROUTINE FOR COMPUTING CONTRIBUTIONS TO CORRELA- |
C| TIONS. PARAMETER K IS THE NUMBER OF THE STARTING TIME |
C| INTERVAL AND PARAMETER M IS THE NUMBER OF THE ELAPSED |
C| TIME INTERVAL. |
C|-----
C| SUBROUTINE CORLAT(K,M)
COMMON X(2,3,420),V(2,3,420),CORREL(2,24,5,210)
. ,ARG(9),NCDR(2,5,210),IRAD,ZSTAR
ITIM=IABS(M-K)+1
I=SIGN(1.0,M-K-0.1)
C
C *** COMPUTE PARTICLE DISPLACEMENTS AND VELOCITY DEVI-
C TIONS
C
ARG(1)=I*(X(1,1,M)-ZSTAR)
ARG(2)=I*(X(1,2,M)-X(1,2,K))
ARG(3)=I*X(1,2,K)*(X(1,3,M)-X(1,3,K))
ARG(4)=V(1,1,M)-VEL(X(1,2,M))
ARG(5)=V(1,2,M)
ARG(6)=V(1,3,M)*X(1,2,K)
I=1+(1+I)/2
NCDR(1,IRAD,ITIM)=NCDR(1,IRAD,ITIM)+1
I3=0
DO 36 I1=1,3
DO 36 I2=1,3
IF (I2 .LT. I1) GOTO 35
I3=I3+1
C
C *** COMPUTE CONTRIBUTION TO CORRELATIONS 1 THROUGH 6
C
CORREL(I,I3,IRAD,ITIM)=CORREL(I,I3,IRAD,ITIM)
. +ARG(I1)*ARG(I2)
35 I4=3*I1+I2
C
C *** COMPUTE CONTRIBUTION TO CORRELATIONS 7 THROUGH 15
C
CORREL(I,I4+3,IRAD,ITIM)=CORREL(I,I4+3,IRAD,ITIM)
. +ARG(I1)*ARG(I2+3)
C
C *** COMPUTE CONTRIBUTION TO CORRELATIONS 16 THROUGH 24
C
36 CORREL(I,I4+12,IRAD,ITIM)=CORREL(I,I4+12,IRAD,ITIM)
. +ARG(I2+3)*ARG(I1+6)
RETURN
END

```

```

C-----
C|*** THIS FUNCTION COMPUTES THE MEAN AXIAL VELOCITY USING |
C| AN EQUATION FORM SUGGESTED BY PA1. THE FORM IS |
C|
C|          UZ/UZ,MAX = A1*(R/R0)**2+A2*(R/R0)**(2*M) |
C|-----
C|
C| FUNCTION VEL(R)
C|   R1=2*R
C|   VEL=1-0.36258*R1*R1
C|   IF(ALOG10(R1) .LT. -0.1) GOTO 10
C|   VEL=VEL-0.63742*R1**150
C| 10 VEL=47.1435*VEL
C|   RETURN
C|   END

```

## BIBLIOGRAPHY

- Abbrecht, P. H. and S. W. Churchill  
 1960 "The thermal entrance region in fully developed turbulent flow," A.I.Ch.E. Journal 6, 268.
- Agostini, L. and J. Bass  
 1950 The theories of turbulence, Publ. Sci. et Techn. der Unin. Air No. 237. Translation in NACA TM 1377 (1955).
- Akerblom, F.  
 1908 "Recherches sur les courants les plus bas de l'atmosphere au dessus de Paris," Nova Acta. Reg. Soc. Upsaliensis (IV) 2, 2.
- Angell, J. K.  
 1964a "Measurements of Lagrangian and Eulerian properties of turbulence at a height of 2,500 ft.," Quart. J. Roy. Meteor. Soc. 90, 57.  
 1964b "Correlations in the vertical component of the wind at heights of 600, 1,600 and 2,600 feet at Cardington," Quart. J. Roy. Meteor. Soc. 90, 307.
- Baldwin, L. V. and W. R. Mickelsen  
 1963 "Turbulent diffusion and anemometer measurements," A.S.C.E. Trans. 128, 1595.
- Baldwin, L. V. and T. J. Walsh  
 1961 "Turbulent diffusion in the core of fully developed pipe flow," A.I.Ch.E. Journal 7, 53.
- Batchelor, G. K.  
 1949 "Diffusion in a field of homogeneous turbulence. I. Eulerian analysis," Austr. J. Sci. Res. 2, 437.  
 1952 "Diffusion in a field of homogeneous turbulence. II. The relative motion of particles," Proc. Camb. Phil. Soc. 48, 345.  
 1953 The theory of homogeneous turbulence, Cambridge University Press, Cambridge.



- Batchelor, G. K.  
1957 "Diffusion in free turbulent shear flows," J. Fl. Mech. 3, 67.
- Batchelor, G. K., A. M. Binnie, and O. M. Phillips  
1955 "The mean velocity of discrete particles in turbulent flow in a pipe," Proc. Phys. Soc. B68, 1095.
- Batchelor, G. K. and A. A. Townsend  
1956 "Turbulent diffusion" in Surveys in mechanics, G. K. Batchelor and R. M. Davies (Eds.), Cambridge University Press, Cambridge.
- Beckers, H. L.  
1956 "Heat transfer in turbulent tube flow," Appl. Sci. Res. A6, 147.
- Beckwith, W. F. and R. W. Fahien  
1963 Determination of turbulent thermal diffusivities for flow of liquid pipes, USAEC Rep. IS-734, Iowa State University of Science and Technology, Ames, Iowa.
- Bernard, R. A. and R. H. Wilhelm  
1950 "Turbulent diffusion in fixed beds of packed solids," C.E.P. 46, 233.
- Bird, R. B., W. E. Stewart, and E. N. Lightfoot  
1960 Transport phenomena, Wiley, New York.
- Bourke, P. J. and D. J. Pulling  
1970 "A turbulent heat flux meter and some measurements of turbulence in air flow through a heated pipe," Int. J. Heat Mass Transfer 13, 1331.
- Boussinesq, J.  
1877 "Essai sur la theorie des eaux courantes," Mem. pres. par. div. savants a l'Acad. Sci. Paris 23, 1.  
  
1897 Theorie de l'ecoulement tourbillonnant et tumultueux des liquides dans les lits rectilignes a grande section, 2 vols., Gauthier-Villars, Paris.
- Brodkey, R. S.  
1967 The phenomena of fluid motions, Addison-Wesley, Reading, Mass.
- Burgers, J. M.  
1951 On turbulent fluid motion, Hydro. Lab. CALTECH, Rep E-341.

- Cavers, S. D., N. T. Hsu, W. G. Schlinger, and B. H. Sage  
1953 "Temperature gradients in turbulent gas streams. Behavior near boundary in two-dimensional flow," I. & E.C. 45, 2139.
- Cermak, J. E. and L. V. Baldwin  
1964 Measurement of Turbulence in Water by Electrokinetic Transducers, FL. Mech. Papers, Colorado State University, Fort Collins.
- Chia, W. S. and B. H. Sage  
1970 "Temperature gradients in turbulent gas streams: Investigation of the limiting value of total Prandtl number," A.I.Ch.E. Journal 16, 37.
- Collis, D. C.  
1948 The diffusion process in turbulent flow, Rep. A.55, Council for Science and Industrial Research, Div. Aero., Fishermen's Bend, Melbourne, Australia.
- Corcoran, W. H.  
1948 I. Temperature gradients in turbulent gas streams.  
II. Thermodynamic properties of methane at low temperatures, Doctoral Dissertation, California Institute of Technology, Pasadena.
- Corcoran, W. H., J. B. Opfell and B. H. Sage  
1956 Momentum transfer in fluids, Academic Press, New York.
- Corcoran, W. H., F. Page, W. G. Schlinger and B. H. Sage  
1952 "Temperature gradients in turbulent gas streams. Methods and apparatus for flow between parallel plates," I. & E.C. 44, 410.
- Corcoran, W. H., B. Roudebush, and B. H. Sage  
1947 "Temperature gradients in turbulent gas streams. Preliminary studies," C.E.P. 43, 135.
- Corcoran, W. H. and B. H. Sage  
1956 "Role of eddy conductivity in thermal transport," A.I.Ch.E. Journal 2, 251.
- Corino, E. R. and R. S. Brodkey  
1969 "A visual investigation of the wall region in turbulent flow," J. Fl. Mech. 37, 1.
- Crum, G. F. and T. J. Hanratty  
1965 "Dissipation of a sheet of heated air in a turbulent flow," Appl. Sci. Res. A15, 177.

Davies, D. R.

- 1954 "A note on the two-dimensional equation of diffusion in the atmosphere," Quart. J. Roy. Meteor. Soc. 80, 429.

Deardorff, J. W.

- 1970 "A numerical study of three-dimensional turbulent channel flow at large Reynolds numbers," J. Fl. Mech. 41, 453.

Deardorff, J. W. and R. L. Peskin

- 1970 "Lagrangian statistics from numerically integrated turbulent shear flow," Phys. Fl. 13, 584.

Defant, A.

- 1921 "Die Bestimmung der Turbulenzgroessen der atmosphärischen Zirkulation aussertropischer Breiten," Sitzungsber. Akad. Wiss. Wien (Abt. IIa) 130, 383.

Deissler, R. G. and C. S. Eian

- 1952 Analytical and experimental investigation of fully developed turbulent flow of air in a smooth tube with heat transfer with variable fluid properties, NACA TN 2629.

Dorweiler, V. P. and R. W. Fahien

- 1959 "Mass transfer at low flow rates in a packed column," A.I.Ch.E. Journal 5, 139.

Fage, A.

- 1936 "Turbulent flow in a circular pipe," Phil. Mag. Ser. T. 21, 81.

Fage, A. and H. C. H. Townend

- 1932 "An examination of turbulent flow with an ultra-microscope," Proc. Roy. Soc. A135, 656.

Fahien, R. W.

- 1954 Mass transfer in packed beds, Doctoral Dissertation, Purdue University, Lafayette, Ind.

Fahien, R. W. and J. M. Smith

- 1955 "Mass transfer in packed beds," A.I.Ch.E. Journal 1, 28.

Fayre, A. (Ed.)

- 1962 Mécanique de la turbulence, Coll. Intern. CNRS, Editions CNRS, Paris.

- Frandolig, J. E. and R. W. Fahien  
 1964 Liquid-phase mass transfer at low flow rates in a packed column, USAEC Rep IS-817, Iowa State University of Science and Technology, Ames, Iowa.
- Frenkiel, F. N.  
 1953 "Turbulent diffusion: mean concentration distribution in a flow field of homogeneous turbulence," Adv. Appl. Mech. 3, 61.
- Frenzen, P.  
 1963 A Laboratory Investigation of the Lagrangian Auto-correlation Function in a Stratified Fluid, Argonne National Lab., ANL-6794.
- Friedlander, S. K. and L. Topper (Eds.)  
 1961 Turbulence--classic papers on statistical theory, Interscience, New York.
- Gielow, R.  
 1965 Problema de Graetz-Nusselt em regime turbulento, M.Sc.Thesis, Universidade do Brasil, Rio de Janeiro.
- 1972 Stochastic modeling of turbulent heat and mass transport in anisotropic shear flow, Doctoral Dissertation, University of Florida, Gainesville.
- Gifford, F. A., Jr.  
 1961 "Use of routine meteorological observations for estimating atmospheric dispersion," Nuclear Safety 2, 47.
- Goering, H.  
 1958 Sammelband zur statistischen theorie der turbulenz, Akademie Verlag, Berlin.
- Goldstein, S. (Ed.)  
 1938 Modern developments in fluid mechanics, Vols. 1, 2, Clarendon Press, Oxford. Reprinted by Dover, New York (1965).
- Grass, A. J.  
 1971 "Structural features of turbulent flow over smooth and rough boundaries," J. Fl. Mech. 50, 233.
- Hanratty, T. J.  
 1956 "Heat transfer through a homogeneous isotropic turbulent field," A.I.Ch.E. Journal 2, 42.
- Hanratty, T. J., G. Latinen and R. H. Wilhelm  
 1956 "Turbulent diffusion in particulate fluidized beds of particles," A.I.Ch.E. Journal 2, 372.

Hay, J. S. and F. Pasquill

1957 "Diffusion from a fixed source at a height of a few hundred feet in the atmosphere," J. Fl. Mech. 2, 299.

1959 "Diffusion from a continuous source in relation to the spectrum and the scale of turbulence," Adv. Geophys. 6, 345.

Hinze, J. O.

1959 Turbulence, McGraw-Hill, New York.

Hogg, R. V. and A. T. Craig

1965 Introduction to mathematical statistics, 2nd Ed., The Macmillan Company, New York.

Hopf, E.

1952 "Statistical hydromechanics of functional calculus," J. Rational Mech. Anal. 1, 87.

1957 "On the application of functional calculus to the statistical theory of turbulence," Proc. Symposia Appl. Math., 8, 41.

Hsu, N. T., K. Sato, and B. H. Sage

1956 "Temperature gradients in turbulent gas streams. Effect of flow conditions upon eddy conductivity," I. & E.C. 48, 2219.

Ibragimov, M. K., V. I. Subbotin and G. S. Taranov

1969 "Determination of the correlation between pulsations of velocity and temperature in turbulent air flow in a tube," Soviet Phys.-Doklady 13, 1208.

1971 "Velocity and temperature fluctuations and their correlations in the turbulent flow of air in pipes," Int. Chem. Eng. 11, 659.

Jenkins, G. M. and D. G. Watts

1969 Spectral analysis and its applications, Holden-Day San Francisco, Calif.

Kakac, S. and E. Paykoc

1968 "Analysis of turbulent forced convection heat transfer between parallel plates," METU J. Pure and Appl. Sci. 1, 27.

Kalinske, A. A. and C. L. Pien

1944 "Eddy diffusion," I. & E.C. 36, 220.

Kampé de Fériet, J.

- 1939 "Les fonctions aleatoires stationnaires et la theorie statistique de la turbulence homogene," Ann. Soc. Sci. Bruxelles 59, 145.

- 1951 Introduction to the statistical theory of turbulence correlation and spectrum, Inst. Fl. Dyn. and Appl. Math. Lect. Ser. No. 8, University of Maryland, Baltimore.

Kennedy, D. A.

- 1965 Some Measurements of the Dispersion of Spheres in a Turbulent Flow, Doctoral Dissertation, Dept. of Mechanics, The Johns Hopkins University, Baltimore, MD.

Kim, H. T., S. J. Kline and W. C. Reynolds

- 1971 "The production of turbulence near a smooth wall in a turbulent boundary layer," J. Fl. Mech. 50, 133.

Kirmse, D. W.

- 1964 A Monte Carlo study of turbulent diffusion, Doctoral Dissertation, Iowa State University of Science and Technology, Ames, Iowa.

Kline, S. J. and P. W. Runstadler

- 1959 "Some preliminary results of visual studies of the flow model of the wall layers of the turbulent boundary layer," J. Appl. Mech. 26, 166.

Kolmogorov, A. N.

- 1941 "Local structure of turbulence in an incompressible fluid at very high Reynolds number," Doklady Akad. Nauk U.S.S.R. 30, 299, Translation in Friedlander, S. K. and L. Topper (Eds.), Turbulence--classic papers on statistical theory, Interscience, New York (1961).

Konopik, A. E. and R. W. Fahien

- 1964 Radial variation of eddy diffusivity tensor components for the three-dimensional mass transport, USAEC Rep IS-830, Iowa State University of Science and Technology Ames, Iowa.

Kraichnan, R. H.

- 1970 "Diffusion by a random velocity field," Phys. Fl. 13, 22.

Lamb, H.

- 1932 Hydrodynamics (6th ed.), Cambridge University Press, Cambridge. Reprinted by Dover, New York (1945).

Laufer, J.

- 1954 The structure of turbulence in fully developed pipe flow, NACA Rep. 1174.

- Lettau, H.  
1951 "On eddy diffusion in shear zones," Geophys. Res. Pap. 97, 369.
- Lin, C. C.  
1948 "Note on the law of decay of isotropic turbulence," Proc. of the Nat. Acad. of Sci. 34, 540.  
1953 "On Taylor's hypothesis and the acceleration terms in the Navier-Stokes equations," Quart. Appl. Math. 10, 295.  
1959 Turbulent flows and heat transfer, Princeton University Press, Princeton, N. J.  
1961 Statistical theories of turbulence, Princeton University Press, Princeton, N. J.
- Lumley, J. L. and H. A. Panofski  
1964 The structure of atmospheric turbulence, Interscience, New York.
- Martin, G. Q. and L. N. Johanson  
1965 Turbulence characteristics of liquids in pipe flow. A.I.Ch.E. Journal 11, 29.
- Mickelsen, W. R.  
1955 An experimental comparison of the Lagrangian and Eulerian correlation coefficients in homogeneous isotropic turbulence, NACA TN 3570.  
1960 "Measurements of the effect of molecular diffusivity in turbulent diffusion," J. Fl. Mech. 7, 397.
- Monin, A. S. and A. M. Yaglom  
1971 Statistical fluid mechanics, vol. 1, M.I.T. Press, Cambridge, Mass.
- Nedderman, R. M.  
1961 "The use of stereoscopic photography for the measurement of velocities in liquids," Chem. Eng. Sci. 16, 113.
- Nunner, W.  
1956 Wärmeübertragung und Druckfall in rauhen Röhren, VDI-Forschungsheft No. 455.
- Obukhov, A. M.  
1941 "Über die Energieverteilung im Spektrum einer turbulenten Strömung," Izvestia Akad. Nauk U.S.S.R., ser. geogr. geofiz. 4-5, 453. Translation in Goering, H., Sammelband zur statistischen Theorie der Turbulenz, Akademie Verlag, Berlin (1958).

- Okubo, A.  
1967 "Study of turbulent dispersion by use of Lagrangian diffusion equation," Phys. Fl. Suppl. 10, S72.
- Opfeli, J. B. and B. H. Sage  
1956 "Turbulence in thermal and material transport," Adv. Chem. Eng. 1, 241.
- Pai, S. I.  
1953 "On turbulent flow between parallel plates," J. Appl. Mech. 20, 109.
- Pasquill, F.  
1961 "The estimation of the dispersion of windborne material," Meteor. Mag. 90, 33.  
1962 Atmospheric diffusion. A study of the dispersion of windborne material from industrial and other sources, D. van Nostrand Publ., London.  
1971 "Atmospheric dispersion of pollution," Quart. J. Roy. Meteor. Soc. 97, 369.
- Patterson, G. K. and J. L. Zakin  
1967 Hot-film anemometry measurements of turbulence in pipe flow: organic solvents, A.I.Ch.E. Journal 13, 513.
- Patterson, G. S., Jr. and S. Corrsin  
1966 "Computer experiments on random walks with both Eulerian and Lagrangian statistics," in S. I. Pai (ed.) Dynamics of fluids and plasmas, Academic Press, New York (1966).
- Philip, J. R.  
1967 "Relation between Eulerian and Lagrangian Statistics," Phys. Fluids Suppl. 10, S69.
- Prandtl, L.  
1904 Ueber Flussigkeitsbewegung bei sehr kleiner Reibung," Verhandlungen d. III Intern. Mathe. Kongr., Heidelberg, 484.  
1925 "Berichtuber Untersuchungen zur ausgebildeten Turbulenz, Z. a. M.M. 5, 136.
- Prandtl, L. and O. G. Tietjens  
1934a Fundamentals of hydro- and aeromechanics, McGraw-Hill, New York. Reprinted by Dover, New York (1957).



- Prandtl, L. and O. G. Tietjens  
 1934b Applied hydro- and aeromechanics, McGraw-Hill, New York. Reprinted by Dover, New York (1957).
- Priestley, C. H. B.  
 1959 Turbulent transfer in the lower atmosphere, Chicago University Press, Chicago.
- Reynolds, O.  
 1883 "An experimental investigation of the circumstances which determine whether the motion of water shall be direct or sinuous, and of the law of resistance in parallel channels," *Phil. Trans. Roy. Soc.* 174, 935.
- 1895 "On the dynamical theory of incompressible viscous fluids and the determination of the criterion," *Phil. Trans. Roy. Soc.* 186, 123.
- Richardson, L. F.  
 1920 "The supply of energy from and to atmospheric eddies," *Proc. Roy. Soc.* A97, 354.
- 1926 "Atmospheric diffusion shown on a distance-neighbour graph," *Proc. Roy. Soc.* A110, 709.
- Roberts, O. F. T.  
 1923 "The theoretical scattering of smoke in a turbulent atmosphere," *Proc. Roy. Soc.* A104, 640.
- Roley, G. and R. W. Fahien  
 1960 Gaseous diffusion at moderate flow rates in circular conduits, USAEC Rep. IS-330, Iowa State University of Science and Technology, Ames, Iowa.
- Rouse, H. and S. Ince  
 1963 History of hydraulics, Dover, New York.
- Russo, C.  
 1965 Tensor diffusividade massica--Estudo dos componentes significativos, M.Sc. Thesis, Universidade do Brasil, Rio de Janeiro.
- Rust, J. H. and A. Sesonske  
 1966 "Turbulent temperature fluctuations in mercury and ethylene glycol in pipe flow," *Int. J. Heat Mass Transfer* 9, 215.
- Saffman, P. G.  
 1962 "Some aspects of the effects of the molecular diffusivity in turbulent diffusion," in Favre, A. (Ed.) Mecanique de la turbulence, Coll. Intern. CNRS, Editions CNRS, Paris (1962).

- Saffman, P. G.  
1960 "On the effect of the molecular diffusivity in turbulent diffusion," J. Fl. Mech. 8, 273.
- Sage, B. H.  
1959 "Some aspects of fluid mechanics in chemical engineering," A.I.Ch.E. Journal 5, 331.
- Schleicher, C. A., Jr.  
1958 "Experimental velocity and temperature profiles for air in turbulent pipe flow," Trans. A.S.M.E. 80, 693.
- Schleicher, C. A., Jr. and M. Tribus  
1957 "Heat transfer in a pipe with turbulent flow and arbitrary wall-temperature distribution," Trans. A.S.M.E. 79, 789.
- Schlichting, H.  
1960 Boundary layer theory, McGraw-Hill, New York.
- Schlinger, W. G., V. J. Berry, J. L. Mason and B. H. Sage  
1953a "Temperature gradients in turbulent gas streams--nonuniform flow," I. & E.C. 45, 662.
- Schlinger, W. G., N. T. Hsu, S. D. Cavers and B. H. Sage  
1953b "Temperature gradients in turbulent gas streams--measurement of temperature, energy and pressure gradient," I. & E.C. 45, 864.
- Schlinger, W. G. and B. H. Sage  
1953 "Velocity distribution between parallel plates," I. & E.C. 45, 2636.
- Schmidt, W.  
1917 "Der Massenaustausch bei der ungeordneten Strömung in freier Luft und seine Folgen," Sitzungsber. Akad. Wiss. Wien (Abt. IIa) 126, 757.
- Schneider, P. J.  
1957 "Effect of axial fluid conduction on heat transfer in the entrance regions of parallel plates and tubes," Trans. A.S.M.E. 79, 765.
- Schubauer, G. B.  
1935 Turbulence indicator utilizing the diffusion of heat, NACA Rep. 524.
- Schubauer, G. B. and C. M. Tchen  
1961 Turbulent flow, Princeton University Press, Princeton, N.J.

- Seagrave, R. C. and R. W. Fahien  
 1961 Turbulent mass transfer in liquid streams, USAEC Rep IS-419, Iowa State University of Science and Technology, Ames, Iowa.
- Smith, F. B.  
 1961 "An analysis of vertical wind-fluctuations at heights between 500 and 5,000 feet," Quart. J. Roy. Meteor. Soc. 87, 180.
- Smith, J. W., R. A. Gowen and B. Wasmund  
 1966 Diffusion coefficients and temperature profiles for turbulent heat transfer to water in pipes, P.P. 10B, 55th Ann. Meeting A.I.Ch.E., Detroit, Mich.
- Snyder, W. H. and J. L. Lumley  
 1971 "Some measurements of particle velocity autocorrelation functions in a turbulent flow," J. Fl. Mech. 48, part 1, 41.
- Sparrow, E. M., T. M. Hallman and R. Siegel  
 1957 "Turbulent heat transfer in the thermal entrance region of a pipe with uniform heat flux," Appl. Sci. Res. A7, 37.
- Sullivan, P. J.  
 1971 "Longitudinal dispersion within a two-dimensional turbulent shear flow," J. Fl. Mech. 49, 551.
- Subbotin, V. I., M. Kh. Ibragimov and E. V. Nomofilov  
 1966 "A generalized relationship for turbulent heat transfer coefficients in fluid streams," Int. Chem. Eng. 6, 81.
- Sutton, O. G.  
 1932 "A theory of eddy diffusion in the atmosphere," Proc. Roy. Soc. A135, 143.  
 1953 Micrometeorology, McGraw-Hill, New York.
- Tanimoto, S. and T. J. Hanratty  
 1963 "Fluid temperature fluctuations accompanying turbulent heat transfer in a pipe," Chem. Eng. Sci. 18, 307.
- Tatarski, V. I.  
 1961 Wave propagation in a turbulent medium, McGraw-Hill, New York.
- Taylor, G. I.  
 1915 "Eddy motion in the atmosphere," Phil. Trans. Roy. Soc. A215, 1.

- Taylor, G. I.  
 1921 "Diffusion by continuous movements," Proc. London Math. Soc. 20, 196.
- 1935a "Statistical theory of turbulence, I.," Proc. Roy. Soc. A151, 421.
- 1935b "Statistical theory of turbulence. II. Measurement of correlation in the Eulerian representation of turbulent flow," Proc. Roy. Soc. A151, 444.
- 1935c "Statistical theory of turbulence. III. Distribution of dissipation of energy in a pipe over its cross-section," Proc. Roy. Soc. A151, 455.
- 1935d "Statistical theory of turbulence. IV. Diffusion in a turbulent air stream," Proc. Roy. Soc. A151, 465.
- 1938 "The spectrum of turbulence," Proc. Roy. Soc. A164, 476.
- 1954 "The dispersion of matter in turbulent flow through a pipe," Proc. Roy. Soc. A223, 446.
- Towle, W. L. and T. K. Sherwood  
 1939 "Eddy diffusion-mass transfer in the central portion of a turbulent air stream," I. & E.C. 31, 457.
- Townsend, A. A.  
 1954 "The diffusion behind a line source in homogeneous turbulence," Proc. Roy. Soc. 229A, 487.
- 1956 The structure of turbulent shear flow, Cambridge University Press, Cambridge.
- Truchasson, C.  
 1964 "Mésures de temperature dans la 'sous-couche laminaire' d'un écoulement d'eau," Chem. Eng. Sci. 19, 305.
- Uberoi, M. S. and S. Corrsin  
 1953 Diffusion of heat from a line source in isotropic turbulence, NACA Rep. 1142.
- Vanoni, V. A. and N. H. Brooks  
 1955 Cal. Inst. Tech., Rep. no. e-46 (ASTIA Reprint Ad 66182), Pasadena.
- Venezian, E. and B. H. Sage  
 1961 "Temperature gradients in turbulent gas streams: effect of viscous dissipation on evaluation of total conductivity," A.I.Ch.E. Journal 7, 688.

Von Karman, T.

- 1934 "Some aspects of the theory of turbulent motion,"  
Proc. Intern. Congr. Appl. Mech. 54, Cambridge.

Von Karman, T. and L. Howarth

- 1938 "On the statistical theory of isotropic turbulence,"  
Proc. Roy Soc. A164, 476.

Von Karman, T., and C. C. Lin

- 1949 "On the concept of similarity in the theory of isotropic turbulence," Rev. of Mod. Phys. 21, 516.

## BIOGRAPHICAL SKETCH

David Lee Breton, son of Henry and Dorothy Breton, was born on August 3, 1940 in Bartow, Florida. In June, 1958 he received his high school diploma from Summerlin Institute in Bartow, Florida. In high school David was awarded the Mathematics Award and the Bausch & Lomb Honorary Science Award for his graduating class.

In September, 1958 he started his undergraduate studies at the University of Florida, Gainesville, Florida and later received his Bachelor of Science degree in chemical engineering in April, 1963. He graduated from the university with High Honors and was also a member of Sigma Tau, an honorary engineering organization.

In September, 1963 David received an Atomic Energy Commission Fellowship to the University of California at Berkeley to study in Nuclear Engineering. Due to a change in interests, in February, 1964 he discontinued graduate studies at Berkeley and went to work for the Nuclear Division of the Union Carbide Corporation in Oak Ridge, Tennessee. While working for Union Carbide Corporation, David investigated processes for recovering Uranium from spent nuclear fuels.

Since September, 1968, David has been enrolled in the Graduate School of the University of Florida. In December, 1969 he received his Master of Engineering degree and he has been working toward his Doctor of Philosophy degree since then. During this period of time he was a graduate assistant in the Department of Chemical Engineering.

He married Frances Louise Daniel of Ocala, Florida in June, 1964 and he is the father of two children. The children are his son, David Lee Breton, Jr., who was born on November 6, 1966, and his daughter, Jeanette Elaine Breton, who was born on February 28, 1968.

I certify that I have read this study and that in my opinion it conforms to acceptable standards of scholarly presentation and is fully adequate, in scope and quality, as a dissertation for the degree of Doctor of Philosophy.



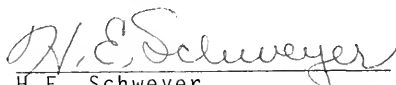
R.W. Fahien, Chairman  
Professor of Chemical  
Engineering

I certify that I have read this study and that in my opinion it conforms to acceptable standards of scholarly presentation and is fully adequate, in scope and quality, as a dissertation for the degree of Doctor of Philosophy.



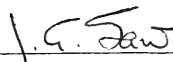
D.W. Kirmse, Co-Chairman  
Assistant Professor of  
Chemical Engineering

I certify that I have read this study and that in my opinion it conforms to acceptable standards of scholarly presentation and is fully adequate, in scope and quality, as a dissertation for the degree of Doctor of Philosophy.



H.E. Schweyer  
Professor of Chemical  
Engineering

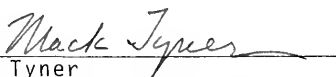
I certify that I have read this study and that in my opinion it conforms to acceptable standards of scholarly presentation and is fully adequate, in scope and quality, as a dissertation for the degree of Doctor of Philosophy.



J.G. Saw  
Professor of Statistics

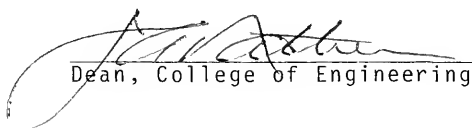


I certify that I have read this study and that in my opinion it conforms to acceptable standards of scholarly presentation and is fully adequate, in scope and quality, as a dissertation for the degree of Doctor of Philosophy.

  
M. Tyner  
Professor of Chemical  
Engineering

This dissertation was submitted to the Graduate Faculty of the College of Engineering and to the Graduate Council, and was accepted as partial fulfillment of the requirements for the degree of Doctor of Philosophy.

August, 1975

  
Dean, College of Engineering

\_\_\_\_\_  
Dean, Graduate School



UNIVERSITY OF FLORIDA



3 1262 08666 273 0